Dissertation

Development and application of *in vitro* cell culture models to investigate vocal fold physiology and pathophysiology on the molecular level

submitted by

Tanja GROSSMANN, BSc, MSc

for the Academic Degree of

Doctor of Medical Science (Dr. scient. med.)

at the

Medical University of Graz

Division of Phoniatrics, ENT Hospital

under the Supervision of

Univ.-Prof. Priv.-Doz. Dr.med.univ.et scient.med. Markus GUGATSCHKA

2020

Statutory Declaration

I hereby declare that this thesis is my own original work and that I have fully acknowledged by name all of those individuals and organizations that have contributed to the research for this thesis. Due acknowledgement has been made in the text to all other material used. Throughout this thesis and in all related publications I followed the “Standards of Good Scientific Practice and Ombuds Committee at the Medical University of Graz”.

Graz, June 2020

Disclosures

Part of this thesis has been published in

The Laryngoscope, article accepted on 23 May, 2020; doi:10.1002/lary.28855.

Exploring the pathophysiology of Reinke´s edema: The cellular impact of cigarette smoke and vibration

Tanja Grossmann, MSc; Barbara Steffan, BSc; Andrijana Kirsch, PhD; Magdalena Grill, PhD; Claus Gerstenberger, MSc; Markus Gugatschka, MD, DMSci.

Division of Phoniatrics, Medical University of Graz, Austria

All co-authors agreed to the use of their data in the thesis and the respective publication:

Contributions of co-authors to the thesis and the respective publication:

Andrijana Kirsch gave input in project design and critically helped in all steps of study performance for the respective publication and the thesis.

Barbara Steffan performed the experiments for the respective publication and was supervised by the doctoral candidate.

Magdalena Grill gave input in project design, co-supervised the project for the respective publication and supported immunohistochemical stainings used in the thesis.

Claus Gerstenberger gave input in project design and supported the project for the respective publication in technical assistance.

Markus Gugatschka supervised the project and the thesis.

The doctoral candidate Tanja Grossmann contributed in supervision to the respective publication:

PLoS One. 2019 Mar 14; 14(3): e0213788. doi: 10.1371/journal.pone.0213788. eCollection 2019.

Development and validation of a novel phonomimetic bioreactor

Andrijana Kirsch, David Hortobagyi, Theresa Stachl, Michael Karbiener, Tanja Grossmann, Claus Gerstenberger, Markus Gugatschka

Division of Phoniatrics, Medical University of Graz, Austria

All co-authors agreed to the use of their data in the thesis and the respective publication:

Contributions of co-authors to the respective publication:

Andrijana Kirsch, Conceptualization, Data curation, Formal analysis, Investigation, Methodology, Supervision, Validation, Visualization, Writing – original draft

David Hortobagyi, Conceptualization, Data curation, Writing – original draft, Writing – review & editing

Theresa Stachl, Methodology

Michael Karbiener, Conceptualization, Formal analysis, Supervision

Claus Gerstenberger, Methodology, Software, Visualization

Markus Gugatschka, Conceptualization, Funding acquisition, Methodology, Project administration, Resources, Supervision, Writing – original draft

All figures and tables within the thesis have been produced by the doctoral candidate without any reproduction/adaptation of previously published figures and tables.

Further co-authors actively contributed to the results of the thesis and agreed to the use of their data in the thesis:

Ruth Birner-Grünberger, Research Unit “Functional Proteomics and Metabolic Pathways”, Medical University of Graz, supported conceptualization and methodology of proteomic analysis for the thesis.

Barbara Darnhofer, Research Unit “Functional Proteomics and Metabolic Pathways”, Medical University of Graz, supported the preparation of proteomic samples and performed preliminary proteomic analysis for the thesis.

Luka Brcic, Diagnostic and Research Institute of Pathology, Medical University of Graz, supported the immunohistochemical stainings for the thesis.

Acknowledgements

At this point, I would like to express my gratitude to all those, without whom this dissertation would not have been possible.

I would like to thank my supervisor Prof. Markus Gugatschka at the Division of Phoniatrics for giving me the opportunity to realize this work. Thank you for choosing this topic for me that I really enjoyed working on and thank for your very positive and friendly way, which always motivated me. I would like to express my gratitude to the team members of the research group Laryngo Tracheal Tissue Engineering Graz, LTTEG that supported me in every possible way. Thanks to Dr. Michael Karbiener, Andrijana Kirsch, PhD and Magdalena Grill, PhD for introducing and supporting me in all biological and technical belongings and guiding parts of my whole work. Thanks to all members of the Center for Medical Research, Graz and the Division of Phoniatrics at the Medical University of Graz for supporting my work.

I am deeply thankful to all members of my dissertation committee Prof. Barbara Obermayer-Pietsch and Prof. Lars Kamolz, who supported me in every possible way.

I would like to express my gratitude to all the co-authors of my paper in “The Laryngoscope”. Thank you all for the good collaboration and for your support in realizing this project!

I would like to thank the Medical University of Graz, from which I received funding through the Doctoral School “Sustainable Health Research”. Furthermore, I want to express my gratitude to the Austrian National Bank (grant No. 16913) and the Austrian Science Fund (grant No. P 30496-B28) for external funding of this work.

Finally, I come to my family and friends. The time of my doctoral thesis was not always an easy one and without all of you, I would not have made it! I am so grateful to my parents for their love, understanding, encouragement and patience that enabled me to start and finish my whole study!

Table of Contents

Abbreviations and Definitions

2D	two-dimensional
3D	three-dimensional
3T3	three-day transfer, inoculum 3 x 10^5 cells
ACTA	alpha smooth muscle actin
ACTN3	actinin alpha 3
ALI	air-liquid-interface
ASC	adipose-derived stromal cells
B2M	beta-2 microglobulin
CAA	chloroacetamide
CaHA	calcium hydroxylapatite
CC	co-cultivation
CDH1	cadherin 1
cDNA	complementary deoxyribonucleic acid
CK	cytokeratin
CMF	Center for Medical Research
COL	collagen
COL4	basal collagen type IV
COVR	cell-based outer vocal fold replacement
COX	cyclooxygenase
CSE	cigarette smoke extract
C_T	cycle threshold
DCN	decorin
ddH_2O	double-distilled water
DLP	deep layer of the lamina propria
DM	decontamination medium
DMEM	Dulbecco´s Modified Eagle´s Medium
DMSO	dimethylsulfoxid
DTPH	dithiobis(propanoid dihydrazide)

DTT	dithiothreitol
DXN	doubly crosslinked network
ECM	extracellular matrix
EDTA	ethylenediaminetetraacetic acid
EGF	epidermal growth factor
eGM	epithelial cell-specific growth medium
ELISA	enzyme-linked immunosorbent assay
ELN	elastin
EtOH	ethanol
FACS	fluorescence-activated cell sorting
FBS	fetal bovine serum
FDR	false discovery rate
FGF	fibroblast growth factor
fGM	fibroblast-specific growth medium
FN	fibronectin
GRABAS	grade, roughness, breathiness, asthenia, strain
GSX	Carbylan-S-crosslinked
Gtn	gelatin
H&E	hematoxylin and eosin
HA	hyaluronic acid
HAADH	hydrazide-modified hyaluronic acid
HAALD	aldehyde-functionalized hyaluronic acid
HAS	hyaluronan synthase
hESC	human embryogenic stem cell
HGF	hepatocyte growth factor
hOMEC	human oral mucosal epithelial cells
HPLC	high-performance liquid chromatography
HSDI	high-speed digital imaging
hTERT	human telomerase reverse transcriptase

HUVEC	human umbilical vein endothelial cells
(h)VFF	(human) vocal fold fibroblast
HYAL	hyaluronidase
IFN	interferon
IGF	insulin-like growth factor
IL	interleukin
ILP	intermediate layer of the lamina propria
ITGA2	integrin subunit alpha 2
ITGB1	integrin subunit beta 1
ITS-G	insulin-transferrin-selenium
KTP	potassium-titanyl-phosphate laser
LC-MS/MS	liquid chromatography-tandem-mass spectrometry
LDH	lactate dehydrogenase
LDV	laser doppler vibrometry
LLLT	low-level laser therapy
LTTEG	Laryngo Tracheal Tissue Engineering Graz
MMP	matrix metalloproteinase
MRI	magnetic resonance imaging
MSC	mesenchymal stromal cells
NaOH	natrium hydroxide
Nd:YAG	Neodymium:Yttrium-Aluminium-Garnet
NGFR	nerve growth factor receptor
NLSM	nonlinear laser scanning microscopy
OCT	optical coherence tomography
PAF	platelet-activating factor
PBS	phosphate buffered saline
PCL	polycaprolactone
PDGF	platelet-derived growth factor
PDL	pulsed-dye laser

PDMS	poly(dimethyl-siloxane)
PDT	photodynamic therapy
PEG	polyethylene glycol
PEGDA	polyethylene glycol diacrylate
PFA	paraformaldehyde
PLGA	poly(lactic-co-glycolic acid)
POM	polyoxymethylene
PSM	peptide-spectra-matches
qPCR	quantitative polymerase chain reaction
RT	reverse transcription
SDS	sodium dodecyl sulfate
siRNA	small interfering ribonucleic acid
SLP	superficial layer of the lamina propria
SM	standard medium
STR	short tandem repeat
SVF	stromal vascular fraction
TCEP	Tris(2-carbocylethyl)phosphine hydrochloride
TEER	transmucosal electrical resistance
TGF	transforming growth factor
THY1	Thy-1 cell surface antigen
TIMP	tissue inhibitor of metalloproteinase
TNF	tumor necrosis factor
UXT	ubiquitously expressed transcript protein
VF	vocal fold
VHI	voice handicap index
VIM	vimentin
VWF	Von Willebrand factor
α-SMA	alpha smooth muscle actin

Abstract in German

Zellkultur ist eine wertvolle, unverzichtbare Methode in der biomedizinischen Forschung und ermöglicht einen besseren Einblick in die grundlegenden zellulären und molekularen Mechanismen von gesunden und pathologisch veränderten Stimmlippen. Bis heute sind die meisten *in vitro* Anwendungen durch die Verwendung eines einzelnen Zelltyps, der Fibroblasten, limitiert. Diese stellen den wichtigsten zellulärer Bestandteil im Stimmlippen-Bindegewebe, der Lamina propria dar. Unter anderem agieren sie als Hauptproduzenten der extrazellulären Matrix und tragen dadurch wesentlich zum Erhalt der einzigartigen Gewebseigenschaften bei. Im Hinblick auf diese komplexe mehrschichtige und –zellige Mikrostruktur der humanen Stimmlippen, ihrer mechanischen Flexibilität während der Lautbildung und ihrer biophysikalischen Umgebung, ist eine Weiterentwicklung der traditionellen zwei-dimensionalen und bisher verwendeten drei-dimensionalen *in vitro* Modelle notwendig.

Ziel dieser Dissertation war die Weiterentwicklung und Anwendung bisher verwendeter Zellkulturmodelle. Dafür etablierten wir ein Verfahren zur Isolierung von primären humanen Epithelzellen aus oraler Schleimhaut. Diese Zellen wurden verwendet, um drei-dimensionale Konstrukte gemeinsam mit humanen Stimmlippen-Fibroblasten unter organotypischen Bedingungen zu generieren. Wir konnten zeigen, dass diese Konstrukte ein mehrschichtiges Epithel und eine durchgehende Basalmembran als morphologische Hauptmerkmale vergleichbar zur nativen Stimmlippen-Schleimhaut während der Kultivierung bildeten. Zusätzlich konnte ein kürzlich etablierter phonomimetischer Bioreaktor genutzt werden, um den kombinierten Effekt von Vibration und Zigarettenrauch auf zellulärer Ebene in immortalisierten, menschlichen Fibroblasten zu untersuchen.

Die verwendeten und entwickelten *in vitro* Modelle können als innovative, stabile und reproduzierbare Strategien genutzt werden. Dadurch kann ein wesentlicher Beitrag zu neuen Einsichen in die (Patho)-Physiology der humanen Stimmlippen geleistet werden. Diese Modelle können zusätzlich als Plattform für präklinische Tests und möglicherweise als Transplantat für laryngeale Stimmlippen-Transplantationen genutzt werden.

Abstract in English

Cell culture is a valuable, indispensable tool for controlled biomedical research, enabling a better insight into the cellular and molecular mechanisms underlying vocal fold function in health, disease and injury. To date, most of the current *in vitro* applications has been limited by the use of a single cell type: fibroblasts. This main cellular component of the vocal fold connective tissue, the lamina propria, has been described to produce large amounts of the extracellular matrix, thereby substantially maintaining the unique tissue characteristics. Regarding the complex multilayered and multicellular microstructure of native vocal folds, its mechanical versatility during sound production and biophysical microenvironment, enhancement of traditional two-dimensional and existing three-dimensional *in vitro* model systems has to be established.

The aim of this thesis was to design possible strategies to develop and apply enhanced cell culture models *in vitro*. Therefore, we established an effective isolation procedure of near primary epithelial cells out of human oral mucosa and used these cells to bioengineer three-dimensional constructs, together with vocal fold fibroblasts, under organotypic conditions. We could show that key morphologic characteristics of co-cultivated constructs resembled the native mucosa, including a mulitlayered epithelium and a continuous basement membrane. Furthermore, we utilized a recently engineered phonomimetic bioreactor to explore the isolated or combined effects of vibration and cigarette smoke on the cellular level of immortalized human vocal fold fibroblasts.

Altogether, the utilized and established strategies will provide innovative, stable and reproducible *in vitro* models. They will substantially contribute to a deeper understanding of vocal fold micro-(patho)physiology, provide an *in vitro* platform for preclinical drug testing and may serve as a graft for laryngeal mucosal transplantation.

1. Introduction

1.1. Phonation in humans – societal and scientific context

One of the most outstanding parts in human evolution is the unique ability for extensive learning and communication of complex vocal behaviors (1). Voice disorders, well-documented to affect up to 30 % of the general population across the lifespan (2), cause significant negative impact on everyday social interactions of affected individuals (3). This wide spectrum of disorders is mostly the consequence of the disruption of the natural pliability of the vocal folds (VF), the soft laryngeal connective tissue performing phonatory and respiratory functions. Various common stimuli including voice overuse, mechanical stresses, deleterious environmental factors, as well as various pathological conditions lead to the damage of the highly complex microstructure of this unique tissue (3–5). Frequently, multiple aformentioned factors are involved.

Current treatment options including behavioral speech therapy, voice rest, as well as phonosurgical methods are still bound to the macroscopical level. However, there has been no consistent or effective strategy. Therefore, newer therapeutic approaches focus on the restoration of VF function on the cellular basis. Most importantly: to identify and study the underlying molecular processes in the context of the VF. Beside animal models, cell culture is an innovative way to extend current knowledge of physiological and pathophysiological mechanisms, so far primarily based on acoustic, visual and histological features (6–12).

1.2. Phonation physiology

Fundamental base of voice production is the complex interaction of three basic anatomic units: (a) the infraglottic respiratory tract, consisting of the lungs, supporting diaphragm, thoracic muscles and back muscles as power source; (b) the supraglottic larynx, pharynx, oral and nasal cavity and the paranasal sinuses acting as resonators; (c) the four cartilages, the thyroid, the cricoid and two arytenoids, as well as their covering mucosa, operating as the oscillator (4,13,14).

The acoustic wave for phonation is produced by the vibratory tissue motion of the VF, which are located medial to the thyroarytenoid muscle on both sides within the larynx.

This process is mainly coordinated by five intrinsic and three extrinsic laryngeal muscles.

The vocalis muscle, the medial proportion of the thyroarytenoid muscle causes adduction, thickening, lowering and shortening of the VF. The lateral cricoarytenoid muscle, adducts, lowers and thins the VF, while the posterior cricoarytenoid muscle, the only one, which enables opening of the glottis, elongates, elevates, and further thins the VF. The interarytenoid muscles (oblique and transverse arytenoid) adduct the VF in the cartilaginous portion and control the glottis closure through rotation and tilting the arytenoid cartilages toward the midline. By approaching the thyroid cartilage towards the cricoid cartilage, VF are elongated, lowered and thinned, which is enabled via contraction of the cricothyroid muscle. Besides the cricothyroid muscle, intrinsic muscles are innervated by the recurrent laryngeal nerve.

Main function of the three extrinsic laryngeal muscles, sternothyroid, sternohyoid and thyrohyoid, is the stabilization of the thyroid cartilage within the neck (4,13,15–18).

The physiological process of phonation was first explained by the “Myoelastic Theory of Voice Production” by Muller (19), and later modified by Van den Berg by the “Myoelastic-aerodynamic Theory of Voice Production and its Control” (20). The myoelastic aspect is related to the neuromuscular control, which adjusts the glottal aperture configuration in addition to tension and elasticity of the VF. The three main principles that are critical for VF vibration are defined by the aerodynamic aspect. These include that (a) air flows from high to low-pressure region; (b) the pressure of a non-compressible flow decreases as the particle speed of the fluid increases - according to Bernoulli´s energy law; and (c) the restricted particle velocity of a non-compressible flow in a duct, increases as the cross-sectional area of the duct decreases (15,20–22).

Expanding this theory, Titze demonstrated VF oscillation to be less initiated by the Bernoulli effect. Rather, frictional energy loss in this tissue is overcome by a continual transfer of energy from the glottal airstream to the tissue through flow-induced oscillation (23).

According to all these theories and aspects, self-sustained oscillation of VF is caused by resulting asymmetry between the aerodynamic driving forces that are produced due periodic opening and closing of the glottis, usually accompanied by collision between

the folds (24,25). Fundamental frequency for normal phonation, dependent on age and gender, typically ranges between 100 and 350 Hz, and VF exhibit strains up to 30 % (26,27). All together, the biomechanical properties of mass and stiffness of VF have to be combined with its typical geometry and histology for adequate voice production in humans.

Fundamental knowledge of VF vibration, laryngeal muscle activity and acoustic output are limited due to limited access to human subject experiments (11,28–34), and sparsely used *in vivo* (35–38) and *in vitro* models (39–42) in animals. Among others, further approaches using synthetic physical models (43–47), the development of three-dimensional biomechanical models (48–51) and computational models (52–56) improved voice research during the past decades.

1.3. Vocal fold composition and anatomy

VF consist of a stratified squamous epithelium, matrix-rich lamina propria, and muscle tissue. The epithelium serves as a protective covering of the tissue and expresses cytokeratin (CK) 13 and 14, nerve growth factor receptor (NGFR), and involucrin. Epithelial cells are joined by junctional complexes including anchoring, occluding and communicating junctions. Basal cells are closely appositioned to the underlying basement membrane zone, which is mainly composed of collagen (COL) but also fibronectin (FN) and secures the epidermis to the lamina propria (57–61). This connective tissue is segmented into three distinct layers. The superficial layer of the lamina propria (SLP) is made up of a loosely arranged network of collagen I and III, elastic fibers, hyaluronic acid (HA) and a low amount of fibroblasts. The intermediate layer of the lamina propria (ILP) consists of more collagen and extracellular matrix (ECM) proteins, a moderate number of fibroblasts and the highest concentration of HA. Elastin (ELN) is most dense in this layer. The deep layer of the lamina propria (DLP) shows a tight accumulation of ECM proteins including fibrous proteins, proteoglycans and HA, many elastic fibers and a high number of fibroblasts. Collagen is most dense in this layer (4,62–67).

The complex microstructure comprises proportions, relationship and organisation of cellular and ECM-related components. It determines, to a large degree, the physiological biomechanical properties of the VF for adequate voice production, as

well as the ability of VF to withstand various mechanical loads such as aerodynamic (~1-10 kPa), contractile (~100 kPa), impact (~0.5-5.0 kPa), shear (~0.8 kPa) and tensile (~1.0 MPa) stresses (63–69). Among others, tissue elastic properties are measured by the Young´s modulus, equated by the relation of stress to strain, whereas stress may be defined as required force for lateral movement or the change in force or the change in force, divided by the tissue contact area over which the force is applied. Strain is defined as the amount of displacement, or the change in length of the tissue (70,71). Location-dependent differences in stiffness among the human VF ranging from 2-4.8 kPa were validated *ex vivo* (72). Characterization of structural and morphological features and changes occurring during pathological processes or surgical intervention procedures contributed substantially among others to this knowledge to date, using histological methods (64,73–75), optical coherence tomography (OCT) (6,76–79), magnetic resonance imaging (MRI) (80), high-resolution synchrotron X-ray microtomography (81), or nonlinear laser scanning microscopy (NLSM) (82).

1.4. Voice disorders

During their lifetime, up to 30 % of the general population develop voice disorders due to numerous and common stimuli (2–5), whereas 22 % of patients seeking treatment present with organic changes of the VF (83). Several studies (84–86) revealed a higher prevalence of voice problems in elderly adults due to age-related physiologic changes including laryngeal muscle atrophy (87), disorganization of collagen fibrils (64) and decreased synthesis of ECM components (12,88–91). Structural changes of the VF due to pathologies like Reinke´s edema (74,92–94), leukoplakia (92,93,95,96), partial or complete paralysis (93,97), age-caused presbyphonia (93,94), benign (e.g. nodules (92,93,98), polyps (92,93,99,100), cysts (92,93), papilloma (92,93)) or malignant lesions (e.g. squamous cell carcinoma (92)) represent the most common form of voice disorders. Roy et al. (101) showed acute and chronic laryngitis, nonspecific dysphonia, and benign VF lesions to be the most frequent diagnoses. Although most of the benign lesions can be relieved temporarily by rest or voice therapy, surgical intervention may be required leading to impaired voice production, conditions with considerable mucosal loss and scar formation (2,3).

1.5. Vocal fold scarring

1.5.1. Causing conditions

To date, scarring of the VF, caused among others by surgical interventions, represents the most severe and difficult to treat option in the context of various voice disorders and remains clinically challenging. Further stimuli such as prolonged phonotrauma (e.g. due to other types or surgery that involve intubation), radiation therapy, inflammatory response to laryngopharyngeal reflux, bacterial laryngotracheitis, rheumatoid arthritis or other biological and chemical changes can lead to scarred VF tissue (4,102–105).

1.5.2. Clinical manifestation and diagnosis

Clinically, patients usually suffer from breathy, hard to sustain, dysphonic voice, long-lasting dysphonia, loss of vocal control and vocal fatigue. Proper diagnosis requires, in addition to a thorough medical history, laryngoscopy and videolaryngostroboscopy (4,105,106). Friedrich et al. (105) revealed two major clinical features typical for scarring: (a) insufficient closure of spindle-shaped glottis during phonation and leaking air, and (b) an impairment of VF vibration with reduced or mostly absent mucosal wave and reduced amplitude.

1.5.3. Pathological features

Normal wound healing response involves sequential, but overlapping phases including inflammation, proliferation and remodeling.

Within the injured tissue, activated platelet aggregation results in degranulation and release of chemotactic factors from platelet α-granules such as platelet-derived growth factor (PDGF), transforming growth factor (TGF)-β, platelet-activating factor (PAF), tumor necrosis factor (TNF)-α, interleukin (IL)-1, FN, and serotonin. The inflammatory phase is characterized by increased vascular permeability and the recruitment of neutrophils and macrophages. Phagocytosis, angiogenesis, regulation of ECM synthesis, cell recruitment and activation is mainly driven by activated macrophages through released cytokines and growth factors such as TGF-β1, TNF-α, interferon (IFN)-γ, epidermal growth factor (EGF), and fibroblast growth factor (FGF). Granulation tissue consistent of proteoglycans, HA, COL, and ELN, is formed during the

proliferation phase. This phase is characterized by a profuse connective tissue and accumulation of fibroblasts, keratinocytes, and endothelial cells. During the remodeling phase, the granulation tissue undergoes maturation or further organization indicated by a diminished density of fibroblasts, declined number of blood vessels and reorganization of connective tissue. Critical therefore is a balanced degradation of profuse ECM and the immature type III collagen and formation of mature type I collagen (107–112).

Any changes within these complex physiological processes lead to the main pathological features of scarred VF - disorganized composition and loss of important ECM constituents, volume deficiency and reduced pliability of the lamina propria (102,113).

Hirano et al. (114) showed excessive levels of disorganized collagen fibers, decreased levels of decorin (DCN) and varying levels of ELN, HA and FN in histologic examination of scarred VF from ten patients. Nevertheless, scarring severity may vary among clinical patients and systematic control of variables thought to impact treatment outcome still remain limitations in research. Therefore, most of reported histologic changes were evaluated and compared to gene expression patterns found in animal models, due to the limited possibility to examine scarring tissues in humans *in vivo*. Differentially abundant gene expression (115–120) and protein synthesis profiles (120–133) of ECM components (e.g. various types of collagens, ELN, HA, DNC, various types of glycosaminoglycans, VIM, FN), ECM-related proteins (e.g. hyaluronan synthases (HAS), hyaluronidases (HYAL), various types of matrix metalloproteinases (MMP)), fibrogenic (alpha smooth muscle actin (α-SMA), HGF) and inflammatory markers (e.g. IL-1β, interferon (IFN)-γ, cyclooxygenases (COX)) were found.

Most of these characteristic features of scarred VF are mainly driven by fibroblasts upon their activation into myofibroblasts caused by various wide-ranging and complex molecular processes within inflammation, wound healing or scar formation. This cellular phenotypic alteration, characterized by increased contraction, collagen and proteoglycan synthesis but decreased proliferation, mainly originates from macrophage-derived growth factors and cytokines (e.g. TGF-β1, TNF-α) (109,111,112,115). Jette et al. (134) validated this using isolated human vocal fold fibroblasts (VFF) derived from scars relative to normal VFF. They could reveal a slower

proliferation rate of scarred VFF and a higher expression of α-SMA, a well-accepted marker gene of fibroblast transdifferentiation (135,136), and an altered relative expression of various ECM-related genes (e.g. COL I, MMP 3 and 10, various types of integrins and laminins).

1.5.4. Current treatment options

Depending on factors such as patient´s individual needs and motivation, as well as the pathology´s severity and impact, the goal of any treatment is to restore the biomechanical function of the VF (137). Despite considerable progress in research of VF scarring, non of existing technical emerging advances, partly mentioned within the following sections, have been established as a fully effective, routine clinical approach.

1.5.4.1. Voice therapy

To date, behavioral voice therapy is primarily implemented as a preventative method to limit further damage to the scarred tissue. Due to the stiffened tissue of scarred VF and resultant changes in quality of voice, patients may develop compensatory hyperfunction behaviors that may result in further deterioration. Engaged voice therapy as well as providing education about vocal hygiene may significantly improve the voice and support returning to normal voice behaviors (4,138,139). Woo et al. (140) revealed in a retrospective study that several patients could improve their voice after speech therapy alone.

1.5.4.2. Laser therapy and cryotherapy

The use of angiolytic lasers such as potassium-titanyl-phosphate (KTP) laser or pulsed-dye laser (PDL), opened a promising approach in the treatment of VF scarring and has increased substantially (141–144).

Sheu et al. (141) propagated an elicited, temporally limited, inflammatory response in an altered ECM metabolism of KTP laser in injured rat VF mucosa, mediated by MMPs. Zhang et al. (142) demonstrated positive effects in rabbit VF scars treated with KTP laser and Neodymium:Yttrium-Aluminium-Garnet (Nd:YAG) laser. They could show a down-regulated production of inflammatory and fibrogenic mediators (e.g. TGF-β1, IL-1β, TNF-α, COX-2), and reduced collagen (COL)-1A1 and - 3A1) expression.

Lou et al. (145) recently demonstrated that low-level laser therapy (LLLT) increased *in vitro* proliferation and migration of human VF epithelial cells and altered expression of wound healing-associated genes (e.g. IL-6 and 10). Zhang et al. (146) described the positive effect of photodynamic therapy (PDT), a treatment using a diode laser at 635 nm, on cytokine-stimulated human VFF *in vitro*. They could show a possible anti-fibrotic effect by changed expression of wound healing-associated genes (e.g. TGF-β1, α-SMA, IL-6). Lou et al. (147) demonstrated similar effects in injured rabbit VF mucosa with decreased amounts of COL and higher levels of HA within the tissue.

The positive effect of cryotherapy, a localized application of extremely cold temperatures up to -40° for 15-20 seconds, was described by Gong et al. (148) using cytokine-stimulated hVFF *in vitro*. They revealed a reduced expression of scarring-associated genes (e.g. TGF-β1, IL-6, COX-2, α-SMA, MMP-1 and HAS-1). These results could partly be validated by Gong et al. (149) in injured rat VF mucosa. Furthermore, decreased amounts of COL and higher levels of HA within the tissue were detected.

1.5.4.3. Injection laryngoplasty

Currently, injection laryngoplasty represents the most common and clinically appropriate treatment of scarred VF besides medialization thyroplasty, frequently dealing with limitations including biocompatibility of materials, immunogenic reaction, restoration of vibratory characteristics, degradation and resorption of augmented materials (138,150,151). Among others, steroids (152,153), collagen (154,155), polytetrafluoroethylene (Teflon) (156,157), autologous fat (158–160) and HA (161,162) have been used. Recently, alternative substances with appropriate structure characteristics, chemical composition and biocompatibility have been employed for addressing VF scarring (138). Some specific advanced materials used for injection or implantation are delineated below.

1.5.4.3.1. Hyaluronic-acid-based materials

As native hyaluronic acid (HA) showed a rapid degradation profile after injection into the VF (163,164), several chemical modifications were generated. Hallén et al. (165) proposed the divinyl sulfone crosslinked HA hydrogel Hylan-B in the treatment of VF

insufficiency due to its non-inflammatory and biocompatible effects after injection into rabbit VF. Hertegard et al. (156) compared injection of Teflon, cross-linked collagen (Zyplast) and Hylan-B using rabbit VF. They could show the lowest dynamic viscosity similar to non-injected VF for Hylan-B. This corresponded to long-term results from Dahlqvist et al. (157).

In order to improve material flexibility and tunable gel properties, a disulfide cross-linked strategy was developed by Shu et al. (166). They coupled HA with dithiobis(propanoid dihydrazide) (DTPH) and reduced it with dithiothreitol (DTT). Obtained HA-DTPH enabled *in vitro* encapsulation of murine fibroblasts (L-929) and supported cell proliferation and viability. Liu et al. (167) transplanted HA-DTPH biofilms into the subcutaneous flank and peritoneal cavity in rats and revealed a very mild tissue reaction after 42 days.

To promote faster gelation (< nine minutes), HA-DTPH was combined with the synthetic polymer polyethylene glycol diacrylate (PEGDA) from Zheng Shu et al. (168). They revealed an increased cell proliferation of human tracheal scar fibroblasts (T31) encapsulated in HA-DTPH-PEGDA hydrogels *in vitro*. They could further show no evidence of biological incompatibility eight weeks after subcutaneous implantation of cell-containing hydrogels into mice flanks and encapsulated fibroblasts were evaluated to maintain their phenotype and secrete extracellular cytokines. Liao et al. (169) studied the effects of mesh size and the initial scaffold elastic modulus on ECM production of porcine VFF encapsulated in PEGDA hydrogels. Material properties, including mesh size, degradation rate, bioactivity and mechanical properties of the used scaffold allowed controlled and systematical modification for the experiments.

In order to reduce the degradation rate and alter viscosity, a new class of HA derivative, Carbylan-S, was generated through modification of HA via carbodiimide-mediated hydrazine. Hansen et al. (170) crosslinked this derivative with PEGDA (Carbylon-SX hydrogel) and injected it in rabbit VF. They could show improved biomechanical properties of viscosity and elasticity for Carbylan-SX-treated VF compared to simultaneously tested HA-DTPH-PEGDA and a lower fibrotic formation after three weeks.

Carbylan-GSX, a cross-linked polymer of Carbylan-S, PEGDA and the thiolated derivative of 3,3´-dithiolbis(propanoic hydrazide)-modified gelatin (Gtn-DTPH), were

generated to improve cell attachment to form stable viscoelastic gels. Chen et al. (171) could show an enhancement of TNF-α-induced remodeling of the lamina propria and potential acceleration of wound healing using immortalized human VFF cultured in three-dimensional Carbylan-GSX hydrogels compared to polystyrene-treated VFF with different concentrations of TNF-α. Positive effects of Carbylan-GSX with a gelatin concentration of 5 % were evaluated by Duflo et al. (172) using a rabbit model. They measured lower viscous properties and elastic shear moduli values and lower expression levels of fibrosis-related genes in Carbylan-GSX treated VF compared to saline-injection six months after treatment.

Microgels containing hydrazide-modified HA (HAADH) and aldehyde-functionalized HA (HAALD), crosslinked with other polymers to form doubly crosslinked networks (DXN) enhanced the surface-to-volume ratio to generate tunable degradation and mechanical properties (173–175). Coppoolse et al. (176) injected HA-gelatin-based microgels in scarred rat VF five days after surgery and revealed no induction of inflammatory or rejection response, indicating its biocompatibility.

1.5.4.3.2. Synthetic polymer materials

Injection of polyethylene glycol (PEG) 30 hydrogel in canine VF was performed by Karajanagi et al. (177). They found no evidence of an inflammatory response and minimal time-dependent resorption of the injected material at the injection site after four months. No impact on normal vibration, amplitude and phonation threshold pressure compared to the non-injected site was evaluated.

Kwon et al. (178) tested Pluronic F127-embedded polycaprolactone (PCL) in rabbit VF. They could show an improvement of asymmetric VF movement and integration into the tissue without induction of inflammatory response indicating its biocompatibility. Another study of Kwon et al. (151) compared injected Pluronic F127/PCL with calcium hydroxylapatite (CaHA). They found a significant reduction of injected CaHA after one week contrary to Pluronic 127/PCL which appeared not to decrease after one year. Furthermore, viscoelastic properties of Pluronic 127/PCL and glottal closure were better restored without inflammation or granuloma formation.

Another synthetic polymer, poly(lactic-co-glycolic acid) (PLGA) combined with Pluronic F127 was evaluated by Lee et al. (179) in rabbit VF. They did not reveal any significant

inflammatory tissue reaction after eight weeks resulting in a regular and symmetric VF movement.

1.5.4.3.3. Growth factors

Hepatocyte growth factor (HGF) (180–182) and basic fibroblast growth factor (bFGF) (183–185) have shown some potential properties in restoring VF scars using several *in vitro* cell culture as well as *in vivo* animal models. For both, among others, increased levels of HA, a decreased collagen deposition, and altered expression of fibrosis-related genes (e.g. HAS1, HAS3, TGF-β1, HGF) could be observed.

Hirano et al. (186) described significant improvements in the Voice Handicap Index (VHI)-10, GRABAS (grade, roughness, breathiness, asthenia, strain) scale, and vibratory amplitude of patients in phase I/II clinical trial using HGF injections in scarred VF after six months.

Ban et al. (187) described significant improvements in subjective parameters (GRABAS scale, VHI-10, mucosal wave grade, glottic closure) after three months in a prospective clinical trial using FGF injections in scarred VF.

1.5.4.3.4. Stromal cells

Svensson et al. (188) injected human mesenchymal stromal cells (MSC) into scarred rabbit VF. After ten weeks, they could show improved biomechanical properties of viscosity and elastic shear modulus and a reduced thickness of the lamina propria. Nagubothu et al. (189) demonstrated that injected MSC reduced inflammation response in scarred rabbit VF due to an altered expression of inflammatory-related genes (e.g. IL-1β and IL-8). They further evaluated a more organized collagen matrix within the tissue.

An *in vitro* co-culture model of isolated cytokine-treated rat VFF, MSC and adipose-derived stromal cells (ASC) from Hiwatashi et al. (190) showed an altered expression of scarring-associated genes (e.g. TGF-β1, α-SMA, COL I and III) for both used cells after 24 hours. Using an *in vivo* model, Hiwatashi et al. (191) used atelocollagen scaffolds containing either MSC or ASC for implantation in scarred dog VF and concluded that ASC showed more potential to decrease collagen deposition and increase HA within the scarred tissue.

Injection of autologous ASC mixed in atelocollagen in dog VF was performed by Lee et al. (192). Injury was performed four days after injection and they could reveal less atrophy and fewer morphological irregularities after 24 weeks in the ASC-treated VF tissues.

A cell-based outer VF replacement (COVR), consistent of rabbit ASC within a three-dimensional fibrin gel, was generated by Long (193) and transplanted into scarred rabbit VF. After one month, an improved glottis closure and furthermore a regular and symmetric VF movement could be revealed.

Recently, Mattei et al. (194) performed a prospective, non-randomized controlled clinical trial using subepithelial injections of autologous adipose-derived stromal vascular fraction (SVF), a heterogeneous population of MSC or ASC, fibroblasts, leukocytes, endothelial cells, progenitors, and pericytes (195). After one year, encouraging improvements in the VHI-10 and a clinically meaningful improvement of roughness could be observed.

1.5.4.4. Gene therapy

The receptor-activated or pathway-restricted Smad3 protein, critical to TGF-β signaling, is described as a potential target for small interfering RNA (siRNA)-based therapeutics (196,197). Paul et al. (196) and Branski et al. (197) revealed a decreased TGF-β-mediated expression of collagen and collagen contraction, respectively, using Smad3-siRNA-transfected human VFF cells (HVOX) *in vitro*. Kraja et al. (198) used the synthetic peptidomimetic oligomer lipitoid as a delivery carrier molecule for effective knock-down of Smad3 expression in HVOX cells and Hiwatashi et al. (199) further improved these results in *vivo* in rabbits.

1.6. Current experimental approaches in laryngeal research

1.6.1. Animal models

Animal models represent an alternative opportunity to systematically study VF function and properties in health, disease, and injury. As mentioned in previous sections, fundamental knowledge in the field of laryngology, especially in the context of VF scarring could be improved by them. Aside from the fact that animal experiments

generally should be tried to kept at a minimum, commonly used species include canine, pig, sheep, rabbit, rat and mouse (138).
Nevertheless, selection of the most appropriate animal depends on differences in research questions, methodological approaches and practical considerations including animal size, available facilities and funding resources to purchase and maintain the animals during the studies. Furthermore, information about physical tissue characteristics including size, shape, structure, organization and relative abundance of ECM components and biomechanical properties in their vibratory behavior comparable to human VF are required (200). Various physiological differences among the species compared to humans and its resulting confined possibility to extrapolate the findings may further constitute an important limitation in the use of animal models.

A widely used model has been the **canine** larynx, employed, among others, in studies of laryngeal muscle physiology (201–206), evaluation and simulation of pre-clinical approaches (207–211) and VF scarring (212–214). Rousseau et al. (215) suggested the canine model as a relevant model for VF scarring due to the amount of tissue that can be provided, the size and composition of the lamina propria and its ability to phonate. Oscillation frequency ranges and amplitudes were measured to be most similar to that of humans (41,216,217). Alipour et al. (217) validated averaged subglottal pressure and sound pressure levels to be close to the corresponding values of humans, whereas averaged phonation threshold pressure was higher in dogs. Elastic behavior and stiffness of canine VF differ from the measured ratios in humans. Histological analyses from Garrett et al. (218) showed a three-layered lamina propria with comparable structural components but a higher amount of COL within the superficial layer than in humans. Furthermore, a thin concentrated elastin band near the basement membrane zone within the superficial layer was detected, whereas human VF showed higher levels of ELN within the deeper layer of the lamina propria. Due to the large size of the canine larynx and described similarities, dogs represent a suitable, but comparatively cost-intensive animal model in laryngology.

Pigs were rarely used, among others, in studies of evaluation and simulation of pre-clinical approaches (218) and VF scarring (132,219). Woodson (220) described advantages using the porcine model to study VF scar due to its similar size and structure compared to human VF. Alipour et al. (217) showed that averaged values of

subglottal pressure, sound pressure and phonation threshold pressure levels were higher in porcine excised larynges than in humans. Elastic behavior in pig VF was validated to be most similar to the humans and stiffness of tissue was comparable to values determined in dogs but lower than in humans. Histological analyses from Garrett et al. (218) showed a two-layered structure of porcine VF in contrast to the three-layered structure in humans. Gill et al. (221) revealed porcine non-keratinized laryngeal epithelium and predominant ciliated, secretory and stratified epithelial cells similar to those found in the human larynx. Furthermore, a similar expression of intercellular junction complex structures (occludin, E-cadherin/catenin, zonula occludens 1) was evaluated. Due to the large size of the porcine larynx and described similarities, pigs represent a suitable, but comparatively cost-intensive animal model in laryngology.

Sheeps represent a widely used *in vivo* model in studies of laryngeal muscle physiology (222,223). Regner et al. (216) published, that oscillation frequency ranges in ovine excised larynges showed lower frequencies and amplitude was higher compared to the values of humans. Averaged values of subglottal pressure and phonation threshold pressure levels were higher whereas sound pressure levels were lower validated in ovine excised larynges than in humans.

Rabbits were rarely used in studies of evaluation and simulation of pre-clinical approaches (224), but represent a widely used model in the area of VF scarring (102,121,122,225,226). Histological analyses showed a three-layered composition of rabbit lamina propria similar to that of humans with a loosely arranged superficial layer, an intermediate layer with a higher amount of COL and a deeper layer mainly consistent of COL (102,156). Gill et al. (221) revealed porcine non-keratinized laryngeal epithelium and predominant ciliated, secretory and stratified epithelial cells similar to those found in the human larynx. Furthermore, a similar, but lower expression of intercellular junction complex structures (occludin, E-cadherin/catenin, zonula occludens 1) was evaluated. Despite the fact of the small animal size and resulting limitations in various experimental settings, rabbits represent a comparatively affordable animal model in laryngology.

Mice and rats were mainly used in studies of VF scarring (117,129–131,133,184,227–229). Tateya et al. (128,130) revealed the advantages using the rat model to study VF scar due to its small costs, short life span, quick healing process and similarities of lamina propria to that of humans. Yamashita et al. (131) described the mouse as a useful model for scar formation. Although no evidence of a distinct layered structure of the lamina propria of mice compared to that of humans could be confirmed, similarities in the abundance of eight ECM components and alterations in response to tissue injury were demonstrated. Gill et al. (221) revealed keratinized laryngeal epithelium in rats contrary to the non-keratinized type in the human larynx. Furthermore, a similar, but lower expression of intercellular junction complex structures (occludin, E-cadherin/catenin, zonula occludens 1) was evaluated. Due to the technical challenge to generate samples from such small animals, valid and reliable data of phonatory properties compared to human parameters have not been reported. Despite the fact of the very small animal size and resulting limitations in various experimental settings, mice and rats represent a comparatively inexpensive and useful animal model in laryngology.

1.6.2. *In vitro* cell culture models

Although homeostasis in VF is maintained by complex interactions between various cell types and ECM components (227,230), most *in vitro* research has been limited by the use of a single cell type. Most of the current *in vitro* applications are limited by the use of fibroblasts, the main cell type of the lamina propria, that produce the ECM and thereby substantially determine the unique tissue characteristics (231).

Branco et al. (232) revealed isolated human VFF treated with the pro-fibrotic growth factor TGF-β1 as an applicable *in vitro* model due to its evaluated similarities in phenotypic myofibroblast-transdifferentiated characteristics compared to native scarred VFF. Recently, our group (Graupp et al. (182)) characterized an innovative laryngeal fibrogenesis model using TGF-β1-stimulated human VFF based on the principle of macromolecular crowding.

Nevertheless, to overcome these limitations, especially in the area of VF scarring, researchers focused on the generation of three-dimensional multi-cellular models over

the last years. Some of these specific advanced models, partly tested *in vivo* in animals to use for VF implantation, are delineated below.

Walimbe et al. (233) assembled a scaffold-free *in vitro* co-culture consistent of immortalized human VFF and primary bronchial/tracheal epithelial cells and induced it with TGF-β1 into a fibrotic model.

Yamaguchi et al. (234) embedded isolated porcine VFF in a Type I collagen solution within nitrocellulose membrane inserts. Resuspended epithelial cell suspension, derived after protease digestion of porcine VF tissue, were poured on the assembled fibroblast-collagen scaffold. Air-liquid-interface (ALI) culture condition was started after three days. Within ten days of cultivation, they could show the assembly of a multilayered epithelium.

Leydon et al. (235) and Lungova et al. (236) generated constructs of Type I collagen-embedded human VFF (cell line 21T) and above seeded isolated human embryogenic stem cell (hESC)-derived simple epithelial cells under ALI culture conditions. After three weeks, they revealed the assembly of a stratified, differentiated epithelium as well as the presence of a basement membrane and intercellular junctions within the constructs.

Mizuta et al. (237) co-cultured isolated rabbit VF epithelial cells in collagen-coated cell culture inserts (1.0 µm pore size) with separately seeded mitomycin C-treated 3T3-feeder cells on collagen-coated plates below the inserts and measured the epithelial barrier function using the method of transepithelial electrical resistance (TEER).

Ling et al. (238) reassembled isolated human VFF and epithelial cells. Type I collagen-embedded fibroblasts were co-cultivated with above seeded isolated epithelial cells in cell culture inserts under ALI culture conditions. After 28 days of cultivation, they revealed the assembly of a stratified, differentiated epithelium as well as the presence of a basement membrane and intercellular junctions within the constructs and further revealed proteomic analyses. Epithelial barrier function was evaluated using TEER measurement. Furthermore, generated constructs were used *ex vivo* in canine larynges to conduct aerodynamic, high-speed digital imaging (HSDI) and acoustic data, and graft survival was documented *in vivo* in humanized mice.

Fukahori et al. (239) reassembled isolated fibroblasts and epithelial cells from canine buccal mucosal tissue. Type I collagen-embedded fibroblasts were co-cultivated with isolated epithelial cells on an oriented collagen sheet in cell culture inserts with a mitomycin C-treated 3T3 feeder layer. After two weeks of cultivation, they revealed an assembly of a multilayered stratified epithelium. Furthermore, fabricated constructs were transplanted *in vivo* into unilateral resected areas of canine VF. After two months, successful integration of the transplanted grafts with the surrounding tissue and a reassembling of morphological and functional characteristics similar to those of the uninjured VF mucosa were found.

1.6.3. Dynamic bioreactors

Generally, bioreactors are designed to achieve a controlled experimental environment to reproduce the phonation-induced biomechanical stimulation of VF tissue or cells *in vitro* as close as possible to the native VF properties.

Wolchok et al. (240) described a simple designed mechanically driven model using an attached electromagnetic voice coil actuator to produce vibrational stimuli on cells seeded in poly(dimethyl siloxane) (PDMS) sheet- or polyurethane foam-based cell culture plates.

Titze et al. (241) developed a more sophisticated, mechanically driven model that provided vibrational as well as tensile stresses. Scaffolds, consistent of isolated cells and porous Tecoflex substrates, could be stimulated at a frequency range of 20-200 Hz with strains up to 25 % by an actuator, connected to a series of levers, which were attached to a moveable vibrational bar. Axial scaffold elongation was provided by a coupled actuator containing manually adjustable threaded rods. Resulting mechanical agitation and fluid perturbation may have limited the achieved frequency ranges. Therefore, the number of moving components has to be minimized.

To overcome the limitations of mechanically-induced vibration, Farran et al. (242) designed a model that created vibration electromagnetically and transferred the energy aerodynamically. Pressure variations were induced by a speaker cone. The created acoustic wave was propagated through the air and transmitted to cell monolayers, seeded on flexible Type I collagen-coated silicone membranes that were placed within

T75 cell culture flasks (vibration stages). Laser Doppler Vibrometry (LDV) measurement at the driving frequency of 110 Hz revealed a maximum displacement, velocity, and acceleration of 19.7 µm, 13.7 mm/s, and 9,43 m/s^2, respectively, at the center of the flexible membranes. Although frequency ranges from 0 to 400 Hz, tensile and compressive stresses (membrane displacement 30 µm, strain level 0.047 %) could be achieved with this model, *in situ* visualization of vibration stages on a standard microscope was not possible and generated pre-strain of silicone membrane was not controllable during device assembly.

Gaston et al. (243) designed a bioreactor that provided vibrational and tensile stress as well as an dynamic angle change. Synthetic strips, consistent of isolated cells and porous fibronectin-coated Tecoflex substrates, were pairwise mounted in a T150 cell culture flask and attached to the vibration platform at one end, and to an aluminum scissor bar at the other end. The sinusoidal vibration signal was produced by a wave-form generator, amplified by a power amplifier and induced by a linear voice coil actuator. Activated linear actuator caused a horizontal translation resulting in a strip contact similar to *in vivo* movement. Stretch was induced by linear stepper motors and an angle change varying from 0 – 39 degrees was induced by mounted rotatory stepper motors, both controlled by computer-based software. Frequency ranges of 0 – 2727 Hz could be achieved with this model device.

Zerdoum et al. (244) designed a bioreactor consisting of custom-made silicone membranes with inserted fibrous poly(ε-caprolactone)-cell scaffolds between a pair of acrylic blocks. Sinusoidal vibration was generated electromagnetically by a speaker and the air between the bottom of the silicone membrane and the underneath mounted mini-woofer was driven into oscillation. LDV measurement at the driving frequency of 200 Hz revealed a displacement, velocity, and acceleration of 40 µm, 52 mm/s, and 66 m/s^2, respectively, at the center of the silicone membranes.

Kim et al. (245) designed a bioreactor containing commercially-available cell culture plates with flexible Type I collagen-covered membranes. Sinusoidal vibrational signals, generated by a generator, were passed through a stereo splitter and mechanically transferred to the cell monolayers by small linear actuators that are directly attached to the membranes. LDV measurement at the driving frequency of 205 Hz revealed a

maximum displacement, velocity, and acceleration of 19.14 µm, 24.6 mm/s, and 31.7 m/s^2, respectively, at the center of the flexible membranes. This model device allowed *in situ* visualization of cellular morphology.

So far, Latifi et al. (25) developed the closest approximation to the complex structure of the human larynx, namely, a flow perfusion bioreactor. They used synthetic replicas of VF, consisting of human VFF, gelatin, hyaluronic acid, and a polyethylene glycol cross-linker, within a silicone body which were placed in lateral contact. Longitudinal stretch was achieved through two sets of bolts and cell culture medium was perfused through a customized secondary flow loop within the scaffold. Phonation was delivered by a connected variable speed centrifugal air blower. Tested reactor frequency ranged from 0.5 – 100 Hz. This model device mimicked the airflow-induced biomechanical stimulation including collisions between the folds and the associated wall pressure changes.

Recently, our group (Kirsch et al. (246)) designed a bioreactor containing a loudspeaker mounted into a custom-made polyoxymethylene (POM) housing for fixation of commercially-available cell culture plates with flexible pronectin-coated membranes. Generated stimulation sound files were exported from a mobile audio player over an audio power amplifier to the loudspeaker to stimulate membranes directly via sound waves. Tested reactor frequency ranged from 50 – 2500 Hz. LDV measurement at the driving frequency of 55 Hz revealed a membrane deflection of ~700 µm at the center of the flexible membranes. This model device enabled us to apply various vibration frequencies and patterns due to the use of custom-designed sound files but reveals limitations by its two-dimensional nature.

1.7. Thesis objectives

Cell culture is a valuable, indispensable tool for controlled biomedical research enabling us to gain a better insight into the cellular and molecular mechanisms underlying VF function in health, disease, and injury. To date, cultures of VFF are applied in basic research (247–250), permitting significant advances in the understanding of disease processes (88,134,232), effective therapeutical strategies (251), and tissue engineering (248,252,253). Regarding the complex and multilayered microstructure of native VF, its mechanical versatility during sound production and the biophysical microenvironment, enhancement of traditional two-dimensional and existing three-dimensional *in vitro* model systems has to be established. Therefore, the aim of this thesis was to design possible strategies to overcome the above-mentioned limitations, develop and apply enhanced cell culture models *in vitro*.

Based on previous work of the research group of Prof. Markus Gugatschka (Laryngo Tracheal Tissue Engineering Graz, LTTEG) in the isolation, *in vitro* cultivation and cryopreservation procedures of near primary human VFF, a reproducible, stable procedure to gain epithelial cells out of human oral mucosa had to be established. Furthermore, these cells were used to bioengineer three-dimensional constructs with VFF under organotypic conditions *in vitro*. Focused to generate a highly comparable state to the native VF, these constructs could be provided as a possible tool to identify and study the underlying physiological and pathophysiological molecular processes in the field of VF research.

Taking into consideration the unique vibratory character of the human VF, several models of dynamic bioreactors have been engineered and published by others (25,240–245), and recently by the research group LTTEG (246). This validated novel phonomimetic bioreactor was used to explore the underlying molecular mechanisms of altered gene and protein expression due to the combination of vibration and several external stimuli *in vitro*.

2. Material and methods

The experiments for this work were performed at the Center for Medical Research (CMF) of the Medical University Graz using the following methods and the referenced materials.

2.1. Primary cell culture of human vocal fold fibroblasts (hVFF)

2.1.1. Cell isolation procedure

A protocol for human tissue processing including primary laryngeal cell cultures for hVFF was successfully established by the working group (254). Human VF tissue samples were collected with approval of the local ethics committee (approval number 27-396 ex 14/15). All data were anonymized, stored and kept separately according to the regulations of the local ethics committee.

In detail, tissue pieces of VF were collected in decontamination medium (DM) consisting of Dulbecco´s Modified Eagle´s Medium (DMEM, 4.5 g/L glucose; Sigma Aldrich, Vienna Austria; Prod.No.D5796) supplemented with 1 % Antibiotic-Antimycotic solution (Gibco, Thermo Fisher Scientific, Waltham, Massachusetts, USA; Prod.No.15240062). and 100 µg/ml Normocin (Invivogen, San Diego, California, USA; Prod.No.ant-nr-1), and immediately decontaminated for ten minutes in fresh DM. Then, small parts of the decontaminated tissue were cut off with scissors and carefully transferred into wells of a 12-well plate (Greiner Bio One, Frickenhausen, Germany; Prod.No.665180). Cultivation of cells was done in fibroblast-specific growth medium (fGM) consisting of DMEM enriched with 23 % Ham´s F-12 Nutrient Mix (Thermo Scientific; Prod.No.21765-029), 1 % Normocin, 5 % fetal bovine serum (FBS; Biowest, Nuaillé, France; Prod.No.S181B), 1 % Insulin-Transferrin-Selenium (ITS-G; Thermo Scientific; Prod.No.41400-045), 0.2 µM 3,3´,5-Triiodo-L-thyronine sodium salt (Prod.No.T6397), 0.1 µg/ml Insulin-like Growth Factor-I-human (IGF; Prod.No.I3769) and 0.0125 µg/ml Fibroblast Growth Factor-Basic human (FGF; Prod.No.F029; all Sigma Aldrich) under standard cell culture conditions (5 % CO_2, 37°C, humidified) with partial medium change every two to three days depending on the outgrowth of cells from the tissue.

2.1.2. Passaging of cells

Passaging of the adherent growing cells was dependent on the density of confluence in a ratio of 1:2 to 1:4. For that, the old medium was removed and cells were washed with phosphate buffered saline (PBS; Gibco; Prod.No.14190144) twice. To detach cells from the dish, Trypsin/EDTA 0.25 % (20 µl/cm^2; Thermo Fisher Scientific; Prod.No.25200056) was added. Cell culture dish was gently swayed to cover the whole bottom of the dish with Trypsin/EDTA solution and then incubated for three minutes at 37°C. After controlling the detachment under the microscope, prewarmed fGM was carefully added to cells. According to the passaging ratio, the appropriate volume of cell suspension was transferred into new dishes and further cultivated under standard cell culture conditions with partial medium change twice a week.

2.1.3. Freezing of cells

Cells were freezed when they reached a confluence of about 80-90 %. For that, cell trypsinization was performed as mentioned above. After centrifugation, the supernatant was decanted and the cell pellet was resuspended in FBS to a final volume of 900 µl per cryovial. The suspension was added to prepared sterile cryovials containing 100 µl dimethylsulfoxid (DMSO; Sigma Aldrich; Prod.No.D2650). Vials were quickly placed on ice and then stored in a -80°C freezer overnight. The following day, vials were transferred to liquid nitrogen tanks for long-term storage at -190°C.

2.1.4. Thawing of cells

To thaw, frozen vials were held in 37°C water bath for few minutes. Then, the cell suspension was diluted with 10 ml of SM and centrifuged at 170 x g for seven minutes at 23°C. Supernatant was decanted, the cell pellet was resuspended in pre-warmed SM and seeded in a T25 cell culture flask (Greiner Bio One; Prod.No.690160). Cultivation was performed under standard cell culture conditions with medium change after 24 hours, followed by partial medium change twice a week.

2.2. Primary cell culture of human oral mucosa epithelial cells (hOMEC)

2.2.1. Cell isolation procedure

For isolation of epithelial cells, previously published protocols (238,239,255,256) were initially used to establish the procedure. Human tissue samples were collected during routine laryngeal surgeries with the confirmed consent of patients and approval of the local ethics committee (approval number 27-396 ex 14/15) or from cadavers during autopsy (Diagnostic and Research Institute of Pathology at the Medical University of Graz, approval number 29-036 ex 16/17), within 12 hours after death of patients without any intubation. In detail, tissue pieces of oral mucosa (Ø ~6 mm during laryngeal surgeries and Ø ~2 cm during autopsy) were collected in DM and immediately decontaminated for ten minutes in fresh DM. Donor demographic is listed in section 3.1.

As cell culture dishes for the cultivation procedure are recommended to be coated, different solutions, combinations of different solutions and concentrations were tested and described in detail within the following sections.

Test 1: Rat tail collagen, Type I (Thermo Fisher Scientific; Prod.No.A1048301) was used according to the manufacturer´s instructions. In detail, wells of a 12-well plate were incubated with 1 ml of collagen solution (5 µg/cm^2) for three hours at 37°C. After incubation, the coating solution was discarded and wells were washed twice with PBS. The decontaminated tissue pieces were digested in a Dispase solution (1.2 U/ml; Thermo Fisher Scientific; Prod.No.17105041) at 37°C for 90 minutes. The epithelial layer was separated carefully from the underlying stroma and small parts were cut off with scissors and transferred into pre-coated wells. After drying for some minutes, 1 ml of epithelial cell-specific growth medium (eGM) consisting of DMEM, 22.5 % Ham´s F-12 supplement, 1 % Normocin, 4 % FBS, 5 µg/ml ITS-G, 10 ng/ml 3,3´,5-Triiodo-L-thyronine sodium salt, 10 ng/ml epidermal growth factor (EGF; Prod.No.E9644), 0.5 µg/ml epinephrine hydrochloride (Prod.No.E4642), 0.5 µg/ml hydrocortisone (Prod.No.H4001), 0.1 ng/ml retinoic acid (Prod.No.R2625) and 1.5 µg/ml albumin from human serum (Prod.No.A1887;all Sigma Aldrich) was added to each well cautiously to

prevent the piece from detaching from the well bottom. Cells were cultivated under standard cell culture conditions with partial medium change every two to three days.

Test 2: Rat tail collagen, Type I (1 mg/ml) was used as coating solution in wells of a 12-well plate. Incubation was performed for two hours at 37°C. After removing the coating solution, the wells were dried shortly without washing steps at 37°C and decontaminated tissue pieces were treated as described in Test 1. Cells were cultivated under standard cell culture conditions with partial medium change of eGM every two to three days.

Test 3: Rat tail collagen, Type I (30 µg/ml) + Fibronectin (10 µg/ml; Sigma Aldrich; Prod.No.F2518) + FBS (10 µg/ml) were used as coating solution in wells of a 12-well plate. Incubation was performed for two hours at 37°C. After removing the coating solution, the wells were dried shortly without washing steps at 37°C. Treatment of decontaminated tissue pieces and all forthcoming steps were performed as described in Test 1.

Test 4: Rat tail collagen, Type I (30 µg/ml) + Fibronectin (10 µg/ml) were used as coating solution in wells of a 12-well plate. Incubation was performed for two hours at 37°C. After removing the coating solution, the wells were dried shortly without washing steps at 37°C. Treatment of decontaminated tissue pieces and all forthcoming steps were performed as described in Test 1.

Test 5: Rat tail collagen, Type I (10 µg/cm^2) was used as coating solution in wells of a 12-well plate. Incubation was performed for two hours at 37°C. After removing the coating solution, the wells were dried shortly without washing steps at 37°C. Treatment of decontaminated tissue pieces and all forthcoming steps were performed as described in Test 1.

Test 6: Rat tail collagen, Type I (15 µg/cm^2) was used as coating solution in wells of a 12-well plate. Incubation was performed for two hours at 37°C. After removing the coating solution, the wells were dried shortly without washing steps at 37°C. Treatment of decontaminated tissue pieces and all forthcoming steps were performed as described in Test 1.

Test 7: Ready-to-use six-well multidish plates pre-coated with collagen (Thermo Fisher Scientific; Prod.No.152034) were used. Decontaminated tissue pieces were treated as described in Test 1 and ready-to-use EpiLife epithelial cell-specific growth medium (Thermo Fisher Scientific; Prod.No.M-EPI-500-CA) was used for cultivation under standard cell culture conditions with partial medium change every two to three days.

Test 8: Human collagen Type IV (6 µg/ml; Sigma Aldrich; Prod.No.C6745) was used as coating solution in wells of a 12-well plate. Incubation was performed for two hours at 37°C. After removing the coating solution, the wells were dried shortly without washing steps at 37°C. Treatment of decontaminated tissue pieces and all forthcoming steps were performed as described in Test 1.

Test 9: Human collagen Type IV (10 µg/ml) was used as coating solution in wells of a 12-well plate. Incubation was performed for two hours at 37°C. After removing the coating solution, the wells were dried shortly without washing steps at 37°C. Treatment of decontaminated tissue pieces and all forthcoming steps were performed as described in Test 1.

Test 10: PureCol (30 µg/ml; Sigma Aldrich; Prod.No.5006) was used as coating solution in wells of a 12-well plate. Incubation was performed for two hours at 37°C. After removing the coating solution, the wells were dried shortly without washing steps at 37°C. Treatment of decontaminated tissue pieces and all forthcoming steps were performed as described in Test 1.

Test 11: Cultivation of immortalized hVFF in wells of a six-well plate was combined with collagen pre-coated inserts (Corning Transwell Collagen; Sigma Aldrich; Prod.No.CLS3491). In detail, hVFF were seeded in wells (1 x 10^5 cells/well) using SM two days before start of the isolation. On the day of isolation, the medium was removed and fresh SM was added to the wells and pre-coated inserts were placed within the wells. Tissue preparation was performed as described in Test 1 and small parts were transferred into the inserts. After drying for some minutes, 800 µl of EpiLife medium was added to the inserts and cells were cultivated under standard cell culture conditions with partial medium change of SM in the wells and EpiLife medium in the inserts every two to three days.

Test 12: Cultivation of immortalized hVFF in wells of a six-well plate was combined with uncoated inserts (Corning Transwell, polyester membrane, 0.4 µm pore size; Sigma Aldrich; Prod.No.3450). All forthcoming steps were performed as described in Test 11.

Test 13: Isolation procedure was tested as recommended by CELLnTec Advanced Cell Systems, “Oral Epithelium Isolation”) (257,258), in uncoated 12-well plates. In detail, the decontaminated tissue piece was digested in a Dispase solution (2.4 U/ml) at 4°C for 15 hours. After incubation, tissue piece was washed in a petri-dish with epithelial cell-specific medium CnT-PR (CellnTec Advanced Cell Systems AG, Bern, Switzerland; Prod.No.CnT-PR) and the epithelial layer was separated carefully from the underlying stroma and digested in an Accutase solution (500-720 U/ml; Sigma Aldrich; Prod.No.A6964) for 10-15 minutes at 37°C. Thereafter. the solution was pipetted up and down carefully and resulting single-cell solution was transferred into a 15 ml Falcon and diluted with 6 ml of CnT-PR medium. The sample was centrifuged at 180 x g for five minutes at room temperature, the supernatant was discarded and the cell pellet was diluted in fresh CnT-PR medium supplemented with IsoBoost (50 µl/50 ml; CellnTec Advancel Cell Systems AG; Prod.No.CnT-ISO-50,) and transferred into uncoated wells of a 12-well plate (1 ml/well). Cell cultivation was performed under standard cell culture conditions using CnT-PR medium supplemented with IsoBoost for five days with daily medium change, followed by a change to CnT-PR medium without IsoBoost with partial medium change every two to three days.

2.2.2. Passaging of cells

The adherent growing cells were passaged depending on the density of confluence in a ratio of 1:2. The old medium was removed and cells were washed with PBS twice. To detach cells from the dish, Accutase solution (50 µl/cm^2) was added. Cell culture dish was gently swayed to cover the whole bottom of the dish with the solution and then incubated for 12-15 minutes at 37°C. After controlling the detachment under the microscope, prewarmed CnT-PR medium was carefully added to cells and resulting single-cell solution was transferred into a 15 ml Falcon and diluted with 2.5 x volume of CnT-PR medium. Sample was centrifuged at 180 x g for five minutes at room temperature, the supernatant was discarded, the cell pellet was diluted in fresh CnT-

PR medium and transferred into new dishes. Cells were cultivated under standard cell culture conditions with partial medium change twice a week.

2.2.3. Freezing of cells

When cells reached a confluence of about 80-90 %, they were freezed. The cells were first detached from the dishes with Accutase as mentioned above. After centrifugation, the supernatant was decanted and the cell pellet was resuspended in FBS to get a final volume of 900 µl for each cryovial. The suspension was added to prepared sterile cryovials containing 100 µl DMSO. Vials were quickly placed on ice and then stored in a -80°C freezer overnight. The following day, vials were transferred to liquid nitrogen tanks for long-term storage at -190°C.

2.2.4. Thawing of cells

A T25 cell culture flask (per cryovial) was equilibrated with 5 ml of CnT-PR medium at room temperature ten minutes before thawing the cells. Frozen vials were held in 37°C water bath for few minutes. Cell suspension was transferred into the flask and cultivated under standard cell culture conditions with medium change after 24 hours, followed by partial medium change twice a week.

2.3. Quantitative polymerase chain reaction (qPCR) for cell-specific characterization

In order to evaluate the purity of the isolated cells and to characterize them, a quantitative polymerase chain reaction (qPCR) of cell-type-specific genes was performed: (Von Willebrand factor (VWF) as endothelial cell marker, actinin alpha 3 (ACTN3) as skeletal muscle cell marker, cytokeratin (CK) 13 and CK14 and cadherin 1 (CDH1) as epithelial cell markers, and vimentin (VIM) and Thy-1 cell surface antigen (THY1) as fibroblast markers. Therefore, total RNA from cells (hVFF: n=1; hOMEC: n=3) and from native VF tissue samples (n=2, procedure described separately in section “Native VF tissue”) as reference set was isolated.

Native VF tissue samples were snap-frozen in liquid nitrogen in MagNa Lyser Green Beads (prefilled with 1.4 mm Ø ceramic beads; Roche, Vienna, Austria; Prod.No.03358941001). Then, 700 µl of QIAzol lysis reagent (Qiagen, Hilden, Germany; Prod.No.55109376) was added to each sample and homogenization was

performed using the MagNa Lyser instrument. For sufficient homogenization, three to five cycles of 20 seconds at 6500 rpm with intermitting one-minute cooling cycles were used.

Cells (hVFF, hOMEC) were seeded in cell-specific growth medium (1.5×10^3 cells/well) and cultivated with partial medium change twice a week. When cells reached a confluence of about 80-90 %, culture plates were transferred into the hood, old medium was aspirated and 700 µl of QIAzol lysis reagent was added to each well and pipetted up and down at least ten times.

RNA isolation of obtained cell lysates and homogenized VF tissue samples was performed with the miRNeasy Mini Kit (Qiagen; Prod.No.217004) according to the manufacturer´s instructions. In detail, 140 µl chloroform (Lactan, Graz, Austria; Prod.No.9065.5) was added to the samples. After vigorous shaking for 15 seconds, followed by a three-minute incubation at room temperature, samples were centrifuged at 13000 rpm for 15 minutes at 4°C. Thereafter, 300 µl of the colorless aqueous phase was transferred into new 1.5 ml tubes, 450 µl of ethanol (>99,8 %; Lactan; Prod.No.K928.4) was added and the solution was mixed thoroughly and pipetted onto the spin column, placed in 2 ml collection tubes. After centrifugation at 9000 rpm for 15 seconds at room temperature, the supernatant was discarded and 700 µl of RWT buffer was added to the spin column. Samples were centrifuged at 13000 rpm for 15 seconds at room temperature and the supernatant was discarded. This step was repeated twice using 500 µl RPE buffer per sample. Purified RNA was eluted in 30-50 µl RNase-free water through centrifugation at 10000 rpm for one minute at room temperature and total concentration was determined using the NanoDrop 2000c spectrophotometer (Thermo Fisher Scientific). Reverse transcription (RT) was perfomed using the QuantiTect Reverse Transcription Kit (Qiagen; Prod.No.205314) according to the manufacturer´s instructions.

The obtained cDNA samples were diluted with RNase-free water to gain a final concentration of 20 ng/µl and reverse transcription quantitative polymerase chain reaction (RT-qPCR) was performed in FrameStar 384 well reaction plates (4titude; Wotton, UK; Prod.No.4ti-0382). Each reaction was pipetted in triplicates consisting of 4 µl cDNA, 5 µl GoTaq Master-Mix (Promega, Mannheim, Germany; Prod.No.A6002) and 1 µl primer mix (forward and reverse primer sequences of used primers, at a final

concentration of 200 nM each are listed in Table 1). RT-qPCR runs were performed on the Light Cycler LC480 device (Roche) with the following program: denaturation at 95°C for two minutes, 45 cycles of ten seconds at 95°C and one minute at 60°C for amplification and ramping at 2.5°C per minute from 55°C to 95°C for melting curve analysis. C_T values were obtained by the AbsQuant/2nd Derivative Max method of the Light Cycler software. Values of technical triplicates were averaged and relative quantification of all mRNAs of interest was performed based on the $2^{(-\Delta\Delta CT)}$ method (259), with slight modifications: C_T values were normalized to the geometric mean of the C_T values of the internal reference genes beta-2 microglobulin (B2M) and ubiquitously expressed transcript protein (UXT).

Table 1. Sequences of used primers for RT-qPCR for cell-specific characterization

Gene symbol	**Forward primer**	**Reverse primer**
ACTN3 (actinin alpha 3)	CACACCAGCTGGAAGGATGG	TGTTCAGGTTTCCGATGGGG
B2M (beta-2 microglobulin)	AGGCTATCCAGCGTACTCCA	CGGATGGATGAAACCCAGACA
CDH1 (cadherin 1)	TGGTTCAGATCAAATCCAACAAAGA	CTGTCACCTTCAGCCATCCT
CK13 (cytokeratin 13)	TCAAGACACGTCTGGAGCAG	AAGTCAGACAGTGAGGGGTCT
CK14 (cytokeratin 14)	AGTCCCTACTTCAAGACCATTGAG	GGTTCAACTCTGTCTCATACTTGG
THY1 (Thy-1 cell surface antigen)	TCTCCTGCTAACAGTCTTGCA	CACGGGTCAGGCTGAACTCG
UXT (ubiquitously expressed transcript protein)	GCAGCGGGACTTGCGA	TAGCTTCCTGGAGTCGCTCA
VIM (vimentin)	GGACCAGCTAACCAACGACA	TCCTCCTGCAATTTCTCCCG
VWF (Von Willebrand factor)	CTCATCGCAGCAAAAGGAGC	ATGCTCATGCACTCCAGGTC

2.4. 3D cultivation of hVFF

The growth of hVFF embedded within a collagen matrix as part of the 3D co-cultivation construct was tested. In detail, immortalized hVFF (isolated from VF of a 21 year-old male donor (252), kindly provided by Prof. S. Thibeault, University of Wisconsin-Madison, USA) were cultured in standard medium (SM) consisting of DMEM supplemented with 1 % Antibiotic-Antimycotic solution. After detaching the cells with 0.25 % Trypsin/EDTA, cell number was determined using a hemocytometer and an appropriate number of cells was used to mix the matrix solution. The matrix consists of purified rat tail collagen, Type I and was prepared to a final concentration of 2.4 mg/ml according to the manufacturer´s instructions as described within the following sections. The calculation scheme is shown in Figure 1. Microscopic examination of the constructs was performed during the cultivation period.

$$Vt = Total\ volume\ of\ collagen\ gel\ desired$$

$$Volume\ of\ collagen\ needed\ [V1] = \frac{(Final\ conc.of\ collagen)\ x\ Total\ Volume\ (Vt)}{Initial\ conc.of\ collagen}$$

$$Volume\ of\ 10X\ PBS\ needed\ [V2] = \frac{Total\ Volume\ (Vt)}{10}$$

$$Volume\ of\ 1N\ NaOH\ needed\ [V3] = (V1)\ x\ 0.025$$

$$Volume\ of\ dH2O\ (cell\ suspension)\ needed\ [V4] = (Vt) - (V1 + V2 + V3)$$

Figure 1. Calculation scheme according to the manufacturer´s instructions for purified rat tail collagen, Type I.

Matrix test 1: hVFF (1 x 10^5 cells/ml; 0.5 ml/well) were embedded in wells of a 24-well plate (Thermo Fisher Scientific; Prod.No.142475) using rat tail collagen, Type I (2.4 mg/ml). Calculated volumes of 10X PBS (Lactan, Prod.No.1058.1) and 1N NaOH (Merck Millipore; Burlington, Massachusetts, USA; Prod.No.6498) were mixed in 1.5 ml tubes. The appropriate volume of cell suspension was calculated, centrifuged at 170 x g for seven minutes at room temperature and resuspended in the appropriate volume of SM. Then, the cell solution was carefully mixed with the appropriate volume of PBS-NaOH mixture, transferred to the collagen solution, slowly pipetted up and down and seeded into the wells. After polymerization at 37°C for 40 minutes, 300 µl of

SM was added to the wells and constructs were cultivated under standard cell culture conditions with partial medium change every two to three days. Microscopic examination of the constructs was performed during ten days of cultivation.

Matrix test 2: hVFF (1×10^5 cells/insert; 2 ml/insert) were embedded in six-well Transwell inserts (Corning Transwell, polyester membrane, 0.4 µm pore size; Sigma Aldrich; Prod.No.3450) using rat tail collagen, Type I (2.4 mg/ml). All steps were performed as described in matrix Test 1, with slight modifications. Polymerization was performed at 37°C for 90 minutes, after which 2 ml of SM were added to the wells and 1.5 ml were carefully added on the top of the matrix within the inserts. Plates were cultivated under standard cell culture conditions with partial medium change every two to three days. Microscopic examination of the constructs was performed during four days of cultivation.

Matrix test 3: hVFF were embedded in 12-well Transwell inserts (Corning Transwell, polyester membrane, 0.4 µm pore size; Sigma Aldrich; Prod.No.3460) in a total volume of 720 µl/insert using rat tail collagen, Type I (2.4 mg/ml). Different concentrations of hVFF per insert were seeded: 5×10^4 cells, 6×10^4 cells, 7×10^4 cells, 8×10^4 cells, 1×10^5 cells and 2×10^5 cells. All steps were performed as described in matrix Test 1, with slight modifications. Polymerization was performed for 45 minutes at 37°C. Thereafter, 1 ml of SM was added to the wells and 500 µl was carefully added on the top of the matrix within the inserts. Plates were cultivated under standard cell culture conditions with partial medium change every two to three days. Microscopic examination of the constructs was performed during 14 days of cultivation. Samples were then allocated to histological analysis (procedure described in section 2.7.1). The collagen-fibroblast matrix containing 2×10^5 cells were allocated to gene expression analysis (sample preparation, RNA-isolation and RT-qPCR procedures described in section 2.3, forward and reverse primer sequences of used primers are listed in Table 2).

Table 2. Sequences of used primers for RT-qPCR for collagen-fibroblast matrix characterization

Gene symbol	Forward primer	Reverse primer
ACTA2 (actin, alpha 2, smooth muscle)	CGTTACTACTGCTGAGCGTGA	GCCCATCAGGCAACTCGTAA
B2M (beta-2 microglobulin)	AGGCTATCCAGCGTACTCCA	CGGATGGATGAAACCCAGACA
COL1A1 (collagen I alpha 1)	GCAGACTGGCAACCTCAAGA	TGTGACTCGTGCAGCCATC
ELN (elastin)	GGTTCCAGGGGTTGTGTCA	GCTCCAACCCCGTAAGTAGG
FN1 (fibronectin)	CTGCAAGCCCATAGCTGAGA	GAAGTGCAAGTGATGCGTCC
HAS1 (hyaluronan synthase 1)	CTTCCTAAGCAGCCTGCGAT	TATATAGGCCTAGAGGACCGCTG
HAS2 (hyaluronan synthase 2)	ATGCTTGACCCAGCCTCATC	TTAAAATCTGGACATCTCCCCCAA
HAS3 (hyaluronan synthase 3)	ATCATGCAGAAGTGGGGAGG	GAGTCGCACACCTGGATGTA
ITGA2 (integrin subunit alpha 2)	GGGAAAGTGCATACAACACTGG	CATCAACCGGCAGGGAGAAT
ITGB1 (integrin subunit beta 1)	CCAAATGGGACACGGGTGAA	TTGCACGGGCAGTACTCATT
MMP1 (matrix metalloproteinase 1)	CACGCCAGATTTGCCAAGAG	GTTGTCCCGATGATCTCCCC
UXT (ubiquitously expressed transcript protein)	GCAGCGGGACTTGCGA	TAGCTTCCTGGAGTCGCTCA
TIMP1 (tissue inhibitor of metalloproteinase 1)	GGAATGCACAGTGTTTCCCTG	GGAAGCCCTTTTCAGAGCCT

2.5. 3D co-cultivation of hVFF and hOMEC

For the 3D co-cultivation (CC) of hVFF and hOMEC, a protocol was established according to a previous publication (238). Performed tests are described in detail within the following sections.

CC test 1: hVFF (6 x 10^4 cells/insert; 400 µl/insert) were embedded within a matrix consisting of rat tail collagen, Type I (2.4 mg/ml) as described in matrix Test 1 into the apical chamber of a 12-well Transwell insert (0.4 µm pore size) and left to polymerize at 37°C for 90 minutes. Then, SM was added to the apical and basolateral sides of the inserts and cultivation was done under standard cell culture conditions. Next day, hOMEC (2 x 10^4 cells/insert, 200 µl/insert) were seeded on top of the established fibroblast-collagen matrix. SM was added to the basolateral sides of the inserts, CnT-PR medium was added to the apical sides of the inserts and constructs were cultivated for additional ten days with partial medium change of the appropriate medium in both sides of the inserts twice a week under standard cell culture conditions. Thereafter, constructs were allocated to histological analysis.

CC test 2: Procedure was performed according to CC Test 1, with slight modifications. hVFF were embedded within the rat tail collagen, Type I matrix at a concentration of 2 x 10^5 cells/insert; 800 µl/insert and left to polymerize at 37°C for 45 minutes and hOMEC were seeded at a concentration of 4 x 10^5 cells/insert, 200 µl/insert. Next day, both media were partially changed and after additional 24 hours, CnT-PR medium was fully aspirated from the apical side of the inserts to create the so-called “air-liquid interface” (ALI). Constructs were cultivated for additional 12 days with partial medium change of SM in basolateral sides of the inserts twice a week under standard cell culture conditions. Thereafter, constructs were allocated to histological analysis.

CC test 3: Procedure was performed according to CC Test 2, with slight modifications. hVFF were seeded within the rat tail collagen, Type I matrix at a concentration of 2 x 10^5 cells/insert; 200 µl/insert, hOMEC were seeded at a concentration of 3.5 x 10^5 cells/insert, 100 µl/insert. Next day, ALI condition was started and constructs were cultivated for additional 12 days with partial medium change of a 1:1 mixture of SM and CnT-PR medium in basolateral sides of the inserts twice a week under

standard cell culture conditions. Thereafter, constructs were allocated to histological analysis.

CC test 4: Procedure was tested as recommended by CELLnTec Advanced Cell Systems (“Full Thickness Skin Models”). In detail, hVFF (5×10^4 cells/insert; 400 µl/insert) were seeded into a 12-well Transwell insert using fibroblast-specific medium CnT-PR-F (CELLnTec Advanced Cell Systems; Prod.No.CnT-PR-F). Cultivation was done for ten days under standard cell culture conditions with partial CnT-PR-F medium change twice a week. Then, hOMEC (1.2×10^4 cells/insert, 600 µl/insert) were seeded into the apical chamber of the inserts on top of the established fibroblast layer using a fully defined co-culture medium CnT-PR-FTAL (CeLLnTec Advanced Cell Systems; Prod.No.CnT-PR-FTAL). CnT-PR-FTAL was added to both sides of the inserts and constructs were cultivated for three days with medium change on day two. Then, sterilized plate spacers were placed on top of new cell culture plates and inserts were carefully transferred into new plates. ALI condition was started. Constructs were cultivated for additional 14 days with partial medium change of CnT-PR-FTAL medium in basolateral sides of the inserts twice a week under standard cell culture conditions. Thereafter, constructs were allocated to histological analysis.

CC test 5: Procedure was performed according to CC Tests 2 and 3, with slight modifications. hVFF were seeded within the rat tail collagen, Type I matrix at a concentration of 1×10^5 cells/insert; 720 µl/insert. Then, CnT-PR-F medium was added to both sides of the inserts and cultivation was done under standard cell culture conditions for ten days with partial medium change twice a week. hOMEC (2.3×10^5 cells/insert, 600 µl/insert) were seeded on top of the established fibroblast-collagen matrix. CnT-PR-FTAL was added to both sides of the inserts and constructs were cultivated for three days with medium change on day two. Sterilized plate spacers were placed on top of new cell culture plates and inserts were carefully transferred into new plates to start ALI condition. Constructs were cultivated for additional 21 days with partial medium change of CnT-PR-FTAL medium in basolateral sides of the inserts twice a week under standard cell culture conditions. Thereafter, constructs were allocated to histological analysis.

CC test 6: Procedure was performed according to CC Test 5, with slight modifications. hVFF were embedded within the rat tail collagen, Type I matrix at a concentration of 2 x 10^5 cells/insert; 720 µl/insert using SM. Cultivation was done under standard cell culture conditions for ten days with partial medium change twice a week. hOMEC (2.4 x 10^5 cells/insert, 600 µl/insert) were seeded on top of the established fibroblast-collagen matrix. CnT-PR-FTAL was added to both sides of the inserts and constructs were cultivated for four days with medium change on day two. Then, ALI condition with sterilized plate spacers was started in new plates and constructs were cultivated for additional 21 days with partial medium change of CnT-PR-FTAL medium in basolateral sides of the inserts twice a week under standard cell culture conditions (schematic illustration of the procedure is shown in Figure 2). Thereafter, constructs were allocated to histological analysis.

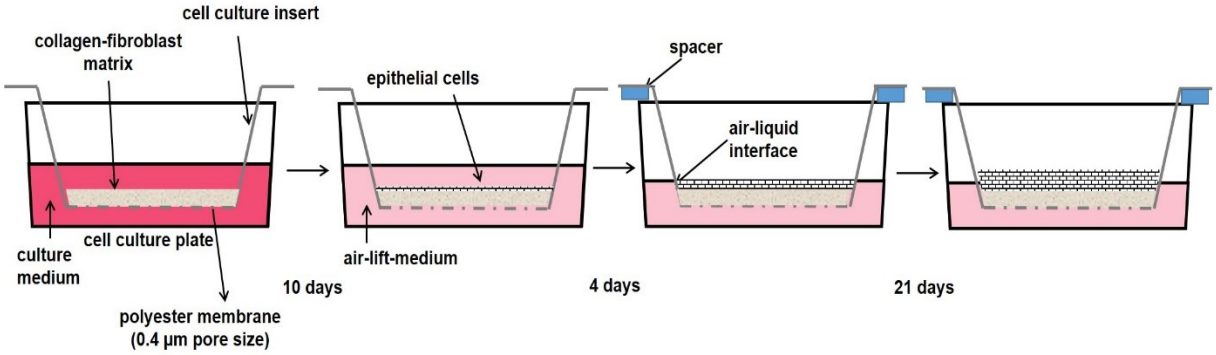

Figure 2. Schematic illustration of the 3D co-cultivation procedure

2.6. Native VF tissue

Native tissue from healthy VF was collected post mortem in collaboration with the Diagnostic and Research Institute of Pathology, Medical University of Graz (valid approval by the local ethics committee no. 29-036 ex 16/17). All data were anonymized, stored and kept separately according to the regulations of the local ethics committee (Donor demographic listed in Table 3). Tissue pieces were collected in DM and transferred to the cell culture laboratory at the ZMF to perform subsequent steps under sterile conditions. Sections of samples were stored at -80°C until further use for histological, gene expression and proteomic analysis (procedures described in sections 2.7.1; 2.7.3.2).

Table 3. Donor demographic of native VF samples

Sample ID	Age	Sex	Cause of death
93	49	female	hepatorenal syndrome
95	69	female	cardiac arrest
99	65	female	cardiac arrest
101	82	male	posterior infarction

2.7. Analysis

2.7.1. Histological analysis

For several histological analysis, the collagen-fibroblast matrix samples, 3D co-cultivation constructs and native VF tissue were fixed in 4 % paraformaldehyde (PFA; Gatt-Koller, Absam, Austria; Prod.No.403150922) for 24 hours, embedded in paraffin using the Tissue Tek VIP (Sakura Finetek USA, Torrance, California, USA) automated embedding machine and cut in 5 µm thick sections.

2.7.1.1. Hematoxylin and Eosin staining (H&E)

In oder to visualize fibroblast distribution and density within the samples, sections were stained with routine H&E staining according to the standard protocol. Briefly, slides were incubated at 65°C for 30 minutes to soak the paraffin. Then, slides were processed with descending alcohol series (2 x 5 min Xylol, 1 x 5 min 100 % EtOH, 1 x 5 min 90 % EtOH, 1 x 5 min 70 % EtOH, 1 x 5 min 50 % EtOH, 1 x 5 min ddH_2O) followed by two minutes incubation with hematoxylin, rinsing in hot running tap water for three minutes. Incubation with eosin solution was performed for two minutes. Then, slides were dehydrated shortly with ascending alcohol series (50 % EtOH, 70 % EtOH, 96 % EtOH, 100 % EtOH, Xylol) and airtight coverslipped.

2.7.1.2. Staining for cytokeratins CK AE1/AE3 and CK 5/6

To visualize the assembly of an epithelial surface layer within the constructs, sections were stained for validation of different epithelial cell-specific cytokeratins CK AE1/AE3 and CK 5/6 in cooperation with the Diagnostic and Research Institute of Pathology,

Medical University of Graz. Detailed automated protocols were performed by the group of Dr. Luka Brcic.

2.7.2. Immunohistochemical analysis

For immunohistochemical analysis, sections were treated according to the manufacturer´s instructions of the used antibodies to visualize the cellular components of the samples. Different concentrations of the antibodies, solutions for antigen retrieval and blocking of non-specific binding sites were tested to establish the staining procedures using sections of native VF tissue. For negative control, staining without primary antibody was performed in parallel for all used primary antibodies. Slides were analyzed on a Nikon A1R+ confocal microscope (Nikon, Tokyo, Japan). Detailed protocols of different stainings are described within the following sections.

2.7.2.1. Basal collagen, Type IV (COL IV)

To visualize the basement membrane within native VF tissue and a successful development of it within the constructs, sections were stained for basal collagen Type IV. In detail, paraffin sections were first deparaffinated at 60°C for 30 minutes and processed with descending alcohol series as mentioned above. Antigen retrieval was performed for 15 minutes at 37°C in a water bath using 0.1 % Proteinase (Sigma Aldrich; Prod.No.P5380), followed by two washing steps with PBS for two minutes each. Then, sections were blocked for non-specific binding sites in a humidified chamber for 45 minutes using a blocking solution (PBS, 0.3 % Triton-X-100 (Lactan; Prod.No.93433), 5 % goat serum (Biolabs, San Diego, California, USA; Prod.No.5425S).

Primary antibody (monoclonal mouse anti-human anti-Collagen Type IV, clone COL-94; Sigma Aldrich; Prod.No.C1926; tested concentrations 1:500; 1:1000; 1:2000) was incubated at 4°C overnight in a humidified chamber followed by three washing steps with PBS for ten minutes each. Incubation with secondary antibody (goat anti-mouse IgG, Alexa Fluor 594; Cell Signaling, Danvers, Massachusetts, USA; Prod.No.8889; 1:1000) was performed light-protected for one hour at room temperature. After three washing steps with PBS for ten minutes each, sections were counterstained with Hoechst (Thermo Fisher Scientific; Prod.No.H1399; 1:1000) light-protected for 15 minutes, further washed with PBS three times for ten minutes each, covered with

mounting medium (Dako, Santa Clara, California, USA; Prod.No.S3023) and coverslipped.

2.7.2.2. Vimentin (VIM)

To visualize the fibroblasts within native VF tissue and the constructs, sections were stained for the fibroblast-specific cytoplasmatic protein vimentin (VIM). In detail, paraffin sections were first deparaffinated and processed with descending alcohol series as mentioned before. Antigen retrieval was performed for 15 minutes at 37°C in a water bath using 0.1 % Proteinase, followed by two washing steps with PBS for two minutes each or for 30 minutes at 110°C in a decloaking chamber using Vector antigen unmasking solution (Szabo Scandic, Vienna, Austria; VECH-330), followed by washing with PBS for five minutes. Then, sections were blocked for non-specific binding sites in a humidified chamber for 45 minutes using a blocking solution.
Primary antibody (monoclonal anti-Vimentin, rabbit monoclonal Ab; Abcam, Camebridge, UK; Prod.No.ab92547, tested concentrations 1:250; 1:500; 1:1000) was incubated at 4°C overnight in a humidified chamber followed by three washing steps with PBS for ten minutes each. Incubation with secondary antibody (goat anti-rabbit IgG, Alexa Fluor 488, Thermo Scientific; Prod.No.A11008; tested concentrations 1:500 1:1000) was performed light-protected for one hour at room temperature. After three washing steps with PBS for ten minutes each, sections were counterstained with Hoechst (1:2000) light-protected for 15 minutes, further washed with PBS three times for ten minutes each, covered with mounting medium and coverslipped.

2.7.2.3. Cadherin 1 (CDH1)

To visualize the epithelial surface layer within native VF tissue and the constructs, sections were stained for cadherin 1 (CDH1). In detail, paraffin sections were first deparaffinated and processed with descending alcohol series as mentioned before. Antigen retrieval was performed for 15 minutes at 37°C in water bath using 0.1 % Proteinase, followed by two washing steps with PBS for two minutes each or for 30 minutes at 110°C in a decloaking chamber using Vector antigen unmasking solution, followed by washing with PBS for five minutes.Then, sections were blocked for non-specific binding sites in a humidified chamber for 45 minutes using a blocking solution.

Primary antibody (polyclonal anti-E-cadherin, IgG; Sigma Aldrich; Prod.No.SAB4503751, tested concentrations 1:100; 1:250; 1:500) was incubated at 4°C overnight in a humidified chamber followed by three washing steps with PBS for ten minutes each. Incubation with secondary antibody (goat anti-mouse IgG, Alexa Fluor 594; tested concentrations 1:500;1:1000) was performed light-protected for one hour at room temperature. After three washing steps with PBS for ten minutes each, sections were counterstained with Hoechst (1:2000) light-protected for 15 minutes, further washed with PBS three times for ten minutes each, covered with mounting medium and coverslipped.

2.7.3. Proteomic analysis

2.7.3.1. Pre-test 1: rat tail collagen, Type I matrix with and without hVFF

Proteomic analysis was performed in cooperation with the research unit “Functional Proteomics and Metabolic Pathways” at the Medical University of Graz. Considering the very high content of rat tail collagen, Type I within the samples of bioengineered 3D constructs, pre-tests were performed to validate the procedures. In detail, scaffolds using rat tail collagen, Type I (2.4 mg/ml) were generated as described in section 2.4 in 12-well Transwell inserts (Corning Transwell, Prod.No. 3460, 0.4 µm pore size) in a total volume of 360 µl/insert. hVFF (1×10^5 cells/insert) were embedded within collagen and at the same density without collagen as control. Cultivation of samples was performed for 30 days with partial medium change of SM every two to three days under standard cell culture conditions. The samples containing collagen were snap-frozen in liquid nitrogen and stored at -80°C. Inserts containing hVFF without collagen were washed twice with PBS, trypsinized and resulting cell suspension was centrifuged at 170 x g for seven minutes at room temperature twice with intermitting discarding of supernatants. The remaining cell pellet was snap-frozen in liquid nitrogen and stored at -80°C. Frozen samples were lysed in 100 µl lysis buffer (100 mM Tris HCl, pH 8.5; Prod.No.252859), 1 % sodium dodecyl sulfate, (SDS; Prod.No.L3771), 10 mM Tris(2-carboxyethyl)phosphine hydrochloride (TCEP; Prod.No.C4706); 40 mM chloroacetamide (CAA; Prod.No.C0267), (all Sigma Aldrich) by sonication for two minutes on ice and used for further preparation for LC-MS/MS as described below.

2.7.3.2. Pre-test 2: tissue preparation of native human VF

Sample preparation represents a critical step in proteomic analysis, depending on the origin of tissue and its reproducible isolation and further preparation. To optimize these procedures for human VF, different homogenization protocols were tested.

Test 1: Snap-frozen tissue samples were homogenized in 700 µL of lysis buffer using the Ultra Thurrax instrument for two minutes on ice.

Test 2: Snap-frozen tissue samples were homogenized in 500 µL of lysis buffer using the MagNa Lyser instrument. For homogenization, five cycles of 20 seconds at 6500 rpm with intermitting cooling cycles for one minute each were used.

Test 3: Snap-frozen tissue samples were homogenized in 700 µL of Tris buffer using the MagNa Lyser instrument. For homogenization, five cycles of 20 seconds at 6500 rpm with intermitting cooling cycles for one minute each were used. 500 µL of the homogenate was diluted with lysis buffer containing 20 % SDS, 500 mM TCEP and 400 mM CAA.

2.7.3.3. NanoLC-MS/MS analysis

Lysates were heat denaturated for ten minutes at 90°C. Supernatants were collected after removal of cell debris by centrifugation at 2000 x g for five minutes at room temperature. Protein concentration was determined using the BCA-RAC assay (Thermo Fisher Scientific; Prod.No.23250). For LC-MS/MS analysis, 100 µg protein or whole matrix constructs were subjected to filter-aided sample preparation as described previously (260), with minor modifications using 3 kD cut off ultracentrifugation filters (Merck Millipore; Prod.No.C7715). Buffer was exchanged three times with 8 M Urea, 100 mM TrisHCl, pH 8.0. The samples were predigested with rLysC (1:100; Promega; Prod.No.V1671) for four hours at 37°C, diluted to 2 M Urea with 100 mM ammonium bicarbonate and digested with trypsin (1:50; Promega; Prod.No.V511B) overnight. Peptides were collected by centrifugation at 14000 x g for 45 minutes at room temperature. Samples were desalted using SDB-RPS tips. 500 ng protein-digest or 1/400 of matrix constructs of each sample were injected and analyzed by nano-HPLC (equipped with an Aurora nanocolumn (C18, 1.6 µm, 250 x 0.075 mm; Ion Optics, Waltham, Massachussetts, USA; Prod.No.AUR2-25075C18A-CSI). Separation was

carried out on the nanocolumn at a flow rate of 150 nl/min at 35°C using the following gradient, where solvent A is 0.1 % formic acid (Thermo Fisher Scientific; Prod.No.85178) in water and solvent B is acetonitrile (VWR International, Radnor, Pennsylvania, USA; Prod.No.83640.32) containing 0.1 % formic acid: 0-0.1 min: 2 % B, 150 µL/min; 0.1-18 min: 2 % 150 µL/min – 300 µL/min; 18-100 min 2 %-25 % B; 100 -107 min: 25-35 % B, 108 – 118 min: 35 – 95 % B; 118-118.1 min: 95 % - 2 % B; 118.1-133 min: 2 % B. The maXis II ETD mass spectrometer (Bruker, Vienna, Austria) was operated with the captive source in positive mode with following settings: mass range: 200-2000 m/z, 2 Hz, capillary 16000 V, dry gas flow 3 L/min with 150°C, nanoBooster 0.2 bar, precursor acquisition control top 17.

2.7.3.4. Data analysis

LC-MS/MS data were analyzed by MaxQuant by searching the public SwissProt human database plus rat collagens (13202466 residues, 20304 sequences) and common contaminants. Carbamidomethylation on cystein was entered as a fixed modification, oxidation on methionine as variable modification. Detailed search criteria were used as follows: trypsin, max. missed cleavage sites: 2; search mode: MS/MS ion search with decoy database search included; precursor mass tolerance ± 0.0006 Da; product mass tolerance ± 40 ppm; acceptance parameters for identification: 1 % peptide-spectra-matches (PSM) false discovery rate (FDR); 1 % protein FDR. In addition, a label free quantitation was performed using MaxQuant (261) requiring a minimum of two ratio counts of quantified razor and unique peptides.

2.8. *In vitro* application of the phonomimetic bioreactor

The recently developed and validated phonomimetic bioreactor (246) was employed to explore the isolated or combined effects of the external stimulation of hVFF through cigarette smoke and vibration to elucidate their influence in the underlying pathophysiological molecular mechanisms of Reinke´s edema. In detail, immortalized hVFF were exposed to cigarette smoke extract (CSE) with, or without additional vibrational stress as part of a master thesis of Barbara Steffan, BSc.; that was maintained by the doctoral candidate in conceptualization, introduction in standard and advanced cell culture techniques, data curation, formal analysis and writing an original draft for publication. Further support was given by the LTTEG group members

Andrijana Kirsch, PhD.; Magdalena Grill, PhD; Magdalena Tschernitz, MSc. and Claus Gerstenberger, DI. This study was granted by the Austrian Science Fund (grant No. P 30496-B28).

Besides cytotoxicity, which was quantified using a lactate dehydrogenase (LDH) assay, RT-qPCR, Western blotting, enzyme-linked immunosorbent assay (ELISA) and Magnetic Luminex assays were employed to assess the influence on ECM production, fibrogenic and inflammatory markers and angiogenesis.

The experiments for this study were described in Grossmann et al. (262) (The Laryngoscope, article accepted on 23 May, 2020; doi:10.1002/lary.28855, “**Exploring the pathophysiology of Reinke´s edema: The cellular impact of cigarette smoke and vibration”**).

3. Results

3.1. Establishment of hOME isolation procedure

After the enzymatic treatment of tissue pieces with Dispase (used for Test 1-12), epithelial layer (~0.5 mm thick) could be separated from the underlying stroma, cut in small pieces and placed within the pre-coated culture plates.

Test 1: Approximately five days after start of the isolation, a high number of small spherical-shaped cells were visible around the tissue pieces and the surrounding area (Figure 3.A). Cultivation was performed for additional 13 days. After trypsinization, the cells died and further cultivation was impossible (Figure 3.B).

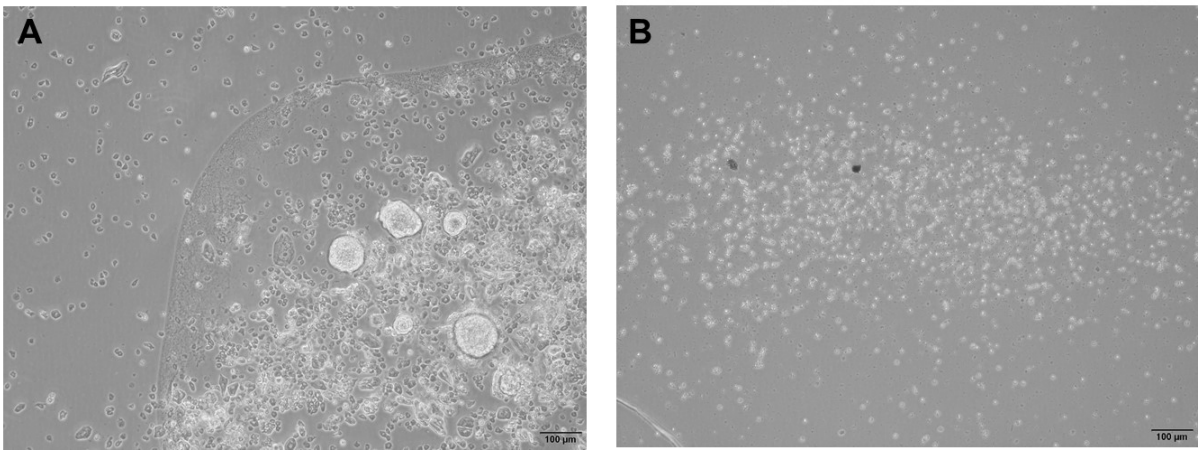

Figure 3. Representative image of growing spherical-shaped cells five days after start of the isolation **(A)**. Representative image of dead cells after trypsinization **(B)**. (both 4x magnification)

Test 2: A high number of spherical- and irregular-shaped cells started to grow tightly packed out of the tissue pieces approximately seven days after start of the isolation (Figure 4.A), but no further growth of cells could be examined over an additional cultivation period of ten days (Figure 4.B).

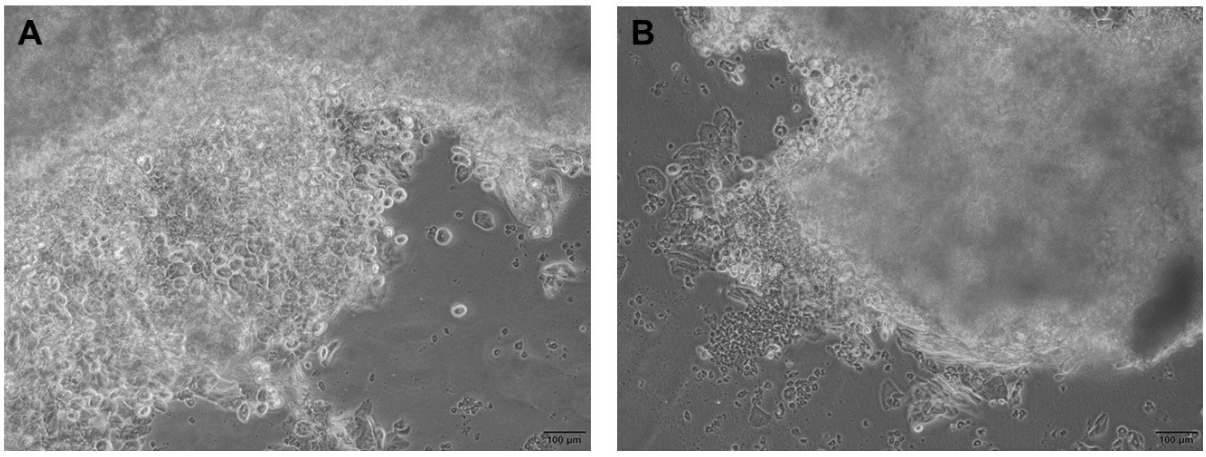

Figure 4. Representative image of growing spherical- and irregular-shaped cells seven days after start of the isolation **(A)**. Representative image of growing spherical- and irregular-shaped cells after additional ten days of cultivation **(B)**. (both 4x magnification)

Test 3: Spherical- and irregular-shaped cells started to grow out of the tissue pieces approximately 12 days after start of the isolation (Figure 5.A), but no further growth of cells could be examined over an additional cultivation period of 17 days (Figure 5.B).

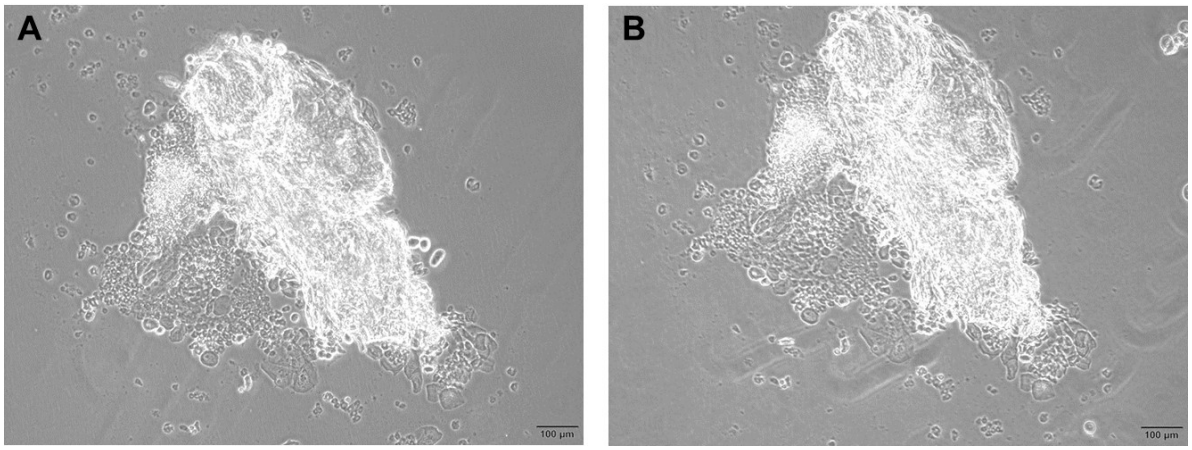

Figure 5. Representative image of growing spherical- and irregular-shaped cells 12 days after start of the isolation **(A)**. Representative image of growing spherical- and irregular-shaped cells after additional 17 days of cultivation **(B)**. (both 4x magnification)

Test 4: Irregular-shaped and fibroblast-like cells started to grow out of the tissue pieces approximately five days after start of the isolation (Figure 6.A). Over an additional cultivation period of six days, cells detached from the bottom of the coated well and died, while few fibroblast-like cells showed no further growth (Figure 6.B).

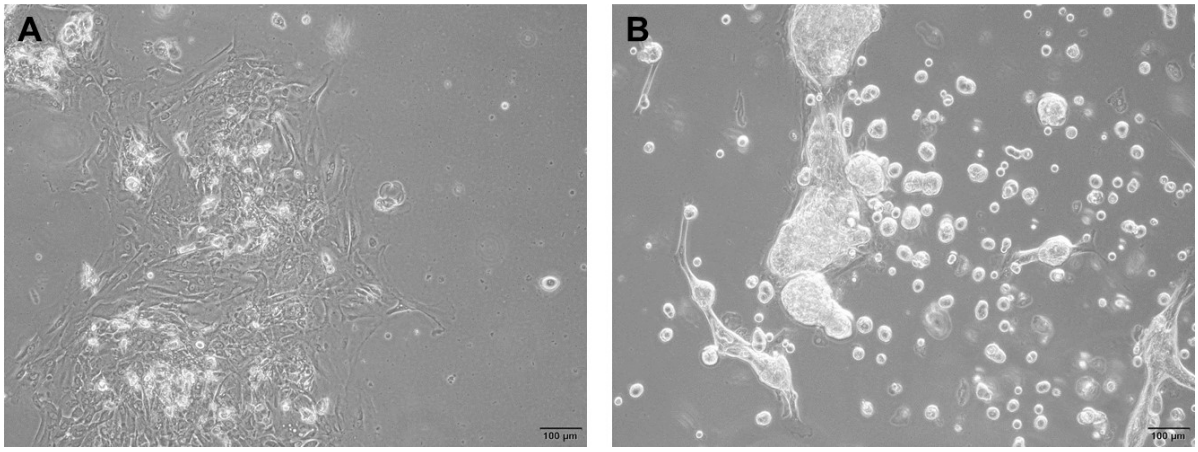

Figure 6. Representative image of growing irregular-shaped and fibroblast-like cells five days after start of the isolation **(A)**. Representative image of dead irregular-shaped cells after additional six days of cultivation **(B)**. (both 4x magnification)

Test 5: Irregular-shaped and a high number of fibroblast-like cells started to grow out of the tissue pieces approximately four days after start of the isolation (Figure 7.A). Over an additional cultivation period of 14 days, unspecific cells detached from the bottom of the coated well and died, while fibroblast-like cells showed further growth (Figure 7.B).

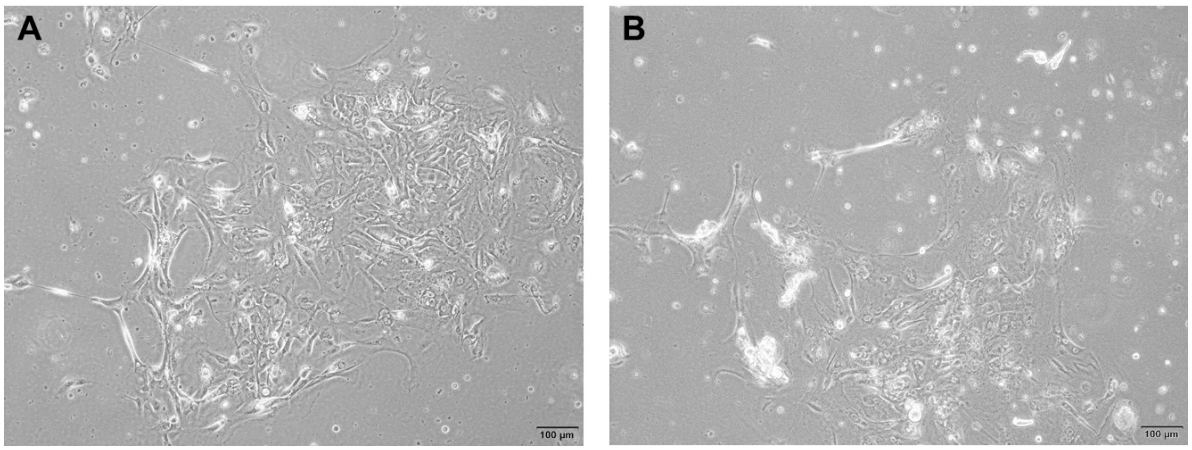

Figure 7. Representative image of growing irregular-shaped and fibroblast-like cells four days after start of the isolation **(A)**. Representative image of fibroblast-like cells after additional 14 days of cultivation **(B)**. (both 4x magnification)

Test 6: Few irregular-shaped cells and a high number of fibroblast-like cells started to grow out of the tissue pieces approximately six days after start of the isolation (Figure

8.A). Over an additional cultivation period of 12 days, only fibroblast-like cells showed further growth (Figure 8.B).

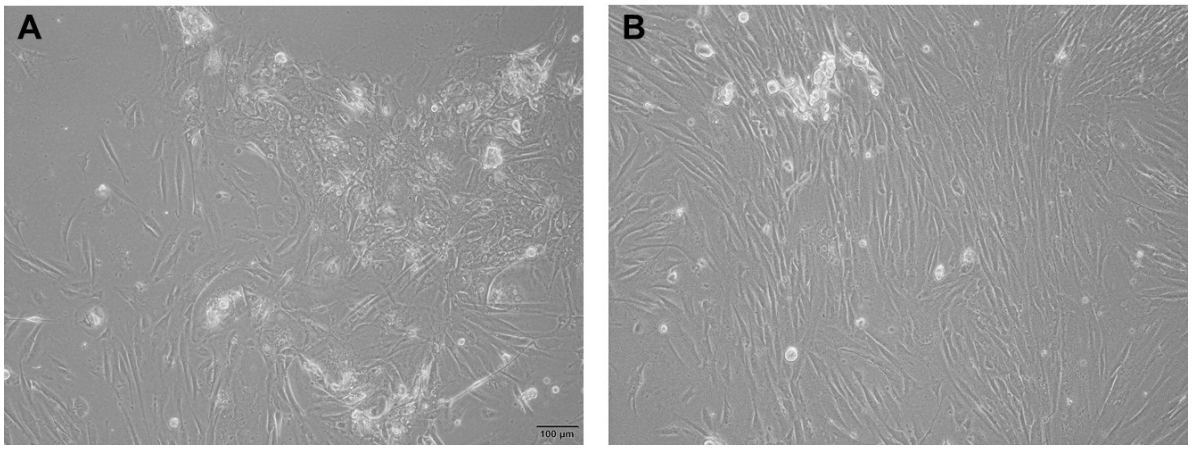

Figure 8. Representative image of growing irregular-shaped and fibroblast-like cells six days after start of the isolation **(A)**. Representative image of fibroblast-like cells after additional 12 days of cultivation **(B)**. (both 4x magnification)

Test 7: Irregular-shaped cells started to grow out of the tissue pieces approximately eight days after start of the isolation (Figure 9.A), but no further growth of cells could be observed over an additional cultivation period of 14 days (Figure 9.B).

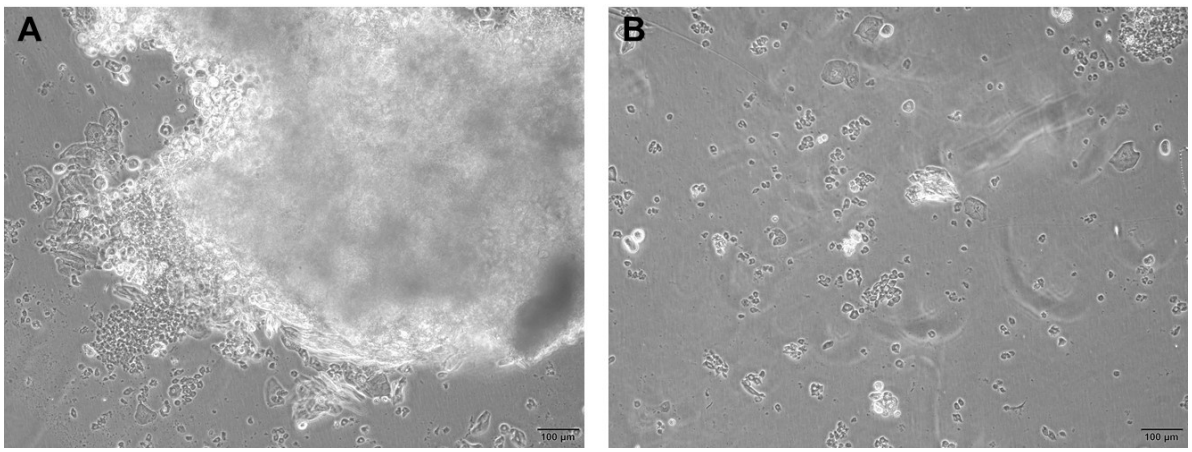

Figure 9. Representative image of growing irregular-shaped cells eight days after start of the isolation **(A)**. Representative image of irregular-shaped cells after additional 14 days of cultivation **(B)**. (both 4x magnification)

Test 8: Small irregular-shaped cells started to grow out of the tissue pieces approximately six days after start of the isolation (Figure 10.A). Over an additional cultivation period of 17 days, no further growth of cells could be observed (Figure 10.B).

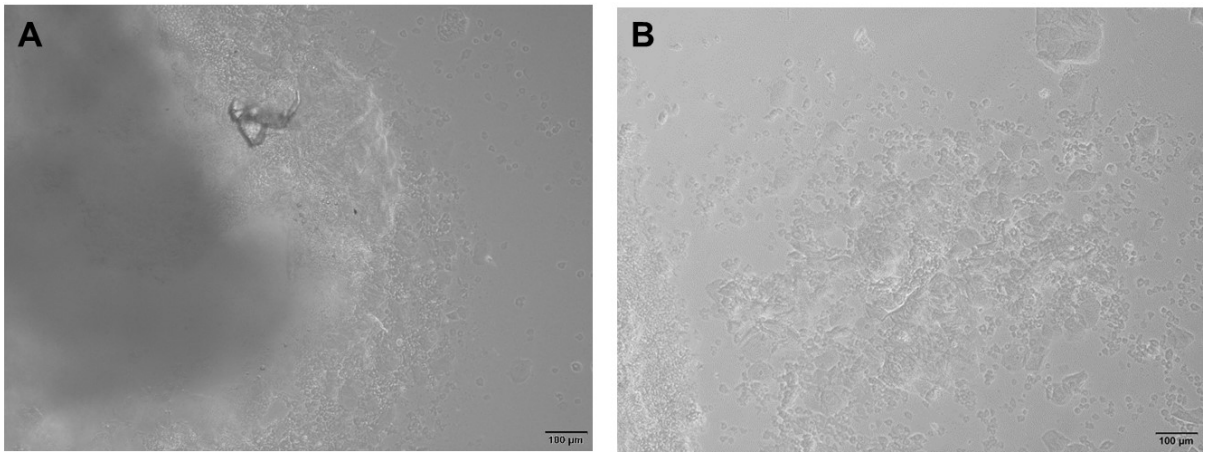

Figure 10. Representative image of growing irregular-shaped cells six days after start of the isolation **(A)**. Representative image of irregular-shaped cells after additional 17 days of cultivation **(B)**. (both 4x magnification)

Test 9: Irregular-shaped cells started to grow out of the tissue pieces approximately nine days after start of the isolation (Figure 11.A). Over an additional cultivation period of eight days, no further growth of cells could be observed (Figure 11.B).

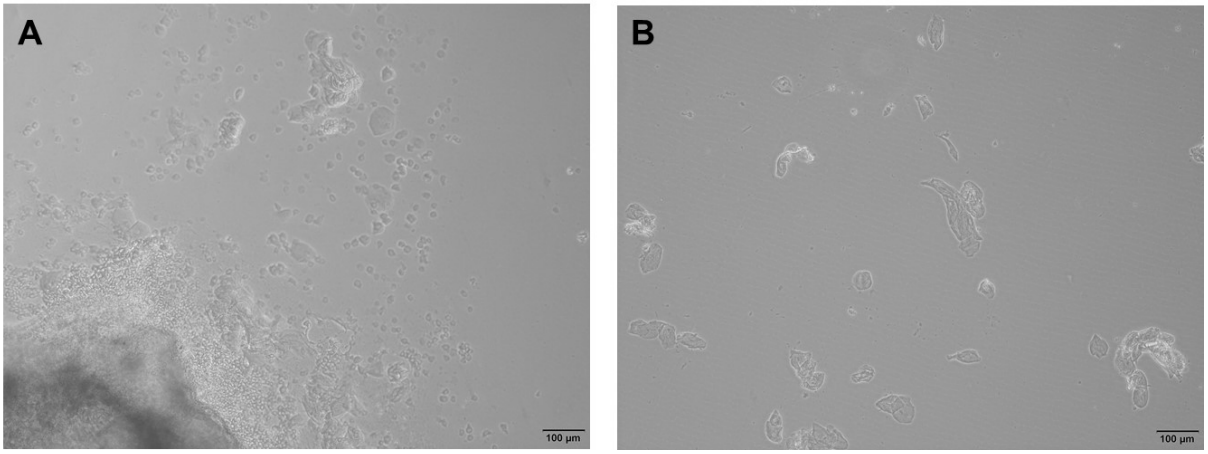

Figure 11. Representative image of growing irregular-shaped cells nine days after start of the isolation **(A)**. Representative image of irregular-shaped cells after additional eight days of cultivation **(B)**. (both 4x magnification)

Test 10: Irregular-shaped cells started to grow out of the tissue pieces approximately five days after start of the isolation (Figure 12.A). Over an additional cultivation period of 18 days, no further growth of cells could be observed (Figure 12.B).

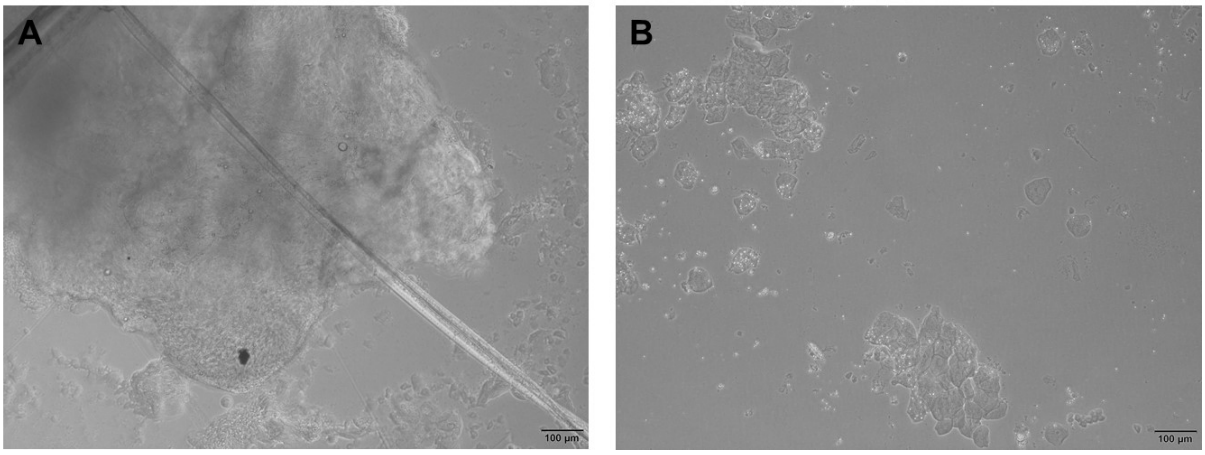

Figure 12. Representative image of growing irregular-shaped cells five days after start of the isolation **(A)**. Representative image of irregular-shaped cells after additional 18 days of cultivation **(B)**. (both 4x magnification)

Test 11: Irregular-shaped cells started to grow out of the tissue pieces approximately three days after start of the isolation (Figure 13.A). Over an additional cultivation period of 15 days, tightly packed cell areas were visible with non-adherent cells within the culture medium but no further growth of cells could be observed (Figure 13.B).

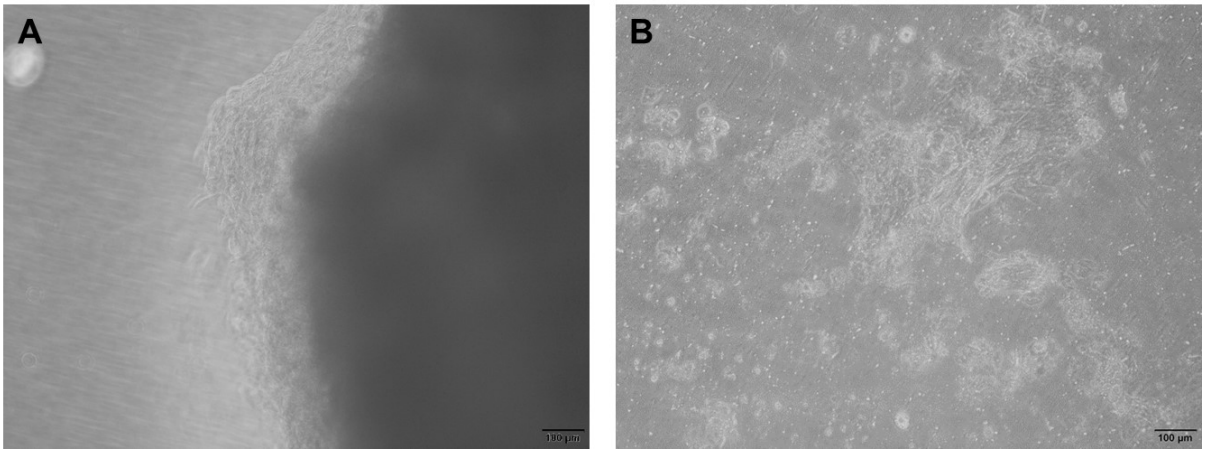

Figure 13. Representative image of growing irregular-shaped cells three days after start of the isolation **(A)**. Representative image of tightly packed cell areas after additional 15 days of cultivation **(B)**. (both 4x magnification)

Test 12: Irregular-shaped cells started to grow out of the tissue pieces approximately five days after start of the isolation (Figure 14.A). Over an additional cultivation period of 18 days, tightly packed irregular-shaped and fibroblast-like cell areas were visible but no further growth of cells could be observed (Figure 14.B).

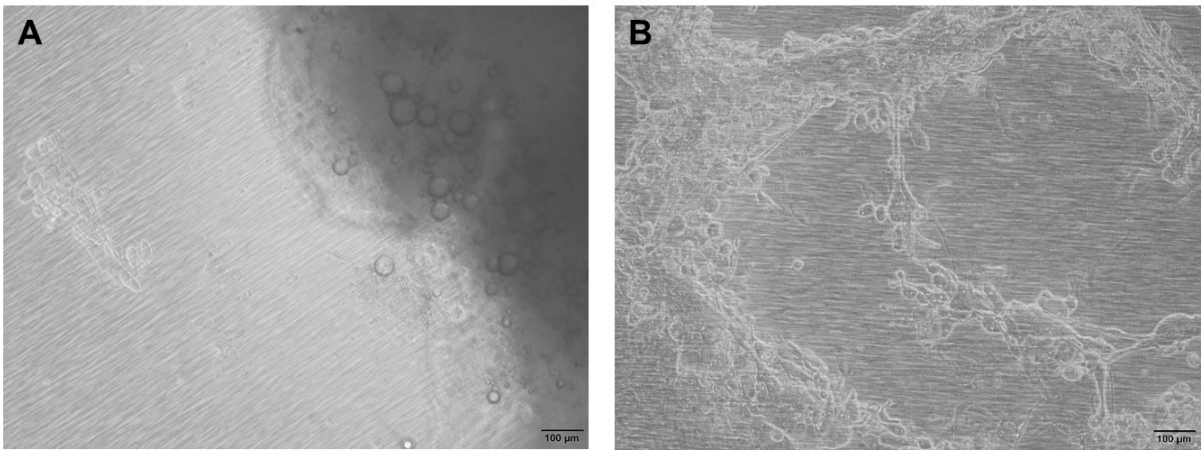

Figure 14. Representative image of growing irregular-shaped cells five days after start of the isolation **(A)**. Representative image of irregular-shaped cells after additional 18 days of cultivation **(B)**. (both 4x magnification)

Test 13: Through the enzymatic treatment with Accutase of the separated epithelial layer for 10-15 minutes, a single-cell suspension could be seeded within uncoated cell culture plates.

One day after the start of the isolation, cobblestone-like cells started to form colonies (Figure 15.A). Over an additional cultivation period of 13 days, cells built a confluent layer (Figure 15.B). This procedure was used for all forthcoming isolations of epithelial cells from different donors.

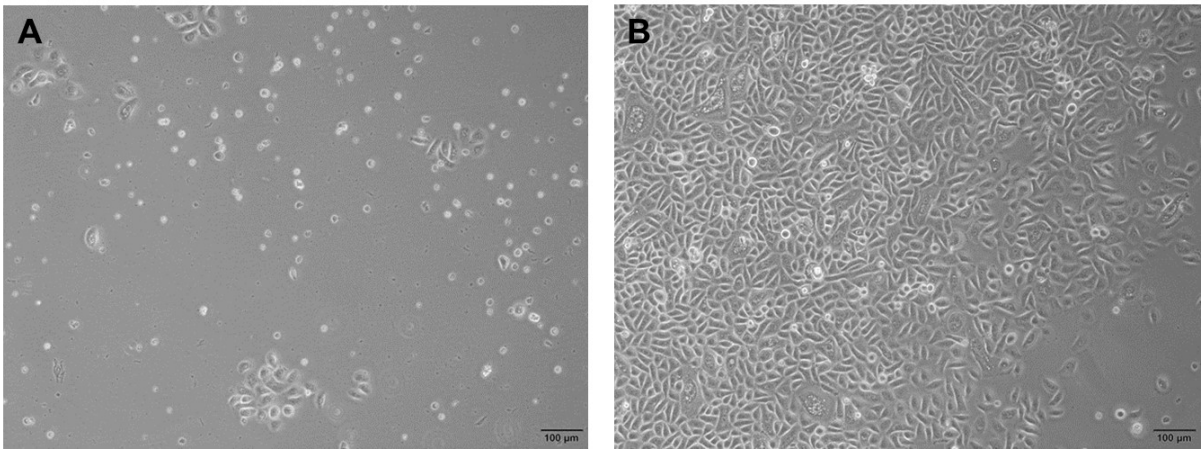

Figure 15. Representative image of colonies of cobblestone-like cells 24 hours after start of the isolation **(A)**. Representative image of confluent cell layer after additional 13 days of cultivation **(B)**. (both 4x magnification)

To date, hOME from four different donors (sample ID 70, 90, 91, 92; demographic data listed in Table 4) could be cultivated and cryovials for long-term storage within the existing biobank of the group could be generated.

Table 4. Donor demographic of isolated OMEC

Sample ID	Age	Sex	Surgical procedure
70	53	female	microlarynx
90	45	female	laryngeal papilloma
91	50	male	microlarynx
92	58	male	panendoscopy

Seven primary hOME cultures (sample ID 82, 88, 93, 95, 98, 99, 101) showed contaminations within four weeks of cultivation and were therefore discarded, four of these cultures (sample ID 93, 95, 99, 101) were derived from tissue collected during autopsies. Cultures of five donors (sample ID 79, 80, 84, 89, 97) formed cobblestone-like colonies but showed moderate cell death after five to seven days in culture and did not show an appropriate number of viable growing cells during the next three weeks of cultivation. Two cultures did not form colonies within five days after start of the isolation (sample ID 83, 85). (Demographic data of donors listed in Table 5).

Table 5. Donor demographic of inefficient OMEC isolations

Sample ID	Age	Sex	Surgical procedure
79	61	male	VF carcinoma
80	39	male	VF cyst
82	45	male	leukoplakia
83	48	male	microlarynx
84	58	female	Reinke´s edema
85	57	female	Reinke´s edema
88	52	male	microlarynx
89	71	male	laryngeal carcinoma
93	49	female	autopsy
95	69	female	autopsy
97	27	male	microlarynx
98	54	male	microlarynx
99	65	female	autopsy
101	82	male	autopsy

3.2. Cell specific characterization

Characterization of isolated hOMEC (n=3) was performed with RT-qPCR using self-designed primers for cell-type specific marker genes. Isolated RNA from one native VF tissue (n=2) was used as reference. The native VF samples had the highest expression of Von Willebrand factor (VWF) as endothelial cell marker and actinin alpha 3 (ACTN3) as skeletal muscle cell marker (Figure 16.A and B, respectively), compared to isolated hOMEC or immortalized hVFF. Immortalized hVFF showed the highest expression of Thy-1 cell surface antigen (THY1) and vimentin (VIM), used as fibroblast markers (Figure 16.C and D, respectively), compared to hOMEC and native VF tissue. The epithelial cell marker cytokeratin (CK) 13 was highly expressed in native VF tissue, followed by hOMEC samples, with nearly no expression in hVFF (Figure 16.E). CK14 expression was highest in hOMEC samples, followed by native VF tissue and very little expression in hVFF (Figure 16.F). Furthermore, a high expression of the epithelial

marker Cadherin 1 (CDH1) was found in hOMEC samples, compared to native VF tissue and hVFF (Figure 16.G).

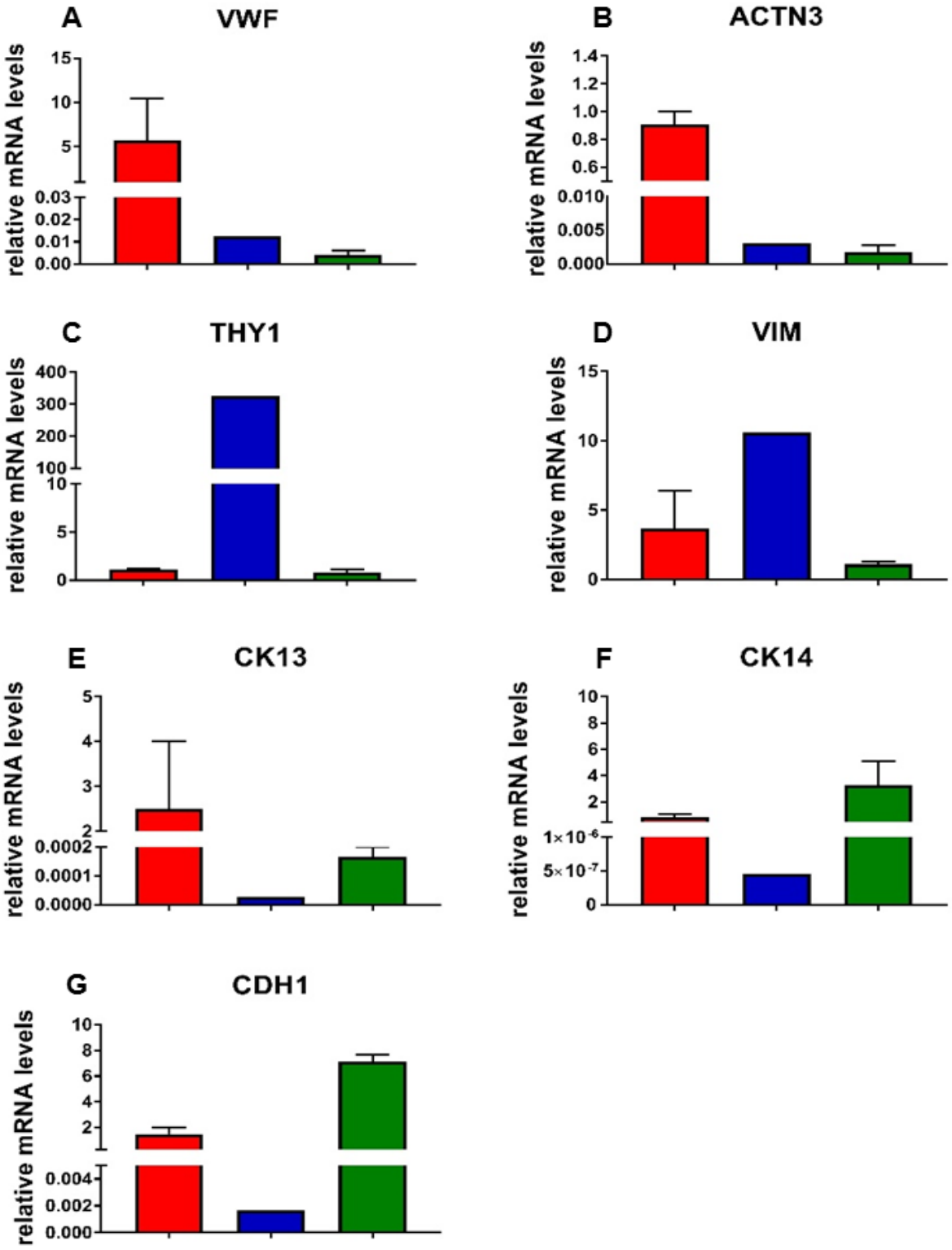

Figure 16. Relative mRNA levels of cell-type specific marker genes of native VF tissue samples (red, n=2), hVFF (blue, n=1) and hOMEC (green, n=3). Von Willebrand factor **(A)**, actinin alpha 3 **(B)**, Thy 1 cell surface antigen **(C)**, vimentin **(D)**, cytokeratin 13 **(E)**, cytokeratin 14 **(F)**, and cadherin 1 **(G)**. Data are presented as means ± SEM (n=1-3), relative to mRNA levels of one native VF tissue sample.

3.3. 3D cultivation of hVFF embedded within rat tail collagen, Type I matrix

Matrix test 1: Although the solutions were mixed carefully, many air bubbles appeared during this procedure. Polymerization was successful in all wells after 40 minutes (Figure 17.A). After a cultivation period of ten days, a low number of hVFF cells were visible within the matrix indicating that cells did not grow (Figure 17.B).

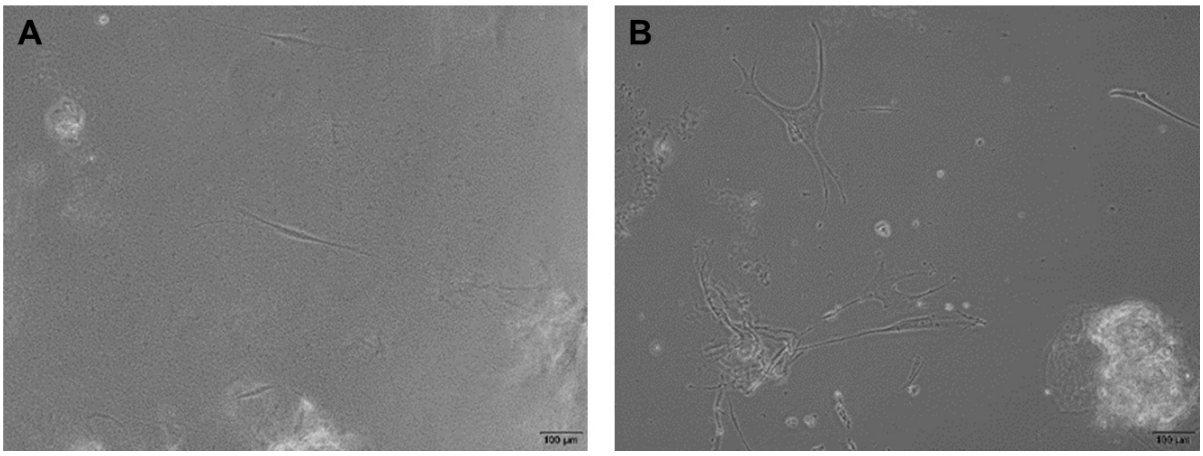

Figure 17. Representative image of embedded hVFF after polymerization **(A)**. Representative image of embedded hVFF after ten days of cultivation **(B)**. (both 4x magnification)

Matrix test 2: After 90 minutes of polymerization, the matrix showed a jellylike texture indicating that the procedure was not successful (Figure 18.A). Further cultivation was started but after a cultivation period of four days, no further growth of hVFF cells was visible within the matrix (Figure 18.B).

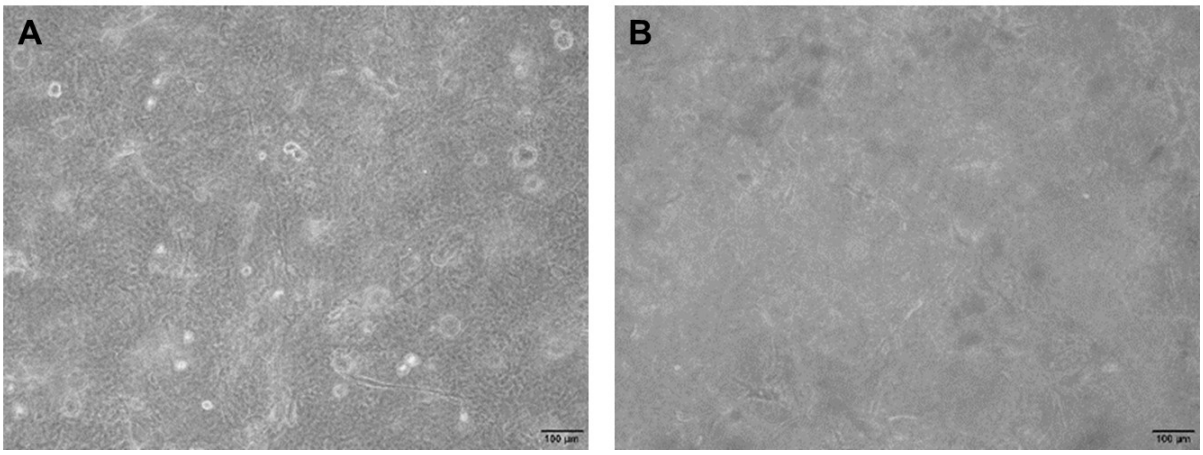

Figure 18. Representative image of embedded hVFF after polymerization **(A)**. Representative image of embedded hVFF after four days of cultivation **(B)**. (both 4x magnification)

Matrix test 3: Polymerization was successful after 45 minutes for all tested concentrations of hVFF. Cell growth of hVFF within the matrix could be observed after a cultivation period of 14 days (images not shown). For all tested concentrations of seeded hVFF, a matrix contraction was observed over the first four days of culture which did not change during the following cultivation period (Figure 19.A-C, 5×10^4 cells/insert, 1×10^5 cells/insert and 2×10^5 cells/insert seeding density, respectively. Images of other tested concentrations not shown). Matrix without hVFF exhibited no contraction, whereas matrix containing hVFF at all tested concentrations reached an averaged plateau of ~ 53 % of initial cross-sectional area over the cultivation period of 14 days (Figure 19.D).

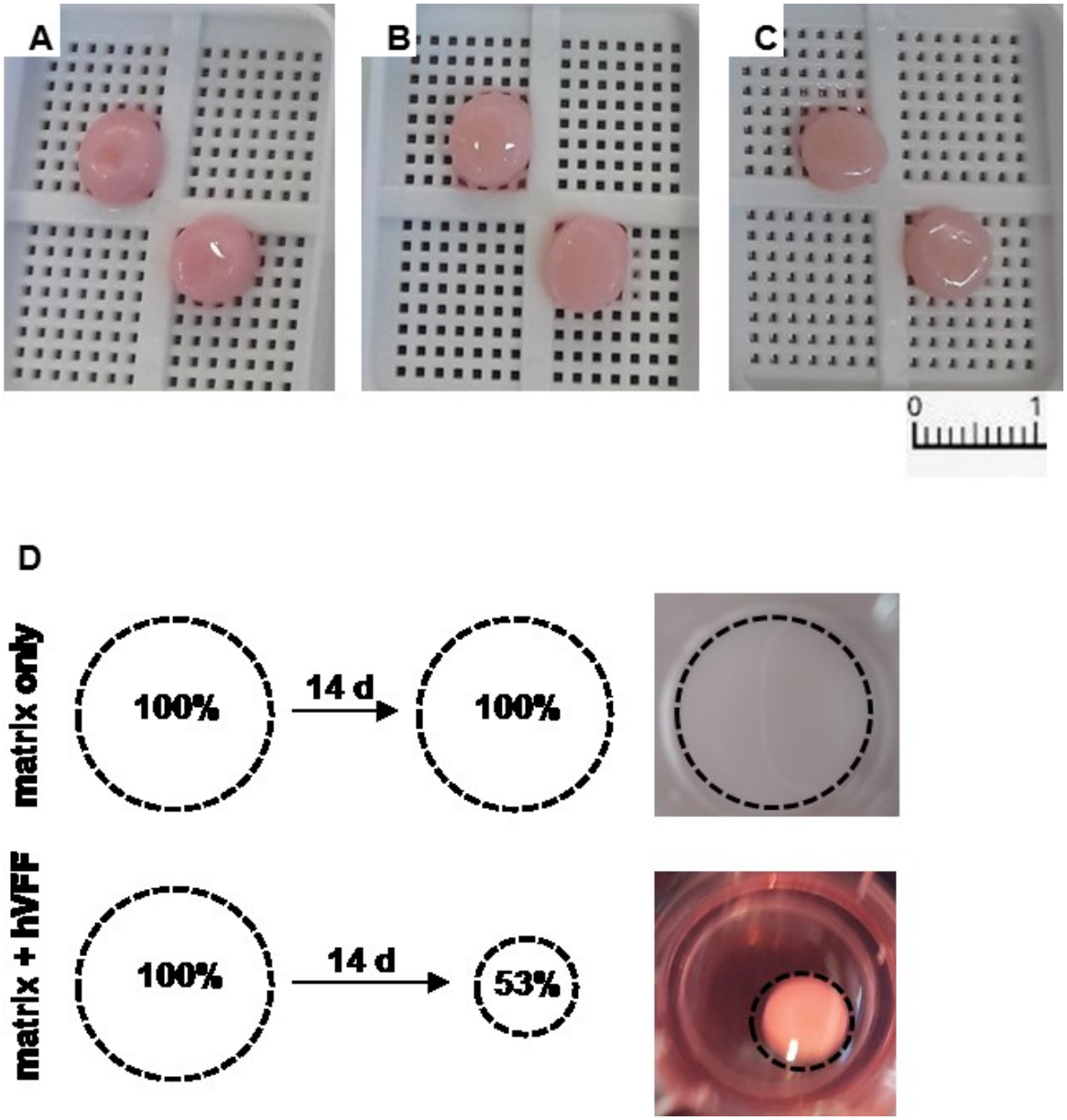

Figure 19. Representative photographs of matrix contraction of embedded hVFF after a cultivation period of 14 days seeded at a density of 5 x 10^4 cells/insert **(A)**, 1 x 10^5 cells/insert **(B)**, and 2 x 10^5 cells/insert **(C)** Scale bar: 1 cm. Representative schematics and photographs illustrating matrix contraction following seeding of hVFF within collagen matrix **(D)**.

Samples were allocated to histology to perform H&E stainings. Density and distribution of fibroblasts within the collagen matrix indicated a successful growth of cells. At lower seeding densities of hVFF (Figure 20.A-E), most cells showed spindle to star-like somata and only a few of them elongated processes. No obvious difference in cell density could be observed. Most of the growing hVFF cells seeded in the highest concentration showed typical fibroblast-like elongated processed (Figure 20.F).

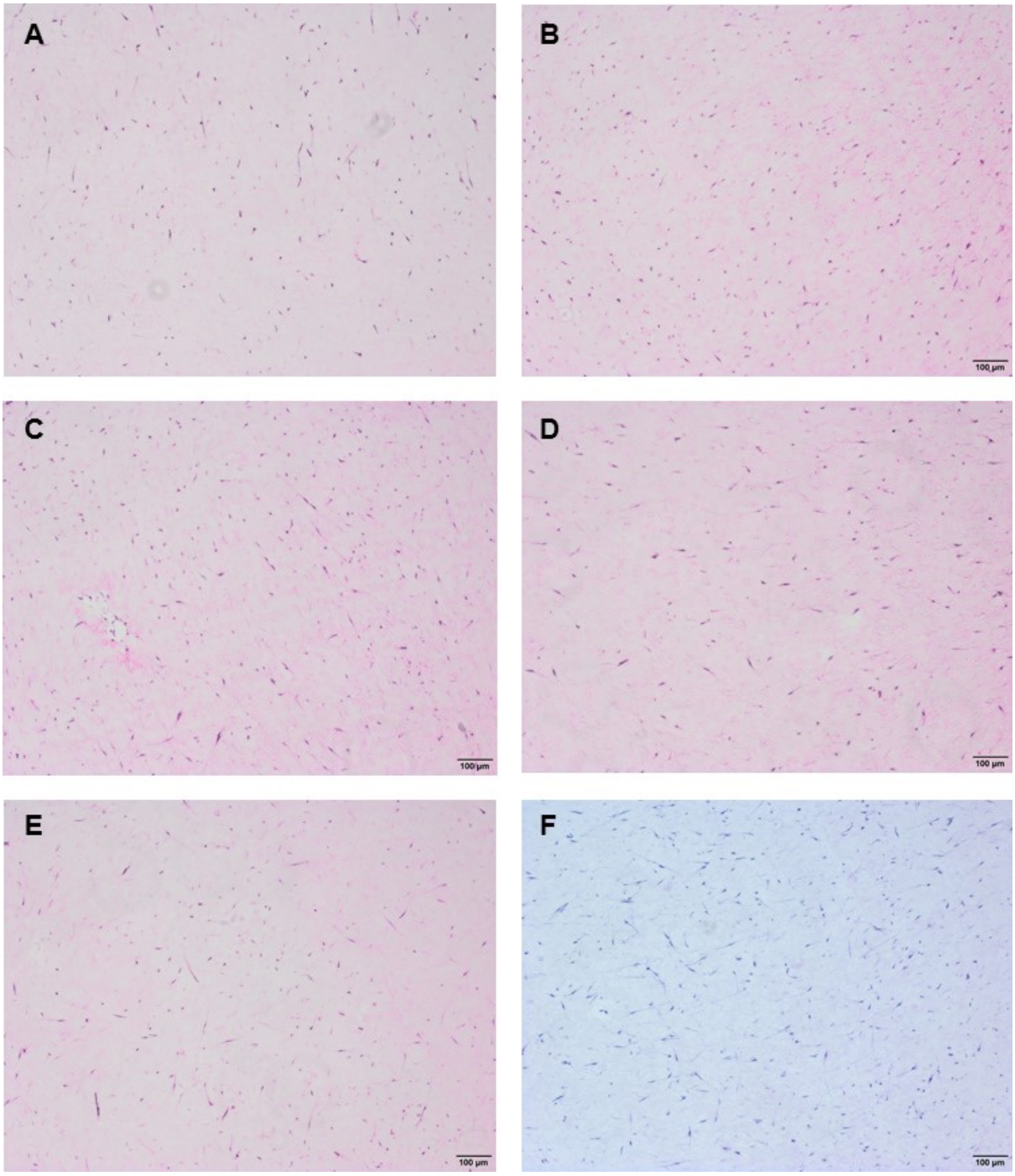

Figure 20. Representative H&E staining of embedded hVFF after a cultivation period of 14 days seeded at a density of 5 x 10^4 cells/insert **(A)**, 6 x 10^4 cells/insert **(B)**, 7 x 10^4 cells/insert **(C)**, 8 x 10^4 cells/insert **(D)**, 1 x 10^5 cells/insert **(E)** and 2 x 10^5 cells/insert **(F)**. (all 4x magnification)

Collagen-fibroblast matrix samples of three experiments performed in technical triplicates containing hVFF at a density of 2 x 10^5 cells were allocated to RT-qPCR, and gene expression levels of embedded hVFF were compared to the hVFF grown

under standard conditions. Gene expression levels of hyaluronan synthases (HAS) 1, 2 and 3 were down-regulated, whereas HAS2 and 3 downregulation reached statistical significance (Figure 21.A-C, respectively). Significant downregulation of gene expression was detected for fibronectin (FN1), collagen I alpha 1 (COL1A1), matrix metalloproteinase 1 (MMP1) and integrin subunit beta 1 (ITGB1) (Figure 21.D, F, H, K, respectively). Gene expression levels of elastin (ELN) and integrin subunit alpha 2 (ITGA2) were up-regulated, whereas ITGA2 upregulation reached statistical significance (Figure 21.E and J, respectively). Actin, alpha 2 (ACTA2) and tissue inhibitor of metalloproteinase 1 (TIMP1) expression levels were not changed (Figure 21.G and I, respectively).

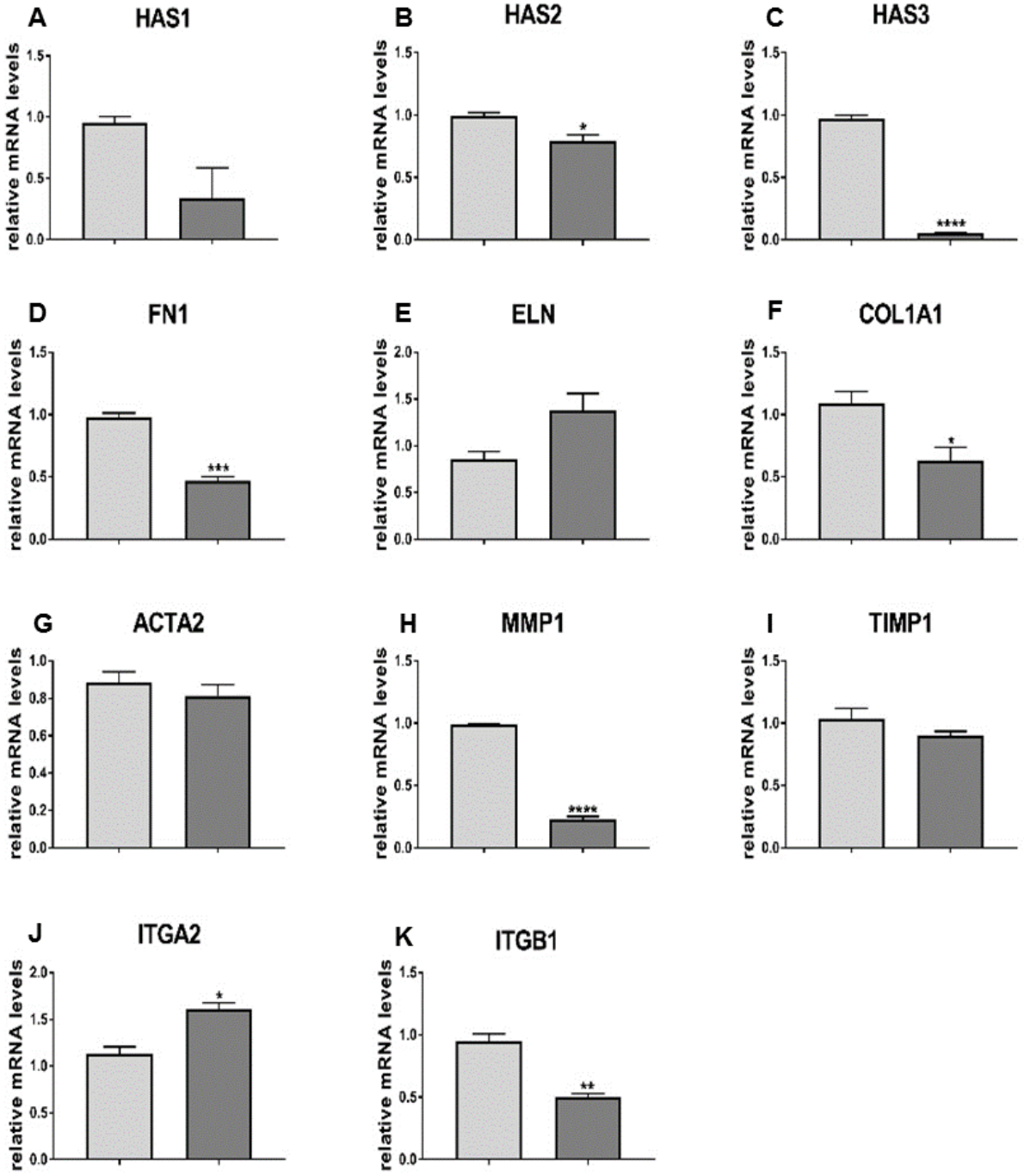

Figure 21. Relative mRNA levels of ECM-related genes of collagen-fibroblast matrix containing 2 x 10^5 hVFF (n=3). Hyaluronan synthase 1 **(A)**, hyaluronan synthase 2 **(B)**, hyaluronan synthase 3 **(C)**, fibronectin **(D)**, elastin **(E)**, collagen I alpha 1 **(F)**, alpha actin 2 **(G)**, matrix metalloproteinase 1 **(H)**, tissue inhibitor of metalloproteinase 1 **(I)**, integrin subunit alpha 2 **(J)** and integrin subunit beta 1 **(K)**. Data are average of three independent experiments performed in triplicates and are represented as means ± SEM, relative to mRNA levels of hVFF cells without collagen matrix. Statistical analysis was performed using a Student´s t test, *p<0.05, **p<0.01, ***p<0.001, ****p<0.0001.

3.4. 3D Co-cultivation of hVFF and hOMEC

For all co-cultivation tests, microscopic examination of cells was only possible during the first steps of the cultivation period within the established fibroblast-collagen layer. After seeding of epithelial cells on top of this matrix, cellular components were not entirely visible under the microscope and further growth of cells could not be observed until the harvest of the constructs. All performed tests are described in detail within the following sections.

CC test 1: Growing hVFF could be observed within the matrix before hOMEC were seeded on top of the construct (Figure 22.A). H&E staining of the construct showed a very low number of stained somata with few elongated procecces, which correspond to the seeded fibroblasts within the collagen matrix. Closely spaced stained somata on both sides of the construct revealed a single cell layer indicating a lack of multiple epithelial layers (Figure 22.B).

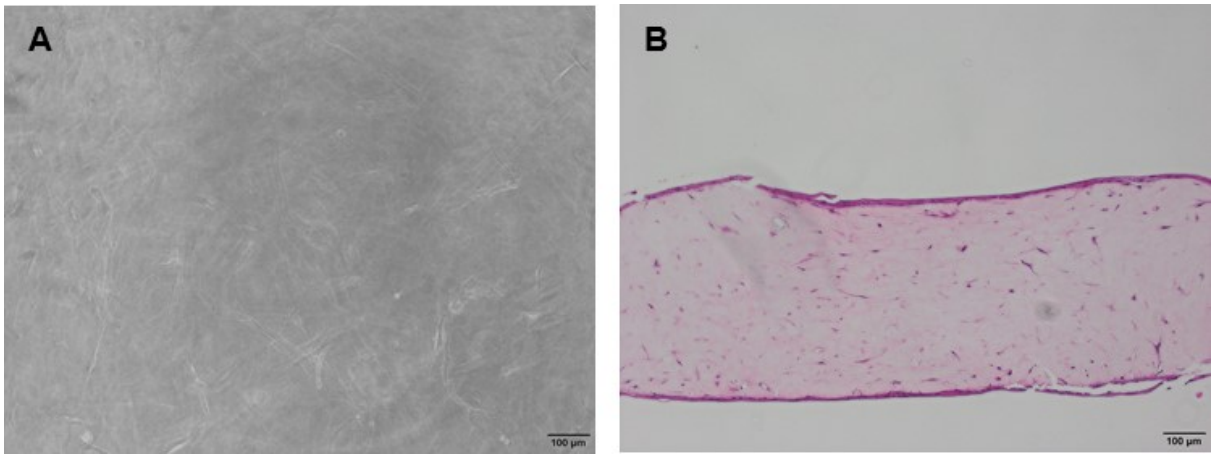

Figure 22. Representative image of embedded hVFF 24 hours after seeding at a density of 6 x 10^4 cells/insert **(A)**. Representative H&E staining of formalin-fixed, paraffin-embedded section of CC Test 1 **(B)**. (both 4x magnification)

CC test 2: Growing hVFF could be observed within the matrix before hOMEC were seeded on top of the construct (Figure 23.A). H&E staining of the construct showed an appropriate density and distribution of cells within the collagen matrix indicating a successful growth of fibroblasts and generation of connective tissue of the *in vitro* model. Most cells showed morphological classic-appearing spindle to star-like somata

and elongated processes. Closely spaced stained somata on top of the construct revealed a single cell epithelial layer (Figure 23.B).

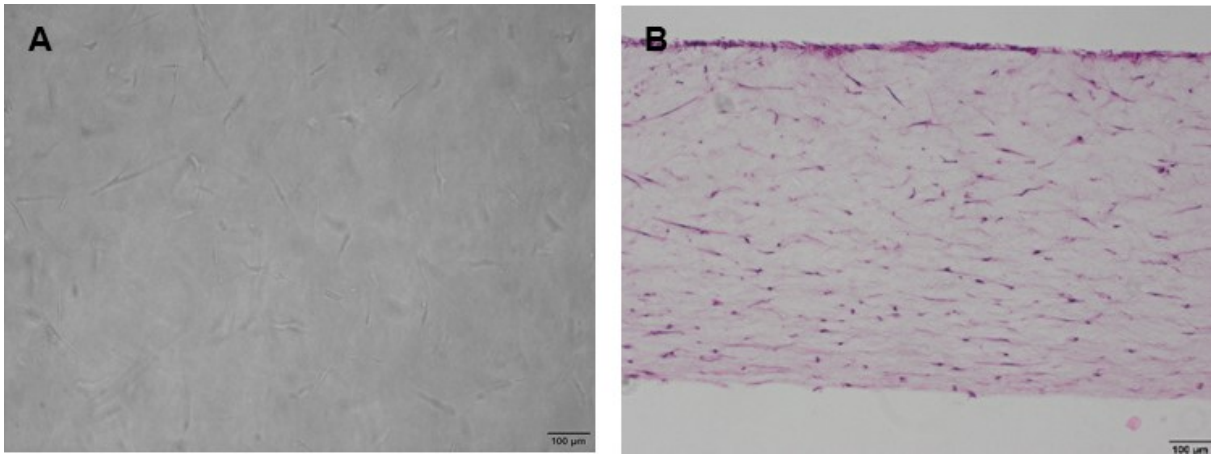

Figure 23. Representative image of embedded hVFF 24 hours after seeding at a density of 2 x 10^5 cells/insert **(A)**. Representative H&E staining of formalin-fixed, paraffin-embedded section of CC Test 2 **(B)**. (both 4x magnification)

CC test 3: Growing hVFF could be observed within the matrix before hOMEC were seeded on top of the construct (Figure 24.A). H&E staining of the construct showed a low density and distribution of fibroblasts within the collagen matrix. Only a few cells showed morphological classic-appearing spindle to star-like somata and elongated processes indicating no successful growth of cells. Closely spaced stained somata on top of the construct revealed a single cell epithelial layer (Figure 24.B).

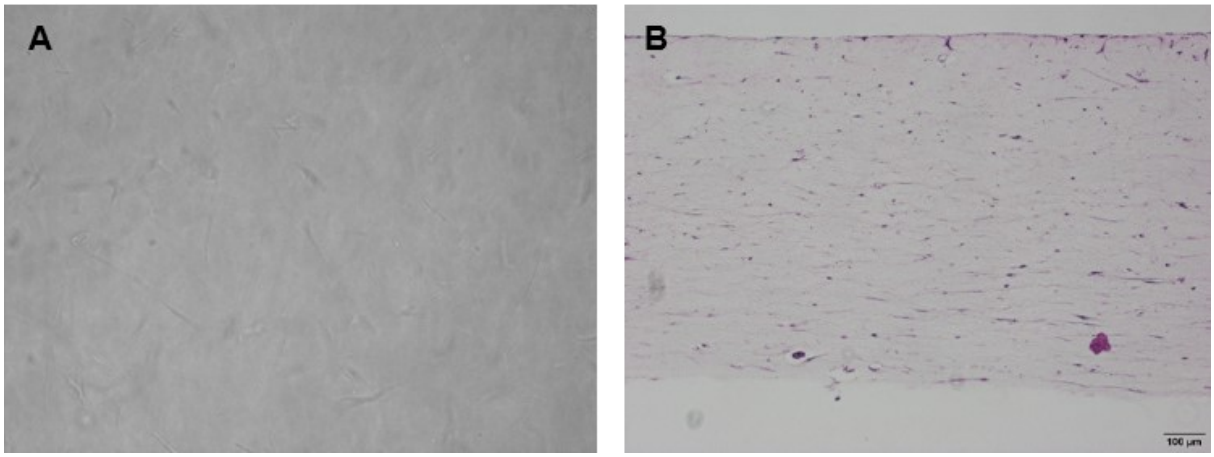

Figure 24. Representative image of embedded hVFF 24 hours after seeding at a density of 2 x 10^5 cells/insert **(A)**. Representative H&E staining of formalin-fixed, paraffin-embedded section of CC Test 3 **(B)**. (both 4x magnification)

CC test 4: The confluent layer of seeded hVFF was observed ten days after seeding, before hOMEC were seeded above (Figure 25.A). H&E staining of the construct showed a low assembly of multilayered structures indicating no generation of connective tissue of the *in vitro* model. Only a few stained somata were visible on top of the membrane (Figure 25.B). Immunohistochemical staining for cytokeratin 5/6 and cytokeratin AE1/AE3 showed an assembly of multiple epithelial layers with a very low number of stained somata (dark red staining in Figure 25.C and brown staining in Figure 25.D, respectively), extending into the underlying fibroblasts (light blue staining in Figure 25.C and D).

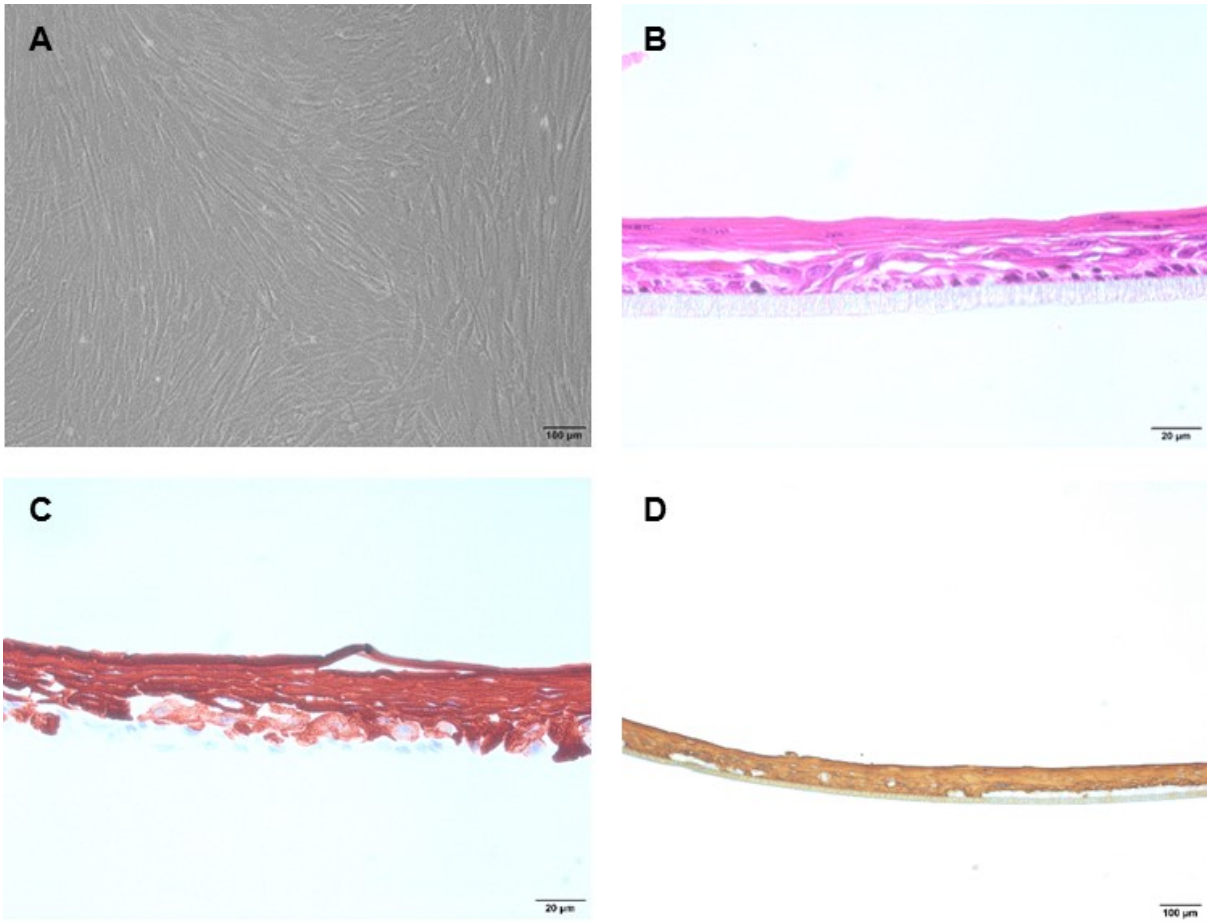

Figure 25. Representative image of seeded hVFF ten days after seeding at a density of 5 x 10^4 cells/insert **(A)**. Representative H&E staining of formalin-fixed, paraffin-embedded section of CC Test 4 **(B)**. Representative staining for cytokeratin 5/6 **(C)** and cytokeratin AE1/AE3 **(D)** of formalin-fixed, paraffin-embedded section of CC Test 4. (A and D 4x magnification; B and C 10x magnification)

CC test 5: Growing hVFF could be observed within the matrix before hOMEC were seeded on top of the construct (Figure 26.A). H&E staining of the construct showed an assembly of multilayered structures. An appropriate number of stained somata were visible within the matrix and closely spaced somata on top of the membrane (Figure 26.B). Immunohistochemical staining for cytokeratin 5/6 and cytokeratin AE1/AE3 showed an assembly of multiple epithelial layers with an appropriate number of stained somata (dark red staining in Figure 26.C and brown staining in Figure 26.D, respectively), extending into the underlying fibroblasts (light blue staining in Figure 26.C and D).

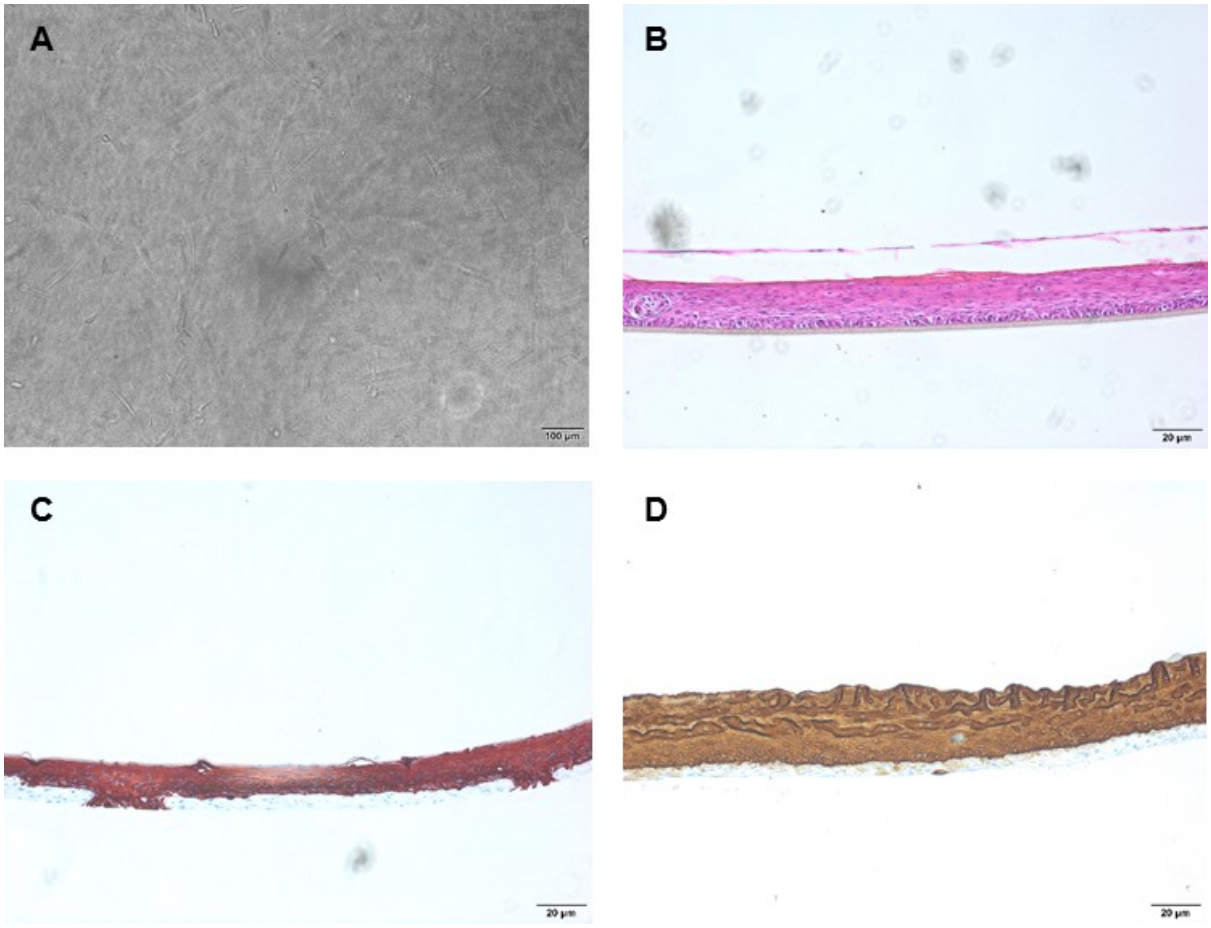

Figure 26. Representative image of embedded hVFF ten days after seeding at a density of 1 x 10^5 cells/insert **(A)**. Representative H&E staining of formalin-fixed, paraffin-embedded section of CC Test 5 **(B)**. Representative staining for cytokeratin 5/6 **(C)** and cytokeratin AE1/AE3 **(D)** of formalin-fixed, paraffin-embedded sections of CC Test 5. (A 4x magnification; B, C and D 10x magnification)

CC test 6: Growing hVFF could be observed within the matrix before hOMEC were seeded on top of the construct (Figure 27.A). H&E staining of the construct showed an appropriate density and distribution of fibroblasts within the collagen matrix indicating a successful growth of cells and generation of connective tissue of the *in vitro* model. Morphologicaly, most cells showed spindle to star-like somata and elongated processes (Figure 27.B). Immunohistochemical staining for cytokeratin 5/6 and AE1/AE3 showed an assembly of multiple epithelial layers with an appropriate number of stained somata (dark red staining in Figure 27.C and brown staining in Figure 27.D, respectively) above the underlying connective tissue with an appropriate number of fibroblasts (light blue staining in Figure 27.C and D).

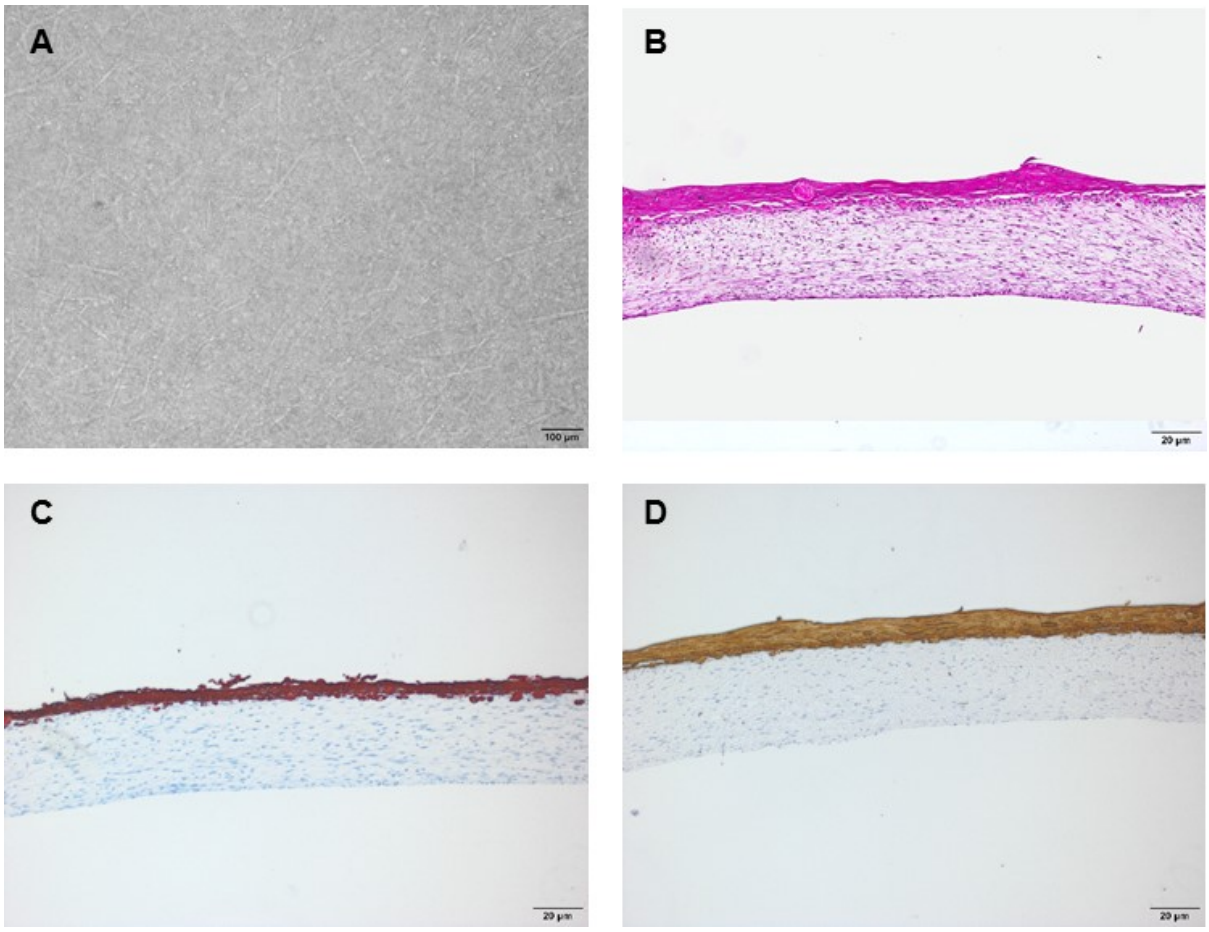

Figure 27. Representative image of embedded hVFF ten days after seeding at a density of 2 x 10^5 cells/insert **(A)**. Representative H&E staining of formalin-fixed, paraffin-embedded section of CC Test 6 **(B)**. Representative staining for cytokeratin 5/6 **(C)** and cytokeratin AE1/AE3 **(D)** of formalin-fixed, paraffin-embedded sections of CC Test 6. (A 4x magnification; B, C and D 10x magnification)

The engineered construct resembled a native mucosa comparable to the native VF after a total cultivation of 35 days. A ~20 µm thick stratified epithelium and an underlying, sparsely cell-populated lamina propria were identified (Figure 27.B-D). Immunohistochemical staining of basal collagen, Type IV (COL IV) showed a basement membrane and vascular basement membrane structures within the native VF tissue, whereas an assembled barrier-like structure within the engineered constructs was found (red signal and white arrows and arrowheads in Figure 28.A and B, respectively). Vimentin (VIM)-stained fibroblasts of the native VF tissue were restricted within the lamina propria, whereas VIM-stained cells were detected throughout the full engineered construct (green signal in Figure 28.C and D, respectively). In native VF, cadherin (CDH)1-stained epithelial cells were preferentially localized to the apical epithelium, a background signal was also detected within the lamina propria (green signal and white arrows in Figure 28.E). Lower, but comparable signal could be detected for the engineered construct (green signal and white arrows in Figure 28.F).

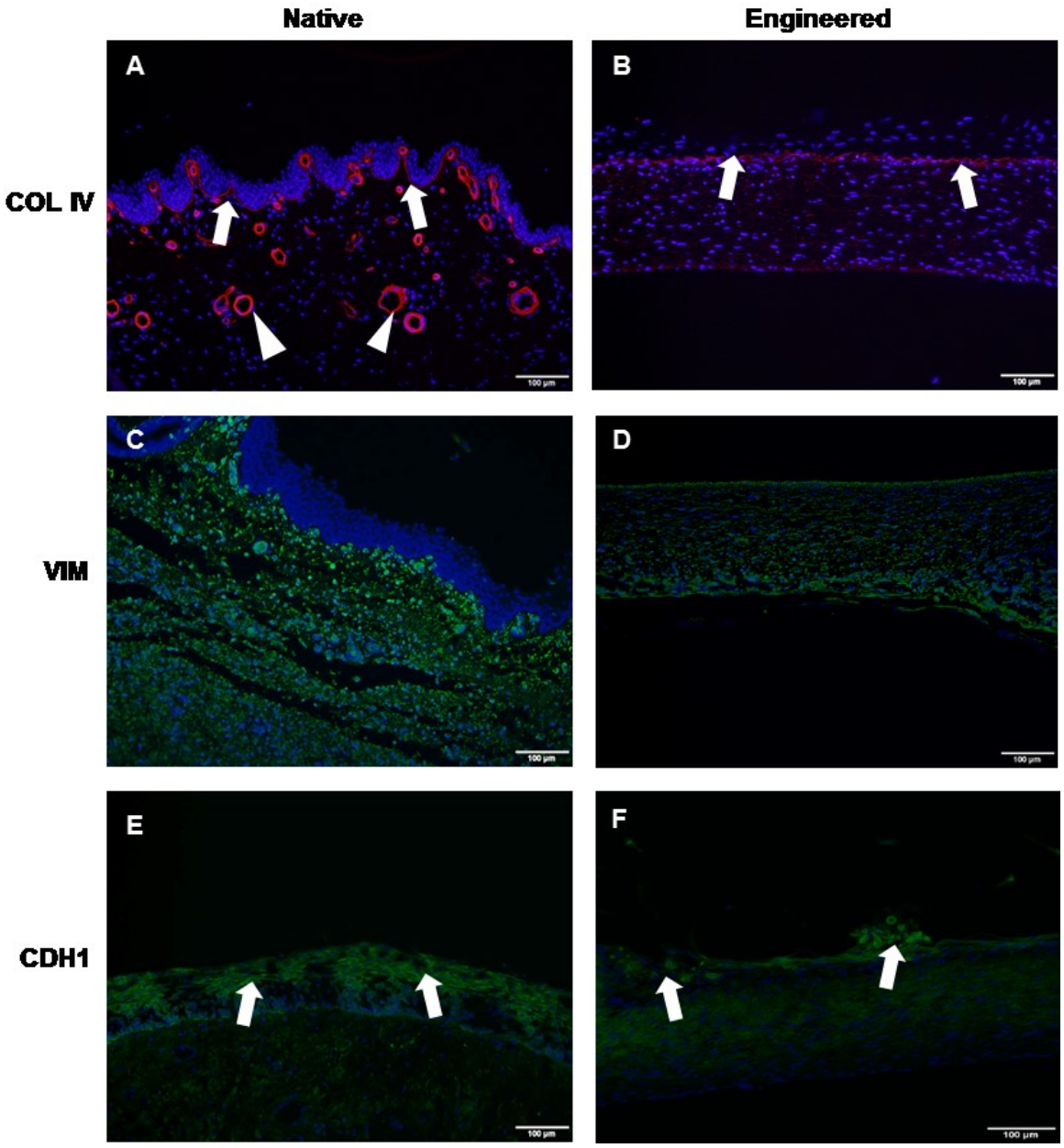

Figure 28. Representative immunohistochemical staining of basal collagen, Type IV (COL IV) indicated by red signal, white arrows and arrowheads in native VF mucosa sections **(A)** and in sections of the bioengineered constructs **(B)**. Representative immunohistochemical staining of vimentin (VIM) indicated by green signal in native VF mucosa sections **(C)** and in sections of the bioengineered construct **(D)** Representative staining for cadherin 1 (CDH1) indicated by green signal and white arrows in native VF mucosa sections **(E)** and in sections of the bioengineered constructs **(F)**. red signal and arrows (B) and the bio-engineered organotypic construct (B,D,E). Counterstaining was performed with Hoechst (blue signal in all stainings) (all 4 x magnification)

This procedure was used to engineer two further 3D co-cultivation constructs with isolated hOMEC of two different donors (sample ID 91 and 92), whereas one of them showed no (Figure 29.A) and the second one (Figure 29.B) only a sparsely assembly of multiple epithelial layers in H&E stained sections. No further stainings and analysis were conducted.

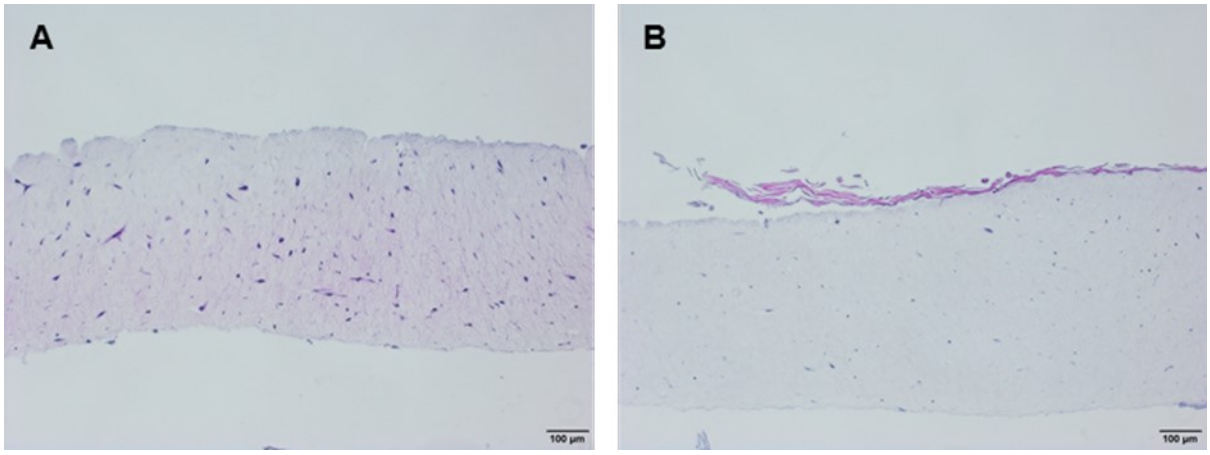

Figure 29. Representative H&E stainings of formalin-fixed, paraffin-embedded section of generated constructs according to the protocol of CC Test 6 using isolated hOMEC of sample ID 91 **(A)** and sample ID 92 **(B)**. (both 4x magnification)

3.5. Establishment of immunohistochemical stainings in native VF tissue

3.5.1. Basal collagen, Type IV (COL IV)

For slides where antigen retrieval was performed with vector antigen unmasking solution, specific stainings for basal collagen, Type IV (COL IV, red signal) were detected at an exposure time of six ms for all tested concentrations (Figure 30.A-C). No background was visible for negative control (Figure 30.D). Tested concentration 1:2000 of primary antibody, 1:1000 for secondary antibody and 1:1000 for nuclear counterstain were used for forthcoming stainings.

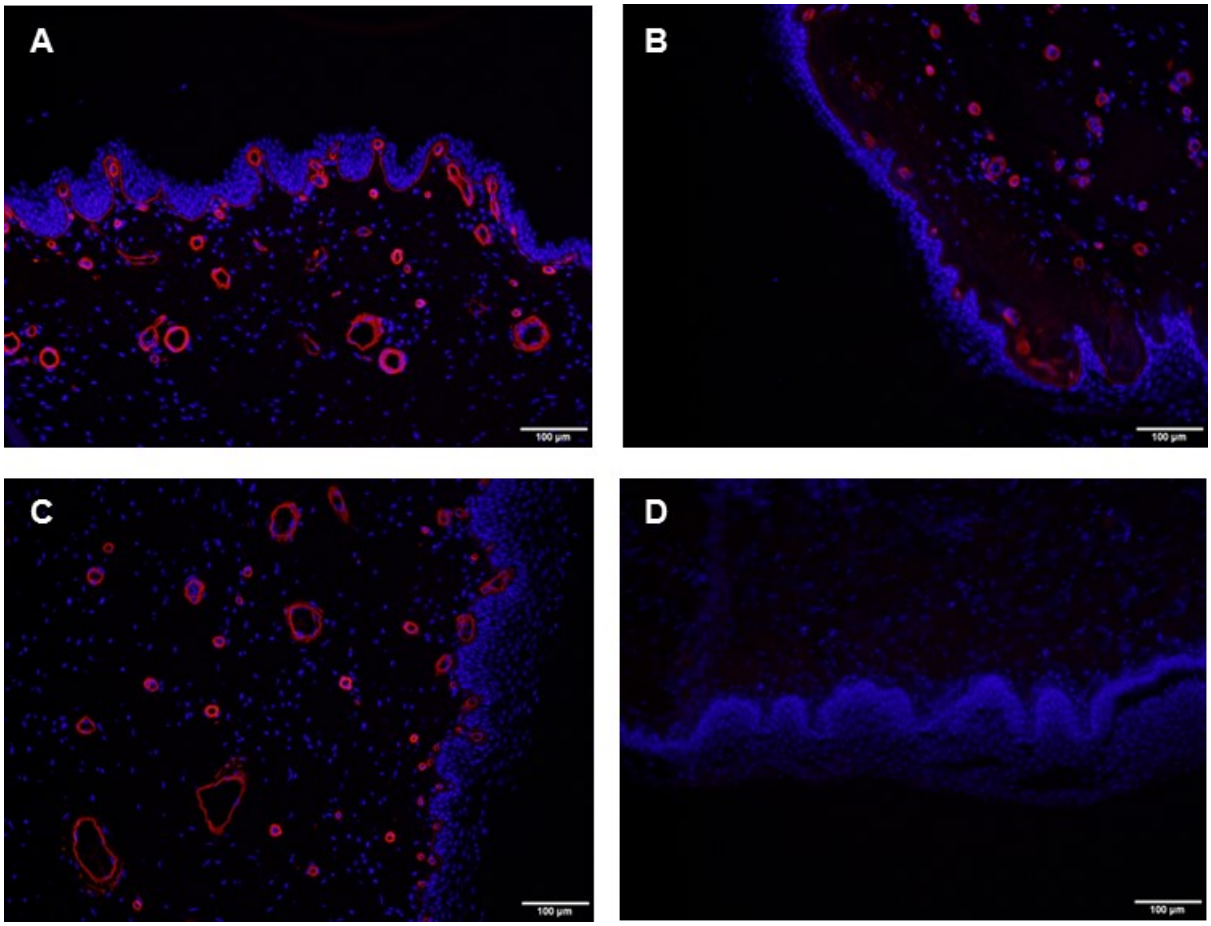

Figure 30. Representative immunohistochemical stainings of basal collagen, Type IV (COL IV, red signal) at a concentration of 1:2000 **(A)**, 1:1000 **(B)** and 1:500 **(C)**. Negative control was performed without primary antibody **(D)**. Counterstaining was performed with Hoechst (blue signal).

3.5.2. Vimentin (VIM)

For slides where antigen retrieval was performed with 0.1 % protease, no specific staining and high background were detected due to the long exposure time of 300 ms for green signal (Figure 31.A and B).

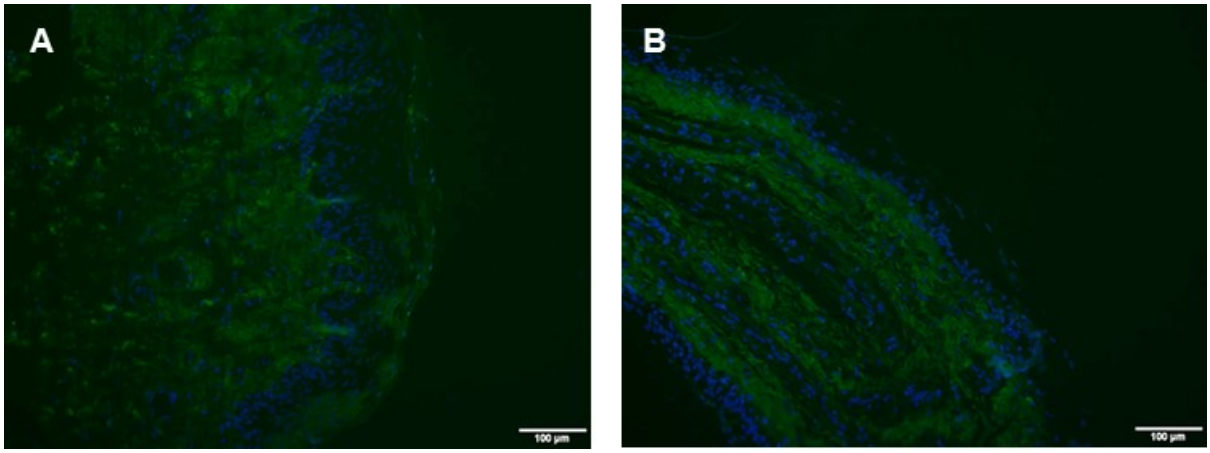

Figure 31. Representative immunohistochemical stainings of vimentin (VIM, green signal) at a concentration of 1:500 using 0.1 % protease for antigen retrieval **(A)** Negative control was performed without primary antibody **(B)**. Counterstaining was performed with Hoechst (blue signal).

For slides where antigen retrieval was performed with vector antigen unmasking solution, specific staining for vimentin (VIM, green signal) was detected at an exposure time of 30 ms for all tested concentrations (Figure 32.A-C). No background was visible for negative control (Figure 32.D). Tested concentration 1:1000 of primary antibody, 1:500 for secondary antibody and 1:2000 for nuclear counterstain were used for forthcoming stainings.

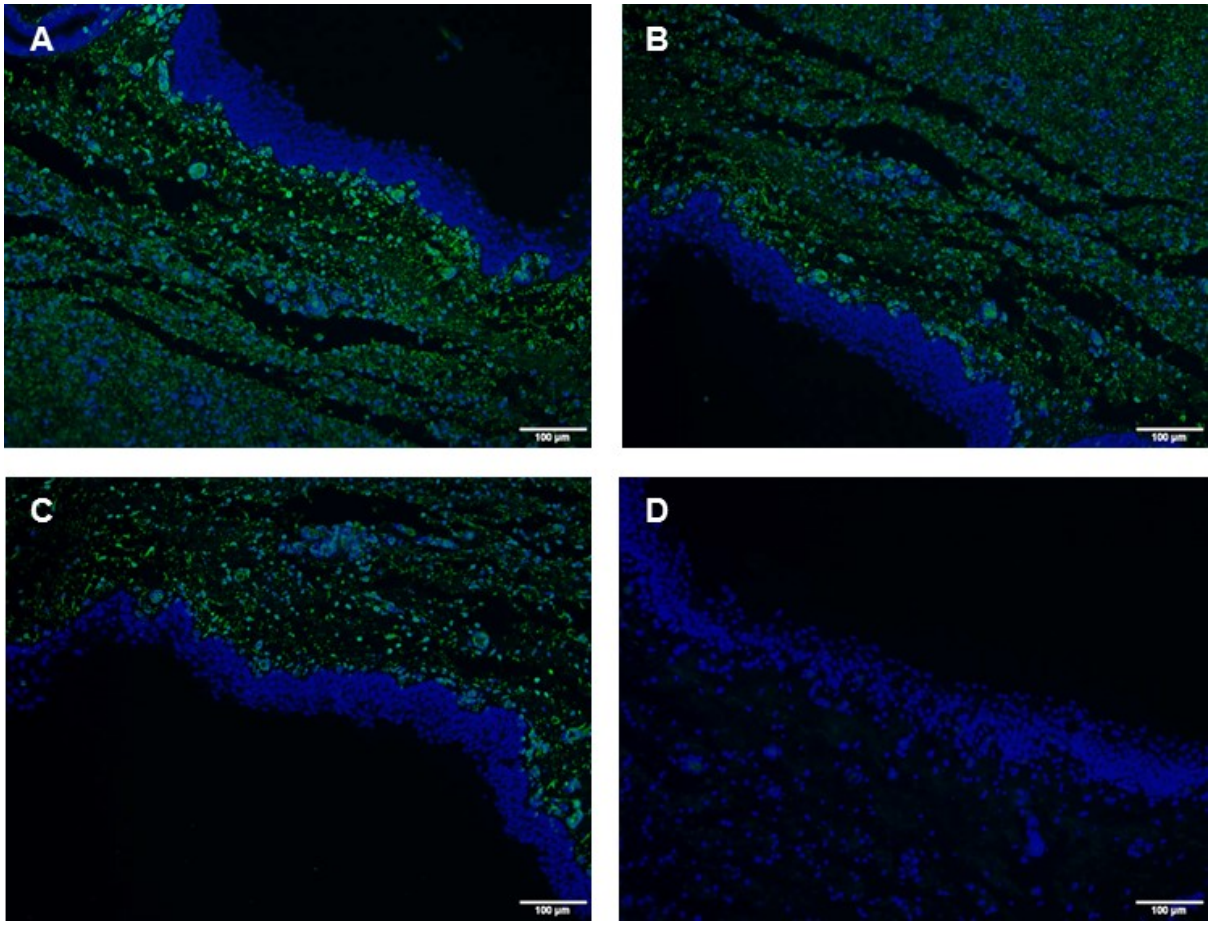

Figure 32. Representative immunohistochemical stainings of vimentin (VIM, green signal) at a concentration of 1:1000 **(A)**, 1:500 **(B)** and 1:250 **(C)** using vector antigen unmasking solution for antigen retrieval. Negative control was performed without primary antibody **(D)**. Counterstaining was performed with Hoechst (blue signal).

3.5.3. Cadherin 1 (CDH1)

For slides where antigen retrieval was performed with 0.1 % protease, no specific staining and high background were detected at an exposure time of 67 ms for the green signal when the first antibody was used at a concentration of 1:100 (Figure 33.C). Higher dilutions of the first antibody (1:500 and 1:250, Figure 33.A and B, respectively) showed more specific stainings, but still a lot of background was detected. No background was detected for negative control (Figure 33.D). Tested concentration 1:500 of primary antibody, 1:500 for secondary antibody and 1:2000 for nuclear counterstain were used for forthcoming stainings.

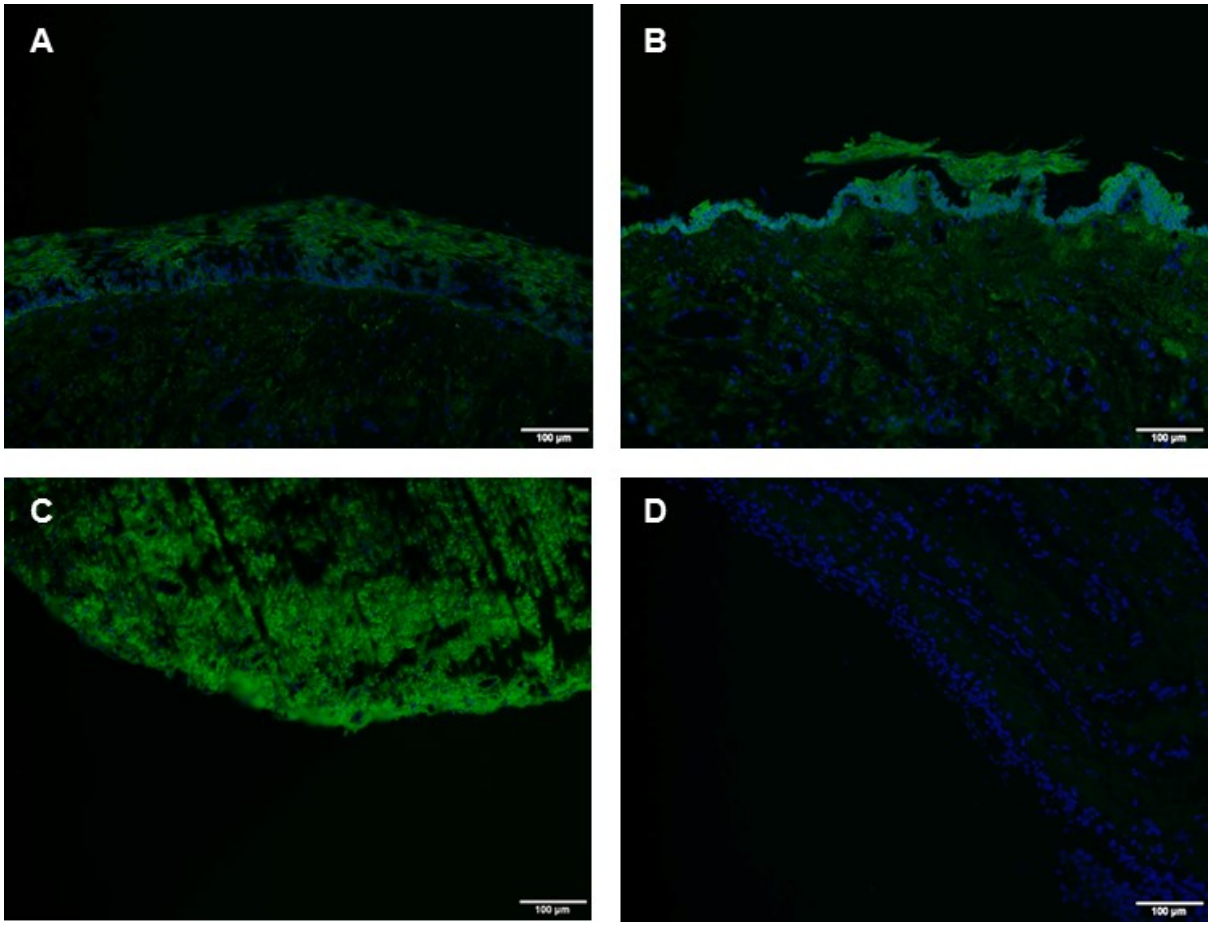

Figure 33. Representative immunohistochemical stainings of cadherin 1 (CDH1, green signal) at a concentration of 1:500 **(A)**, 1:250 **(B)** and 1:100 **(C)** using 0.1 % protease for antigen retrieval. Negative control was performed without primary antibody **(D)**. Counterstaining was performed with Hoechst (blue signal).

For slides where antigen retrieval was performed with vector antigen unmasking solution, no specific staining for cadherin 1 (CDH1, green signal) for all tested concentrations (1:250 and 1:100, Figure 33.A and B, respectively) was detected. Background was still detected for negative control (Figure 33.C).

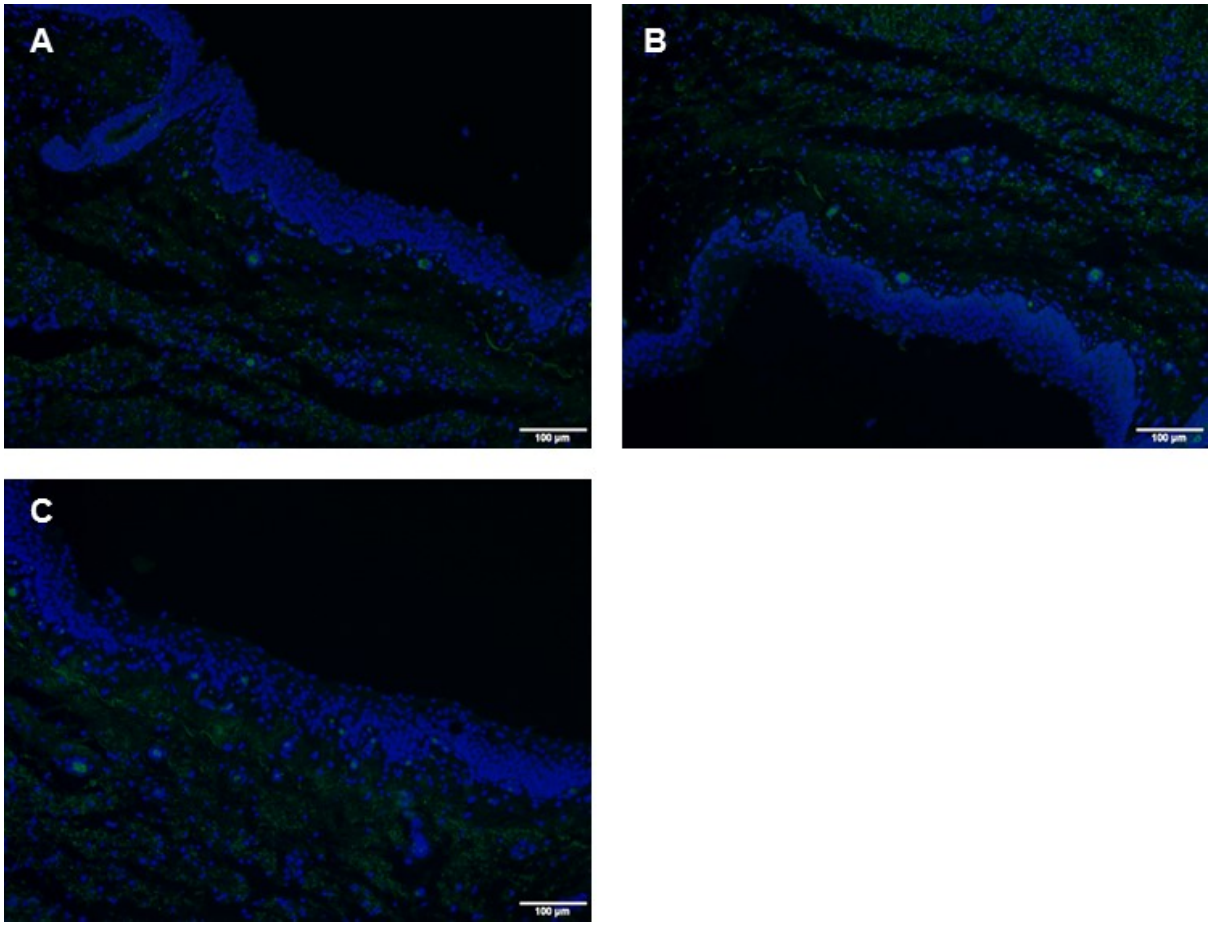

Figure 34. Representative immunohistochemical stainings of cadherin 1 (CDH1, green signal) at a concentration of 1:250 **(A)**, 1:100 **(B)** using vector antigen unmasking for antigen retrieval. Negative control was performed without primary antibody **(C)**. Counterstaining was performed with Hoechst (blue signal).

3.6. Pre-tests for proteomic analysis

3.6.1. Rat tail collagen, Type I matrix with and without hVFF

Proteomic analysis was done in cooperation with the research unit “Functional Proteomics and Metabolic Pathways” at the Medical University of Graz. Sufficient sample preparation and amount of injected samples could be validated by testing collagen matrix samples with and without embedded hVFF. Due to the missing biological and technical replicates for these analyses, different protein intensities within the samples were measured but no statistical analysis was performed. A total number of 986 proteins were detected for the hVFF cell pellet (see supplementary data, Table S 1), 185 proteins for collagen matrix with embedded hVFF (see supplementary data,

Table S 2) and 83 proteins for the collagen matrix without hVFF (see supplementary data, Table S 3).

3.6.2. Tissue preparation of native human VF

During the homogenization of native human VF tissue samples using lysis buffer, a lot of air bubbles were produced using the MagNa Lyser instrument (Test 2) resulting in an insufficient homogenization of tissue pieces after five cycles. No further cycles were performed to avoid protein degradation within the samples. A lower air bubble production was observed using the Ultra Thurrax (Test 1). Production of air bubbles could be avoided using Tris buffer for homogenization (Test 3).

Although different protein concentrations were determined for the samples (Test 1: 32.2 µg protein/mg tissue; Test 2: 20.5 µg protein/mg tissue; Test 3: 8.8 µg protein/mg tissue), similar intensity peaks for all tests and 1175 unique proteins for Test 3 could be detected.

3.7. In *vitro* application of the phonomimetic bioreactor

The application of the established phonomimetic bioreactor allowed us to gain a more detailed insight into the molecular effects of cigarette smoke and vibration, alone or in combination, on hVFF. Detailed results are prepared within the publication Grossmann et al. (262) (The Laryngoscope, article accepted on 23 May, 2020; doi:10.1002/lary.28855, “**Exploring the pathophysiology of Reinke´s edema: The cellular impact of cigarette smoke and vibration”**).

4. Discussion and future perspectives

4.1. Isolation procedure of hOMEC as part of the bioengineered 3D co-culture constructs

VF epithelium represents the first layer of cellular interaction and epithelial cells have been implicated in the development of voice disorders resulting from various stimuli (263–266). Normally, VF epithelium consists of five to ten closely packed non-keratinized stratified squamous cell layers, in contrast to keratinized cells, such as those found in the skin (267). The isolation and cultivation of human VF epithelial cells are described sparsely to date (238,255) and the established protocols are limited to use by the extremely rare possibility to obtain healthy VF mucosa biopsies. Other tissues containing proportions of non-keratinized epithelial cells include the esophagus (268), vagina (269), cornea (270) and the oral cavity (268). Therefore, epithelial cells from human oral mucosa were regarded as an alternative cell type as oral mucosa is easier to harvest with a lower risk of scarring for the donors and has already been used in laryngology (105,239). Hence, we decided to use isolated oral mucosa epithelial cells for the generation of bioengineered 3D co-culture constructs.

The isolation procedure of fibroblasts was already established by our group (254) and could be successfully used to extend the group´s existing biobank. The epithelial cell isolation was not yet performed by the group, therefore the procedure within this thesis was started according to previously published protocols (238,239,255,256). Different coatings of cell culture plates and two different growth media were used for cell isolation out of the tissue, previously enzymaticly digested using Dispase. Although unspecific cells started to grow out of the tissue within a few days, cells did not adhere to the dishes after the first passaging step. Additional literature search provided protocols using an epithelial cell-specific growth medium from CELLnTEC Advanced cell systems (257,258). Tests using this growth medium and the recommended protocol was successful. Through an additional enzymatic Accutase digestion of the separated epithelial layer, a single-cell suspension could be revealed. Recommended incubation for 10-15 minutes did not fully decompose the tissue, but longer treatment disturbed living cells within the solution. One day after seeding, cells formed multiple colonies and after approximately five to seven days, cells could be passaged and

further cultivated without any kind of coating, in contrast to previously published procedures (271–273).

Although this procedure was successfully applied, only four cultures could be established (donor age range 45-58 years, two female, two male). A relatively high number of cultures showed no colony forming, moderate cell death and reduced proliferation, or contaminations and had to be discarded. This may indicate for a highly donor-specific correlation regarding the broad margin of ages that existed within the donors (27-82 years), different sexes and medical history. In contrast to the small tissue pieces of the oral mucosa, collected during routine laryngeal surgeries, samples from autopsies were regarded as a more sufficient source to isolate a higher number of hOMEC over a lower number of passages. However, no isolation using these samples was successful due to occurred contaminations, although antibiotics and antimycotics were added to the culture medium. This probably may be caused by enhanced bacterial colonization within the oral cavity postmortem. A reduction of sampling time after death would help to overcome this limitation and should be favored but furthermore will restrict the number of available donors.

Typical cobblestone-like morphology of growing cells was microscopically observed during cultivation over a number of four to six passages. At higher passages, a shift to a spindle-shaped, fibroblast-like morphology could be observed, indicating a possible donor-related replicative senescence that may change gene expression and metabolism of isolated cells, as it is described for different types of cells (88,271,274). In the literature, only a few studies have reported the maintenance of the primary cell culture for more than ten generations (275,276). Based on this, cells up to passage number three were used for RNA-isolation and the generation of 3D-co-cultivated constructs. This further limited the experimental scope for the epithelial cell utilization, representing a major limitation of the present thesis. Reasoned by the time-consuming establishment of the isolation procedure and the limited number of tissue samples in accordance with the ethical standards, hOMEC from four different donors could be cultivated to date and also cryovials for long-term storage within the existing biobank of the group could be generated. To overcome these limitations, the traditionally used technique of immortalization of primary cells, namely transduction of the human telomerase reverse transcriptase (hTERT) gene or other oncogene-based strategies

(252,277–283) could be used in the future. Nevertheless, this procedure is accompanied by higher technical, financial and temporal requests.

Additional to the microscopical observation of cell-typical morphology, isolated hOMEC could be characterized by mRNA expression profiles of cell-type-specific marker genes (VWF, ACTN3, THY1, VIM, CK13, CK14, CDH1). Although differentially abundant expression profiles compared to the physiological levels in native VF tissue could be revealed, results have to be regarded critically due to measured variations within these samples, caused by donor-related properties (e.g. age, sex, medical history, cause of death), variable postmortem sampling time and tissue preparation. Furthermore, isolated and cultured cells may undergo a phenotypic change characterized by altered expression profiles of cell-type-specific markers *in vitro* compared to the *in vivo* state (284–286). Cultivated cell lines of endothelial cells (HUVEC) and muscle cells, besides already used hVFF, have to be included in cell-type-specific marker evaluation through RT-qPCR- and fluorescence-activated cell sorting (FACS) analysis and immunohistochemical stainings. As the limited number of isolated hOMEC was further used to start the generation of 3D co-cultivations, forthcoming isolations must be focused on the improvement and establishment of extended characterization protocols to validate the procedure as stable and highly reproducible. Additionally, profiling of microsatellite loci in the human genome harboring short tandem repeat (STR) DNA marker (287–290) should be performed to exclude cell-line cross contaminations in the isolated hOMEC. Furthermore, the growth characteristics of cells and the effect of liquid-nitrogen preservation have to be validated.

The stratified, non-keratinized squamous VF epithelium mainly acts as a functional barrier through its structural integrity that is maintained by the junctional complex consisting of tight junctions, adherens junctions, gap junctions and desmosomes (58,59). The *in vitro* measurement of this physiological function represents an important tool to quantify the barrier integrity of generated epithelial cell layers with or without the co-cultivation with other types of cells. Transepithelial electrical resistance (TEER) has been validated and used as a reliable method for this measurement (291,292). Mizuta et al. (237) developed an experimental protocol using rabbit VF epithelial cells to evaluate the epithelial barrier function over time, in response to endogenous experimental treatments. Furthermore, it is an innovative tool for the

preclinical testing of novel approaches for VF epithelium restoration after injury. The barrier function has to be validated for the isolated hOMEC in monolayer culture as well as in the reassembled epithelial layer of the bio-engineered 3D co-cultivated constructs.

4.2. Generation of bioengineered 3D co-cultivated constructs

In healthy VF, homeostasis is maintained by complex interactions between various types of cells and the ECM (227,230,231,293). Besides the protective epithelium, acting as a selective biochemical barrier (58,230,294), underlying fibroblasts within the lamina propria synthesize most of the ECM in response to signals from the surrounding environment (190,293). It is widely accepted that direct signaling events between multiple cell types are crucial in growth, migration, and differentiation of cells, but the underlying mechanisms remain largely unexplored (295–297). Most research, has either focused on fibroblasts (214,298–301) or epithelial cells (227,237), while little is known about the epithelial-fibroblast signaling within the VF. To overcome this, the field of tissue engineering and 3D co-cultivation *in vitro,* simulating the direct contact between cell types, have reached broad interest of researchers for applications in regenerative medicine, basic research and pharmacy. Various scaffolds including natural derivatives, ECM protein-based scaffolds, synthetic materials and cross-linking technologies are described (253,302–304).

The collagen-based technique was applied in this thesis according to its abundance in native human VF tissue, cytocompatibility, and use in previous organotypic cultures and engineered tissues (305–307). Collagen from different non-human origins was described to be used for the generation of 3D *in vitro* models of the human oral mucosa (308) and of the human VF mucosa (238,239).

As the main structural component of the engineered 3D construct, the generation of a rat tail collagen-fibroblast matrix was successfully established within this thesis. Considering that differentiation of the unique complexity of the native lamina propria of the VF during human development lasts more than ten years (309), we could not fully recapitulate this *in vitro*. Similar to results from Ling et al. (238), a relatively high matrix contraction was observed in our experiments, whereas no correlation with the seeding density of hVFF could be confirmed. In contrast, Hahn et al. (299) observed no

reduction in gel diameter but a mass loss of about 55 % for constructs consistent of isolated porcine VFF within a rat tail collagen-hyaluronic acid scaffold, whereas collagen was used at a higher final concentration. For our procedure, a stable averaged plateau of ~ 53 % of the initial cross-sectional area compared to the collagen matrix without fibroblasts was seen, comparable to results from Jetté et al. (134). Slight differences can be explained by a possible altered cellular interaction of used immortalized hVFF instead of isolated primary cells.

Fibroblasts are described to produce a large proportion of the ECM components (197,310). Thus, contraction and augmentation of the collagen matrix seemed to be mainly driven by stress-related endogenous ECM production of collagen-embedded fibroblasts (134,238,299,311,312). This could be demonstrated by validated gene and protein expression profiles of ECM-related genes that are considered critical for the biomechanical function of native VF mucosa (63,313), whereas evaluated preliminary results of initial, but limited proteomic analysis have to be interpreted critically due to the lack of biological and technical replicates.

Embedded fibroblasts showed down-regulated gene expression of all three isoforms of hyaluronan synthases (HAS1, 2, and 3) that are responsible for the synthesis of hyaluronic acid (HA) (314), an important component of the native VF lamina propria providing the viscoelasticity of the tissue (313). Elastin (ELN) is a fibrous protein and major component of elastic fibers and is critical to biomechanical tissue performance by facilitating elasticity of the lamina propria (63,313). We revealed a slightly up-regulated gene expression of ELN within the collagen-fibroblast matrix. Nevertheless, both mature proteins could not be detected. Hence, protein abundance of HA and ELN have to be validated within the full 3D co-cultivated constructs due to their effect on elastic tissue properties.

Fibronectin (FN), the most abundant ECM glycoprotein (315) is described to function as an adhesion molecule for cell-cell and cell-ECM interactions generally (316) and even in VF (313). Although FN1 gene expression of fibroblasts embedded in collagen was significantly down-regulated, the mature protein was assembled within the collagen-fibroblast matrix compared to the collagen scaffold alone (317). The same was evaluated for collagen I alpha 1 (COL1A1), whereas COL1A1 was also detected

in the scaffold alone, but at a lower intensity, indicating a higher existing stiffness of the collagen-fibroblast matrix.

The collagen matrix did not significantly change fibroblast gene expression of actin alpha 2 smooth muscle (ACTA2) but the mature protein was detected, whereas protein levels in the collagen scaffold alone were not measured. ACTA2 overexpression is a well-accepted marker of fibroblast transdifferentiation (135,136) into myofibroblasts, mainly responsible for excessive ECM deposition and scar contraction. However, this phenotypic cellular change has also been shown to be normal during differentiation of fibroblasts in culture (134,318,319).

Matrix metalloproteinases (MMP) are involved in the degradation of ECM molecules, including FN, ELN, and type I and III collagens (320). Our finding, a significant downregulation of MMP1 gene expression in collagen-embedded fibroblasts with no detected protein levels, corresponded to the fibroblast-augmented endogenous ECM production within the constructs. This could be further improved, as gene expression of tissue inhibitor of MMP (TIMP)-1 was not altered and protein levels were not detected within the collagen-fibroblast matrix.

Both integrin subunit proteins (ITGA2 and ITGB1) were exclusively detected within the collagen matrix containing fibroblasts, although their gene expression levels were differentially changed by collagen (ITGA2 up-regulated and ITGB1 down-regulated). These membrane receptor proteins participate in binding interactions between fibroblasts and the surrounding collagen fibrils (134,311).

A greater maturation of the collagen-fibroblast matrix, closer to the native complex structure of the lamina propria, could be accomplished by an extended cultivation time, addition of HA- and ELN-based matrix components or the use of more architecturally relevant scaffold materials, such as decellularized VF mucosa (321,322).

Nevertheless, the established collagen-fibroblast matrix co-cultivated with isolated hOMEC reassembled native mucosa comparable to the native VF after a total cultivation of 35 days. The engineered construct demonstrated key morphologic characteristics of native mucosa including a multilayered epithelium and a continuous basement membrane. This was achieved in the presence of a so-called air-liquid interface (ALI) during cultivation, embedded fibroblasts and appropriate media. It is well documented that the presence of both fibroblasts and epithelial cells is needed for

the growth of a multilayered epithelium (234,235). Although we confirmed this in our experiments, we could further show that a high density of embedded fibroblasts, as well as the presence of collagen acting as scaffold, was critical for generating a complex structure of the underlying lamina propria *in vitro*.

Further analysis of the ongoing work must focus on the characterization of the epithelial cell layers using immunohistochemical stainings for cell-type-specific markers. In the native VF epithelium, closely to the basement membrane appositioned basal cells express nerve growth factor receptor (NGFR/p75) and cytokeratin (CK) 14 within the bottom three to four layers. The majority of basal cells sparsely express CK13 which is expressed throughout the entire epithelium but at the highest levels within the suprabasal layers (57,235). Intercellular junctions, including adherens junctions (221), tight junctions (221,323), gap junctions (324), and desmosomes (323) within the native VF epithelium represent important components of barrier function. The presence of E-cadherin (CDH1), a marker of adherens junctions, could be revealed in our construct, further evidence of intercellular junctions was not provided and has to be processed in ongoing work. In the native VF tissue, CDH1-stained epithelial cells were preferentially localized to the apical epithelium, whereas background signal was also detected throughout the entire lamina propria. Lower, but comparable signal could be detected for the engineered construct. Additionally, cells throughout the entire construct expressed vimentin (VIM), a mesenchymal marker, contrary to the native VF tissue showing VIM-stained cells restricted within the lamina propria. Based on results from Walimbe et al. (233), this might be explained by a possible epithelial-mesenchymal transition (EMT), characterized by a reduced expression of epithelial adhesion proteins like CDH1 and an increased expression of mesenchymal markers such as VIM and alpha smooth muscle actin (α-SMA) (325,326). Further evaluation of EMT in monocultures of isolated hOMEC has to be analyzed.

In line with results from Leydon et al. (235), but contrary to studies from Yamaguchi et al. (234) and Long et al. (327), we could show an assembly of a basement membrane within our engineered construct. Besides its critical role in tissue development (328), cell differentiation (329), and growth factor cell signaling (330), the basement membrane presents an important component of the native VF mucosa by attaching epithelial cells to the underlying ECM.

The major limitation of the present study is the lack of replicates as we were only able to engineer one construct that reassembled native mucosa comparable to the native VF. Two further constructs using hOMEC from other donors were cultured but did not reassemble a multilayered epithelium, indicating a possible donor-specific effect, not only in the isolation, but also in the utilization of cells *in vitro*. Ongoing work is needed to improve the culture microenvironment (e.g. by addition of supplements to the culture medium or by an enhanced seeding density of hOME), to produce a suffice number of constructs to assess gene expression- and proteome-level evidence of mucosal morphogenesis and ECM complexity compared to native VF mucosa. Future applications of the bioengineered 3D cultivated constructs will include the identification and manipulation of mechanisms underlying fibroblasts and epithelial cells, comparison of cellular crosstalk in response to daily irritants alone or combined with vibration using the engineered dynamic bioreactor of our group LTTEG (246).

4.3. Phonomimetic bioreactor and its *in vitro* application

Several models of dynamic bioreactors have been engineered and published by us and others (25,240–245) taking into consideration the unique biomechanical character of the VF. Nevertheless, none fully integrates the complex biomechanical environment combined with the unique structure of the native VF tissue. The engineered phonomimetic bioreactor (246) from our LTTEG research group allowed us to explore the combined effects of the external stimulus cigarette smoke and vibration on the cellular level of fibroblasts *in vitro*.

Compared to previous more sophisticated models (25,241), our used bioreactor represents a simple, cost-effective device that showed similar effects of vibration on the cultured cells (246). The application of custom-designed sound files enabled us to vary vibration frequencies and patterns within the broad tested reactor frequency range (50-2500 Hz). Propagated sound waves from the loudspeaker were directly transferred to the used cell culture plates and enabled simultaneous vibration of all six wells. This enhanced the experimental scope which could be utilized, compared to other used bioreactors (242,243). Similar to the designed model from Kim et al. (245), we were able to visualize the cells *in situ* on a standard microscope, but our device could avoid any agitation and fluid perturbation within the wells, as vibration was not mechanically-

induced. Nevertheless, we could not simulate all physiologically relevant *in vivo* forces acting the VF mucosa, as vibration is only one isolated biomechanical factor.
Aerodynamic driving forces, caused by periodic opening and closing of the glottis during phonation and usually accompanied by a collision between the folds (25) could not be simulated. Development strategies to mimic the airflow-induced biomechanical stimulation by an integrated flow perfusion, as described by Latifi et al. (25), will be focused in ongoing work.
Simulation of other physiological forces, such as tensile stress and dynamic angle changes (243), or the collisions between the folds (25), provided in previously designed bioreactors, will probably not be possible with our device.
In the current study (262) we focused our work on fibroblasts as they produce a large proportion of the ECM components and thereby substantially determine the native VF mucosa characteristics (231,310) and play a central role in the development of Reinke´s edema (331–334). Although we were able to simulate external stimulation *in vitro*, the two-dimensional nature of the experiments represents a further limitation of the used bioreactor. The next step would be to evaluate the effects of vibration using the collagen-fibroblast matrix which was established within this thesis as biomechanical stimulation is described as a decisive factor in the development of the lamina propria microstructure (335). This will provide an innovative, stable and reproducible *in vitro* model to study and identify the underlying molecular processes in the context of VF (patho)physiology, and thereby will significantly enhance current knowledge of physiological and pathophysiological mechanisms.

A more sophisticated strategy will be to use the bioengineered 3D cultivated constructs of fibroblasts and epithelial cells in the dynamic bioreactor. This would resemble the native VF mucosa and would allow studying cell interactions within the VF, as well as provide an *in vitro* platform for preclinical drug testing and alternative treatments such as laryngeal mucosal transplantation.
Nevertheless, there are plenty of aspects that need to be considered. The limited number of epithelial cells will substantially restrict this application. Therfore, the isolation procedure has to be honed as mentioned above. The full construct has to withstand physiologically relevant mechanical conditions during vibration probably requiring a greater maturation *in vitro*. Besides an extended cultivation time, and the

use of more architecturally relevant scaffold materials as previously described, this might be provided by phonation-relevant exposure to mechanical forces (243). Nevertheless, the validated secured anchoring to the underlying lamina propria and emergence of intercellular junctional complexes within our constructs let us hypothesize a low risk of shearing of the engineered epithelium from the construct due to the vibrational stimulation.

To conclude, the present thesis substantially contributed to the ongoing projects of the LTTEG working group and provided additional basic data to enhance the recently used *in vitro* cell culture models, in order to gain a better insight into the cellular and molecular mechanisms underlying VF function in health, disease and injury. Nevertheless, more precise and frequent experiments have to be performed, to hone the isolation procedure of epithelial cells and thereby improve the construction of multicellular constructs and the use of the phonomimetic bioreactor.

5. Literature

1. Kumar V, Croxson PL, Simonyan K. Structural Organization of the Laryngeal Motor Cortical Network and Its Implication for Evolution of Speech Production. J Neurosci. 2016 Apr 13;36(15):4170–81.

2. Roy N, Merrill RM, Gray SD, Smith EM. Voice disorders in the general population: prevalence, risk factors, and occupational impact. Laryngoscope. 2005 Nov;115(11):1988–95.

3. Ramig LO, Verdolini K. Treatment efficacy: voice disorders. J Speech Lang Hear Res. 1998 Feb;41(1):S101-116.

4. Benninger MS, Alessi D, Archer S, Bastian R, Ford C, Koufman J, et al. Vocal fold scarring: current concepts and management. Otolaryngol Head Neck Surg. 1996 Nov;115(5):474–82.

5. Koufman JA, Blalock PD. Functional voice disorders. Otolaryngol Clin North Am. 1991 Oct;24(5):1059–73.

6. Nourmahnad A, Benboujja F, Hartnick CJ. Using intraoperative optical coherence tomography to image pediatric unilateral vocal fold paralysis. Int J Pediatr Otorhinolaryngol. 2019 Jun;121:72–5.

7. Pham TT, Chen L, Heidari AE, Chen JJ, Zhukhovitskaya A, Li Y, et al. Computational analysis of six optical coherence tomography systems for vocal fold imaging: A comparison study. Lasers Surg Med. 2019 Jan 25;

8. Heris HK, Miri AK, Ghattamaneni NR, Li NYK, Thibeault SL, Wiseman PW, et al. Microstructural and mechanical characterization of scarred vocal folds. J Biomech. 2015 Feb 26;48(4):708–11.

9. Miri AK, Heris HK, Tripathy U, Wiseman PW, Mongeau L. Microstructural characterization of vocal folds toward a strain-energy model of collagen remodeling. Acta Biomater. 2013 Aug;9(8):7957–67.

10. Tanaka S, Gould WJ. Relationships between vocal intensity and noninvasively obtained aerodynamic parameters in normal subjects. J Acoust Soc Am. 1983 Apr;73(4):1316–21.

11. Holmberg EB, Hillman RE, Perkell JS. Glottal airflow and transglottal air pressure measurements for male and female speakers in soft, normal, and loud voice. J Acoust Soc Am. 1988 Aug;84(2):511–29.

12. Roberts T, Morton R, Al-Ali S. Microstructure of the vocal fold in elderly humans. Clin Anat. 2011 Jul;24(5):544–51.

13. Gunter HE. Modeling mechanical stresses as a factor in the etiology of benign vocal fold lesions. J Biomech. 2004 Jul;37(7):1119–24.

14. Redford MA, editor. The Handbook of Speech Production: Redford/The Handbook of Speech Production [Internet]. Hoboken, NJ: John Wiley & Sons, Inc; 2015 [cited 2020 May 12]. Available from: http://doi.wiley.com/10.1002/9781118584156

15. Jiang J, Lin E, Hanson DG. Vocal fold physiology. Otolaryngol Clin North Am. 2000 Aug;33(4):699–718.

16. Jürgens U. Neural pathways underlying vocal control. Neurosci Biobehav Rev. 2002 Mar;26(2):235–58.

17. Rubin AD, Sataloff RT. Vocal fold paresis and paralysis. Otolaryngol Clin North Am. 2007 Oct;40(5):1109–31, viii–ix.

18. Li NYK, Heris HK, Mongeau L. Current Understanding and Future Directions for Vocal Fold Mechanobiology. J Cytol Mol Biol. 2013 Apr 1;1(1):001.

19. Sataloff RT. Sataloffs Comprehensive Textbook of Otolaryngology: Head and Neck Surgery. Head and Neck Surgery: Pediatric Otolaryngology 6 6. 2016.

20. Van Den Berg J. Myoelastic-aerodynamic theory of voice production. J Speech Hear Res. 1958 Sep;1(3):227–44.

21. van den Berg Jw, Zantema JT, Doornenbal P. On the Air Resistance and the Bernoulli Effect of the Human Larynx. The Journal of the Acoustical Society of America. 1957 May;29(5):626–31.

22. Titze IR, Martin DW. *Principles of Voice Production*. The Journal of the Acoustical Society of America. 1998 Sep;104(3):1148–1148.

23. Titze IR. The physics of small-amplitude oscillation of the vocal folds. J Acoust Soc Am. 1988 Apr;83(4):1536–52.

24. Story BH. Mechanisms of Voice Production. In: Redford MA, editor. The Handbook of Speech Production [Internet]. Hoboken, NJ: John Wiley & Sons, Inc; 2015 [cited 2020 May 12]. p. 34–58. Available from: http://doi.wiley.com/10.1002/9781118584156.ch3

25. Latifi N, Heris HK, Thomson SL, Taher R, Kazemirad S, Sheibani S, et al. A Flow Perfusion Bioreactor System for Vocal Fold Tissue Engineering Applications. Tissue Eng Part C Methods. 2016;22(9):823–38.

26. Patel R, Dubrovskiy D, Döllinger M. Characterizing vibratory kinematics in children and adults with high-speed digital imaging. J Speech Lang Hear Res. 2014 Apr 1;57(2):S674-686.

27. Titze IR. On the relation between subglottal pressure and fundamental frequency in phonation. J Acoust Soc Am. 1989 Feb;85(2):901–6.

28. Isshiki N. REGULATORY MECHANISM OF VOICE INTENSITY VARIATION. J Speech Hear Res. 1964 Mar;7:17–29.

29. Hirano M, Ohala J, Vennard W. The function of laryngeal muscles in regulating fundamental frequency and intensity of phonation. J Speech Hear Res. 1969 Sep;12(3):616–28.

30. Hirano M, Vennard W, Ohala J. Regulation of register, pitch and intensity of voice. An electromyographic investigation of intrinsic laryngeal muscles. Folia Phoniatr (Basel). 1970;22(1):1–20.

31. Gay T, Hirose H, Strome M, Sawashima M. Electromyography of the intrinsic laryngeal muscles during phonation. Ann Otol Rhinol Laryngol. 1972 Jun;81(3):401–9.

32. Stathopoulos ET, Sapienza C. Respiratory and laryngeal function of women and men during vocal intensity variation. J Speech Hear Res. 1993 Feb;36(1):64–75.

33. Henrich N, D'Alessandro C, Doval B, Castellengo M. Glottal open quotient in singing: measurements and correlation with laryngeal mechanisms, vocal intensity, and fundamental frequency. J Acoust Soc Am. 2005 Mar;117(3 Pt 1):1417–30.

34. Van Den Berg J, Tan TS. Results of experiments with human larynxes. Pract Otorhinolaryngol (Basel). 1959 Nov;21:425–50.

35. Moore DM, Berke GS. The effect of laryngeal nerve stimulation on phonation: a glottographic study using an in vivo canine model. J Acoust Soc Am. 1988 Feb;83(2):705–15.

36. Sloan SH, Berke GS, Gerratt BR, Kreiman J, Ye M. Determination of vocal fold mucosal wave velocity in an in vivo canine model. Laryngoscope. 1993 Sep;103(9):947–53.

37. Slavit DH, McCaffrey TV, Yanagi E. Effect of superior laryngeal nerve on vocal fold function: an in vivo canine model. Otolaryngol Head Neck Surg. 1991 Dec;105(6):857–63.

38. Berke GS, Moore DM, Gerratt BR, Hanson DG, Natividad M. Effect of superior laryngeal nerve stimulation on phonation in an in vivo canine model. Am J Otolaryngol. 1989 Jun;10(3):181–7.

39. Alipour F, Jaiswal S, Vigmostad S. Vocal fold elasticity in the pig, sheep, and cow larynges. J Voice. 2011 Mar;25(2):130–6.

40. Alipour F, Jaiswal S. Glottal airflow resistance in excised pig, sheep, and cow larynges. J Voice. 2009 Jan;23(1):40–50.

41. Alipour F, Jaiswal S. Phonatory characteristics of excised pig, sheep, and cow larynges. J Acoust Soc Am. 2008 Jun;123(6):4572–81.

42. Döllinger M, Kniesburges S, Berry DA, Birk V, Wendler O, Dürr S, et al. Investigation of phonatory characteristics using ex vivo rabbit larynges. J Acoust Soc Am. 2018;144(1):142.

43. Murray PR, Thomson SL. Vibratory responses of synthetic, self-oscillating vocal fold models. J Acoust Soc Am. 2012 Nov;132(5):3428–38.

44. Shaw SM, Thomson SL, Dromey C, Smith S. Frequency response of synthetic vocal fold models with linear and nonlinear material properties. J Speech Lang Hear Res. 2012 Oct;55(5):1395–406.

45. Titze IR, Schmidt SS, Titze MR. Phonation threshold pressure in a physical model of the vocal fold mucosa. J Acoust Soc Am. 1995 May;97(5 Pt 1):3080–4.

46. Chan RW, Titze IR, Titze MR. Further studies of phonation threshold pressure in a physical model of the vocal fold mucosa. J Acoust Soc Am. 1997 Jun;101(6):3722–7.

47. Ruty N, Pelorson X, Van Hirtum A, Lopez-Arteaga I, Hirschberg A. An in vitro setup to test the relevance and the accuracy of low-order vocal folds models. J Acoust Soc Am. 2007 Jan;121(1):479–90.

48. Yang A, Berry DA, Kaltenbacher M, Döllinger M. Three-dimensional biomechanical properties of human vocal folds: parameter optimization of a numerical model to match in vitro dynamics. J Acoust Soc Am. 2012 Feb;131(2):1378–90.

49. Yang A, Lohscheller J, Berry DA, Becker S, Eysholdt U, Voigt D, et al. Biomechanical modeling of the three-dimensional aspects of human vocal fold dynamics. J Acoust Soc Am. 2010 Feb;127(2):1014–31.

50. Zhang Z. Regulation of glottal closure and airflow in a three-dimensional phonation model: implications for vocal intensity control. J Acoust Soc Am. 2015 Feb;137(2):898–910.

51. Zhang Z. Cause-effect relationship between vocal fold physiology and voice production in a three-dimensional phonation model. J Acoust Soc Am. 2016;139(4):1493.

52. Ishizaka K, Flanagan JL. Synthesis of Voiced Sounds From a Two-Mass Model of the Vocal Cords. Bell System Technical Journal. 1972 Jul 8;51(6):1233–68.

53. Pickup BA, Thomson SL. Identification of geometric parameters influencing the flow-induced vibration of a two-layer self-oscillating computational vocal fold model. J Acoust Soc Am. 2011 Apr;129(4):2121–32.

54. Yang A, Stingl M, Berry DA, Lohscheller J, Voigt D, Eysholdt U, et al. Computation of physiological human vocal fold parameters by mathematical optimization of a biomechanical model. J Acoust Soc Am. 2011 Aug;130(2):948–64.

55. Döllinger M, Gómez P, Patel RR, Alexiou C, Bohr C, Schützenberger A. Biomechanical simulation of vocal fold dynamics in adults based on laryngeal high-speed videoendoscopy. PLoS ONE. 2017;12(11):e0187486.

56. Jiang W, Xue Q, Zheng X. Effect of Longitudinal Variation of Vocal Fold Inner Layer Thickness on Fluid-Structure Interaction During Voice Production. J Biomech Eng. 2018 01;140(12).

57. Dowdall JR, Sadow PM, Hartnick C, Vinarsky V, Mou H, Zhao R, et al. Identification of distinct layers within the stratified squamous epithelium of the adult human true vocal fold. Laryngoscope. 2015 Sep;125(9):E313-319.

58. Levendoski EE, Leydon C, Thibeault SL. Vocal fold epithelial barrier in health and injury: a research review. J Speech Lang Hear Res. 2014 Oct;57(5):1679–91.

59. Tsukita S, Furuse M, Itoh M. Multifunctional strands in tight junctions. Nat Rev Mol Cell Biol. 2001 Apr;2(4):285–93.

60. Hirschi SD, Gray SD, Thibeault SL. Fibronectin: an interesting vocal fold protein. J Voice. 2002 Sep;16(3):310–6.

61. Gray SD, Pignatari SS, Harding P. Morphologic ultrastructure of anchoring fibers in normal vocal fold basement membrane zone. J Voice. 1994 Mar;8(1):48–52.

62. Hammond TH, Zhou R, Hammond EH, Pawlak A, Gray SD. The intermediate layer: a morphologic study of the elastin and hyaluronic acid constituents of normal human vocal folds. J Voice. 1997 Mar;11(1):59–66.

63. Gray SD, Titze IR, Alipour F, Hammond TH. Biomechanical and histologic observations of vocal fold fibrous proteins. Ann Otol Rhinol Laryngol. 2000 Jan;109(1):77–85.

64. Madruga de Melo EC, Lemos M, Aragão Ximenes Filho J, Sennes LU, Nascimento Saldiva PH, Tsuji DH. Distribution of collagen in the lamina propria of the human vocal fold. Laryngoscope. 2003 Dec;113(12):2187–91.

65. Buhler RB, Sennes LU, Mauad T, Melo ECM, Silva LFF, Saldiva PHN. Collagen fiber and versican distribution within the lamina propria of fetal vocal folds. Laryngoscope. 2008 Feb;118(2):371–4.

66. Tang SS, Mohad V, Gowda M, Thibeault SL. Insights Into the Role of Collagen in Vocal Fold Health and Disease. J Voice. 2017 Sep;31(5):520–7.

67. Moore J, Thibeault S. Insights into the role of elastin in vocal fold health and disease. J Voice. 2012 May;26(3):269–75.

68. Gunter HE, Howe RD, Zeitels SM, Kobler JB, Hillman RE. Measurement of vocal fold collision forces during phonation: methods and preliminary data. J Speech Lang Hear Res. 2005 Jun;48(3):567–76.

69. Hirano M. Morphological structure of the vocal cord as a vibrator and its variations. Folia Phoniatr (Basel). 1974;26(2):89–94.

70. Min YB, Titze IR, Alipour-Haghighi F. Stress-strain response of the human vocal ligament. Ann Otol Rhinol Laryngol. 1995 Jul;104(7):563–9.

71. Tran QT, Berke GS, Gerratt BR, Kreiman J. Measurement of Young's modulus in the in vivo human vocal folds. Ann Otol Rhinol Laryngol. 1993 Aug;102(8 Pt 1):584–91.

72. Chhetri DK, Zhang Z, Neubauer J. Measurement of Young's modulus of vocal folds by indentation. J Voice. 2011 Jan;25(1):1–7.

73. Sakae FA, Imamura R, Sennes LU, Tsuji DH, Mauad T, Saldiva PHN. Elastic fibers in Reinke's edema. Ann Otol Rhinol Laryngol. 2010 Sep;119(9):609–14.

74. Sakae FA, Imamura R, Sennes LU, Mauad T, Saldiva PH, Tsuji DH. Disarrangement of collagen fibers in Reinke's edema. Laryngoscope. 2008 Aug;118(8):1500–3.

75. Tateya T, Tateya I, Bless DM. Collagen subtypes in human vocal folds. Ann Otol Rhinol Laryngol. 2006 Jun;115(6):469–76.

76. Maturo S, Benboujja F, Boudoux C, Hartnick C. Quantitative distinction of unique vocal fold subepithelial architectures using optical coherence tomography. Ann Otol Rhinol Laryngol. 2012 Nov;121(11):754–60.

77. Burns JA, Zeitels SM, Anderson RR, Kobler JB, Pierce MC, de Boer JF. Imaging the mucosa of the human vocal fold with optical coherence tomography. Ann Otol Rhinol Laryngol. 2005 Sep;114(9):671–6.

78. Jungheim M, Donner S, Bleeker S, Ripken T, Krueger A, Ptok M. Effect of saline inhalation on vocal fold epithelial morphology evaluated by optical coherence tomography. Laryngoscope. 2016;126(10):E332-336.

79. Benboujja F, Hartnick C. Clinical and surgical implications of intraoperative optical coherence tomography imaging for benign pediatric vocal fold lesions. Int J Pediatr Otorhinolaryngol. 2018 Nov;114:111–9.

80. Zhang Z, Wu L, Gray R, Chhetri DK. Three-dimensional vocal fold structural change due to implant insertion in medialization laryngoplasty. PLoS ONE. 2020;15(1):e0228464.

81. Bailly L, Cochereau T, Orgéas L, Henrich Bernardoni N, Rolland du Roscoat S, McLeer-Florin A, et al. 3D multiscale imaging of human vocal folds using synchrotron X-ray microtomography in phase retrieval mode. Sci Rep. 2018 18;8(1):14003.

82. Miri AK, Tripathy U, Mongeau L, Wiseman PW. Nonlinear laser scanning microscopy of human vocal folds. Laryngoscope. 2012 Feb;122(2):356–63.

83. Coyle SM, Weinrich BD, Stemple JC. Shifts in relative prevalence of laryngeal pathology in a treatment-seeking population. J Voice. 2001 Sep;15(3):424–40.

84. Bertelsen C, Zhou S, Hapner ER, Johns MM. Sociodemographic Characteristics and Treatment Response Among Aging Adults With Voice Disorders in the United States. JAMA Otolaryngol Head Neck Surg. 2018 01;144(8):719–26.

85. Golub JS, Chen P-H, Otto KJ, Hapner E, Johns MM. Prevalence of perceived dysphonia in a geriatric population. J Am Geriatr Soc. 2006 Nov;54(11):1736–9.

86. Turley R, Cohen S. Impact of voice and swallowing problems in the elderly. Otolaryngol Head Neck Surg. 2009 Jan;140(1):33–6.

87. Pontes P, Yamasaki R, Behlau M. Morphological and functional aspects of the senile larynx. Folia Phoniatr Logop. 2006;58(3):151–8.

88. Chen X, Thibeault SL. Characteristics of age-related changes in cultured human vocal fold fibroblasts. Laryngoscope. 2008 Sep;118(9):1700–4.

89. Branco A, Rodrigues SA, Fabro AT, Fonseca-Alves CE, Martins RHG. Hyaluronic acid behavior in the lamina propria of the larynx with advancing age. Otolaryngol Head Neck Surg. 2014 Oct;151(4):652–6.

90. Branco A, Todorovic Fabro A, Gonçalves TM, Garcia Martins RH. Alterations in extracellular matrix composition in the aging larynx. Otolaryngol Head Neck Surg. 2015 Feb;152(2):302–7.

91. Butler JE, Hammond TH, Gray SD. Gender-related differences of hyaluronic acid distribution in the human vocal fold. Laryngoscope. 2001 May;111(5):907–11.

92. Altman KW. Vocal fold masses. Otolaryngol Clin North Am. 2007 Oct;40(5):1091–108, viii.

93. Verdolini K, Rosen CA, Branski RC, Andrews ML, American Speech-Language-Hearing Association, editors. Classification manual for voice disorders-I. Mahwah, N.J: Lawrence Erlbaum; 2006. 284 p.

94. Reiter R, Hoffmann TK, Pickhard A, Brosch S. Hoarseness-causes and treatments. Dtsch Arztebl Int. 2015 May 8;112(19):329–37.

95. Ahn A, Wang L, Slaughter JC, Nguyen AM, Ossoff RH, Francis DO. Serial full-thickness excision of dysplastic vocal fold leukoplakia: Diagnostic or therapeutic? Laryngoscope. 2016 Apr;126(4):923–7.

96. Cervigne NK, Machado J, Goswami RS, Sadikovic B, Bradley G, Perez-Ordonez B, et al. Recurrent genomic alterations in sequential progressive leukoplakia and oral cancer: drivers of oral tumorigenesis? Hum Mol Genet. 2014 May 15;23(10):2618–28.

97. Walton C, Conway E, Blackshaw H, Carding P. Unilateral Vocal Fold Paralysis: A Systematic Review of Speech-Language Pathology Management. J Voice. 2017 Jul;31(4):509.e7-509.e22.

98. Patel RR, Unnikrishnan H, Donohue KD. Effects of Vocal Fold Nodules on Glottal Cycle Measurements Derived from High-Speed Videoendoscopy in Children. PLoS ONE. 2016;11(4):e0154586.

99. Martins RHG, Defaveri J, Domingues MAC, de Albuquerque e Silva R. Vocal polyps: clinical, morphological, and immunohistochemical aspects. J Voice. 2011 Jan;25(1):98–106.

100. Gu J, Huang Y. β-Defensin-2 is overexpressed in human vocal cord polyps. Eur Arch Otorhinolaryngol. 2017 Feb;274(2):901–7.

101. Roy N, Kim J, Courey M, Cohen SM. Voice disorders in the elderly: A national database study. Laryngoscope. 2016 Feb;126(2):421–8.

102. Thibeault SL, Gray SD, Bless DM, Chan RW, Ford CN. Histologic and rheologic characterization of vocal fold scarring. J Voice. 2002 Mar;16(1):96–104.

103. Hirano S. Current treatment of vocal fold scarring. Curr Opin Otolaryngol Head Neck Surg. 2005 Jun;13(3):143–7.

104. Graupp M, Bachna-Rotter S, Gerstenberger C, Friedrich G, Fröhlich-Sorger E, Kiesler K, et al. The unsolved chapter of vocal fold scars and how tissue engineering could help us solve the problem. Eur Arch Otorhinolaryngol. 2016 Sep;273(9):2279–84.

105. Friedrich G, Dikkers FG, Arens C, Remacle M, Hess M, Giovanni A, et al. Vocal fold scars: current concepts and future directions. Consensus report of the Phonosurgery Committee of the European Laryngological Society. Eur Arch Otorhinolaryngol. 2013 Sep;270(9):2491–507.

106. Sataloff RT, Spiegel JR, Hawkshaw MJ. Strobovideolaryngoscopy: results and clinical value. Ann Otol Rhinol Laryngol. 1991 Sep;100(9 Pt 1):725–7.

107. Lindley LE, Stojadinovic O, Pastar I, Tomic-Canic M. Biology and Biomarkers for Wound Healing. Plast Reconstr Surg. 2016 Sep;138(3 Suppl):18S-28S.

108. Eming SA, Martin P, Tomic-Canic M. Wound repair and regeneration: mechanisms, signaling, and translation. Sci Transl Med. 2014 Dec 3;6(265):265sr6.

109. Witte MB, Barbul A. General principles of wound healing. Surg Clin North Am. 1997 Jun;77(3):509–28.

110. Wang P-H, Huang B-S, Horng H-C, Yeh C-C, Chen Y-J. Wound healing. J Chin Med Assoc. 2018;81(2):94–101.

111. Ehrlich HP, Krummel TM. Regulation of wound healing from a connective tissue perspective. Wound Repair Regen. 1996 Jun;4(2):203–10.

112. Serini G, Gabbiana G. Modulation of alpha-smooth muscle actin expression in fibroblasts by transforming growth factor-beta isoforms: an in vivo and in vitro study. Wound Repair Regen. 1996 Jun;4(2):278–87.

113. Allen J. Cause of vocal fold scar. Curr Opin Otolaryngol Head Neck Surg. 2010 Dec;18(6):475–80.

114. Hirano S, Minamiguchi S, Yamashita M, Ohno T, Kanemaru S-I, Kitamura M. Histologic characterization of human scarred vocal folds. J Voice. 2009 Jul;23(4):399–407.

115. Lim X, Tateya I, Tateya T, Muñoz-Del-Río A, Bless DM. Immediate inflammatory response and scar formation in wounded vocal folds. Ann Otol Rhinol Laryngol. 2006 Dec;115(12):921–9.

116. Welham NV, Lim X, Tateya I, Bless DM. Inflammatory factor profiles one hour following vocal fold injury. Ann Otol Rhinol Laryngol. 2008 Feb;117(2):145–52.

117. Ohno T, Hirano S, Rousseau B. Gene expression of transforming growth factor-beta1 and hepatocyte growth factor during wound healing of injured rat vocal fold. Laryngoscope. 2009 Apr;119(4):806–10.

118. Ohno T, Hirano S, Rousseau B. Extracellular matrix gene expression during wound healing of the injured rat vocal fold. Otolaryngol Head Neck Surg. 2009 May;140(5):757–61.

119. Rousseau B, Ge PJ, Ohno T, French LC, Thibeault SL. Extracellular matrix gene expression after vocal fold injury in a rabbit model. Ann Otol Rhinol Laryngol. 2008 Aug;117(8):598–603.

120. Tateya I, Tateya T, Watanuki M, Bless DM. Homeostasis of hyaluronic acid in normal and scarred vocal folds. J Voice. 2015 Mar;29(2):133–9.

121. Mau T, Du M, Xu CC. A rabbit vocal fold laser scarring model for testing lamina propria tissue-engineering therapies. Laryngoscope. 2014 Oct;124(10):2321–6.

122. Rousseau B, Hirano S, Chan RW, Welham NV, Thibeault SL, Ford CN, et al. Characterization of chronic vocal fold scarring in a rabbit model. J Voice. 2004 Mar;18(1):116–24.

123. Thibeault SL, Rousseau B, Welham NV, Hirano S, Bless DM. Hyaluronan levels in acute vocal fold scar. Laryngoscope. 2004 Apr;114(4):760–4.

124. Branski RC, Rosen CA, Verdolini K, Hebda PA. Biochemical markers associated with acute vocal fold wound healing: a rabbit model. J Voice. 2005 Jun;19(2):283–9.

125. Li-Jessen NYK, Powell M, Choi A-J, Lee B-J, Thibeault SL. Cellular source and proinflammatory roles of high-mobility group box 1 in surgically injured rat vocal folds. Laryngoscope. 2017;127(6):E193–200.

126. Hahn MS, Jao CY, Faquin W, Grande-Allen KJ. Glycosaminoglycan composition of the vocal fold lamina propria in relation to function. Ann Otol Rhinol Laryngol. 2008 May;117(5):371–81.

127. Welham NV, Montequin DW, Tateya I, Tateya T, Choi SH, Bless DM. A rat excised larynx model of vocal fold scar. J Speech Lang Hear Res. 2009 Aug;52(4):1008–20.

128. Tateya T, Tateya I, Sohn JH, Bless DM. Histologic characterization of rat vocal fold scarring. Ann Otol Rhinol Laryngol. 2005 Mar;114(3):183–91.

129. Tateya I, Tateya T, Lim X, Sohn JH, Bless DM. Cell production in injured vocal folds: a rat study. Ann Otol Rhinol Laryngol. 2006 Feb;115(2):135–43.

130. Tateya T, Tateya I, Sohn JH, Bless DM. Histological study of acute vocal fold injury in a rat model. Ann Otol Rhinol Laryngol. 2006 Apr;115(4):285–92.

131. Yamashita M, Bless DM, Welham NV. Morphological and extracellular matrix changes following vocal fold injury in mice. Cells Tissues Organs (Print). 2010;192(4):262–71.

132. Rousseau B, Sohn J, Montequin DW, Tateya I, Bless DM. Functional outcomes of reduced hyaluronan in acute vocal fold scar. Ann Otol Rhinol Laryngol. 2004 Oct;113(10):767–76.

133. Yamashita M, Bless DM, Welham NV. Surgical method to create vocal fold injuries in mice. Ann Otol Rhinol Laryngol. 2009 Feb;118(2):131–8.

134. Jetté ME, Hayer SD, Thibeault SL. Characterization of human vocal fold fibroblasts derived from chronic scar. Laryngoscope. 2013 Mar;123(3):738–45.

135. Desmoulière A. Factors influencing myofibroblast differentiation during wound healing and fibrosis. Cell Biol Int. 1995 May;19(5):471–6.

136. Hinz B, Mastrangelo D, Iselin CE, Chaponnier C, Gabbiani G. Mechanical tension controls granulation tissue contractile activity and myofibroblast differentiation. Am J Pathol. 2001 Sep;159(3):1009–20.

137. Speyer R, Wieneke GH, van Wijck-Warnaar I, Dejonckere PH. Effects of voice therapy on the voice range profiles of dysphonic patients. J Voice. 2003 Dec;17(4):544–56.

138. Li L, Stiadle JM, Lau HK, Zerdoum AB, Jia X, Thibeault SL, et al. Tissue engineering-based therapeutic strategies for vocal fold repair and regeneration. Biomaterials. 2016;108:91–110.

139. Bartlett RS, Thibeault SL, Prestwich GD. Therapeutic potential of gel-based injectables for vocal fold regeneration. Biomed Mater. 2012 Apr;7(2):024103.

140. Woo P, Casper J, Colton R, Brewer D. Diagnosis and treatment of persistent dysphonia after laryngeal surgery: a retrospective analysis of 62 patients. Laryngoscope. 1994 Sep;104(9):1084–91.

141. Sheu M, Sridharan S, Paul B, Mallur P, Gandonu S, Bing R, et al. The utility of the potassium titanyl phosphate laser in modulating vocal fold scar in a rat model. Laryngoscope. 2013 Sep;123(9):2189–94.

142. Zhang J, Zhen R, Wei C. Potassium titanyl phosphate laser-induced inflammatory response and extracellular matrix turnover in rabbit vocal fold scar. Eur Arch Otorhinolaryngol. 2018 Jun;275(6):1525–32.

143. Tibbetts KM, Simpson CB. Office-Based 532-Nanometer Pulsed Potassium-Titanyl-Phosphate Laser Procedures in Laryngology. Otolaryngol Clin North Am. 2019 Jun;52(3):537–57.

144. Prufer N, Woo P, Altman KW. Pulse dye and other laser treatments for vocal scar. Curr Opin Otolaryngol Head Neck Surg. 2010 Dec;18(6):492–7.

145. Lou Z, Zhang C, Gong T, Xue C, Scholp A, Jiang JJ. Wound-healing effects of 635-nm low-level laser therapy on primary human vocal fold epithelial cells: an in vitro study. Lasers Med Sci. 2019 Apr;34(3):547–54.

146. Zhang C, Wang J, Chou A, Gong T, Devine EE, Jiang JJ. Photodynamic therapy induces antifibrotic alterations in primary human vocal fold fibroblasts. Laryngoscope. 2018;128(9):E323–31.

147. Lou Z, Gong T, Kang J, Xue C, Ulmschneider C, Jiang JJ. The Effects of Photobiomodulation on Vocal Fold Wound Healing: In Vivo and In Vitro Studies. Photobiomodul Photomed Laser Surg. 2019 Sep;37(9):532–8.

148. Gong T, Zhang C, Kang J, Lamb JJ, Jiang JJ. Cryotherapy has antifibrotic and regenerative effects on human vocal fold fibroblasts. Laryngoscope. 2019;129(4):E143–50.

149. Gong T, Zhang C, Kang J, Lou Z, Scholp A, Jiang JJ. The effects of cryotherapy on vocal fold healing in a rabbit model. Laryngoscope. 2019;129(4):E151–7.

150. Courey MS. Injection laryngoplasty. Otolaryngol Clin North Am. 2004 Feb;37(1):121–38.

151. Kwon SK, Kim H-B, Song J-J, Cho CG, Park S-W, Choi J-S, et al. Vocal fold augmentation with injectable polycaprolactone microspheres/pluronic F127 hydrogel: long-term in vivo study for the treatment of glottal insufficiency. PLoS ONE. 2014;9(1):e85512.

152. Wang C-T, Liao L-J, Cheng P-W, Lo W-C, Lai M-S. Intralesional steroid injection for benign vocal fold disorders: a systematic review and meta-analysis. Laryngoscope. 2013 Jan;123(1):197–203.

153. Mortensen M. Laryngeal steroid injection for vocal fold scar. Curr Opin Otolaryngol Head Neck Surg. 2010 Dec;18(6):487–91.

154. Ford CN, Staskowski PA, Bless DM. Autologous collagen vocal fold injection: a preliminary clinical study. Laryngoscope. 1995 Sep;105(9 Pt 1):944–8.

155. Courey MS. Homologous collagen substances for vocal fold augmentation. Laryngoscope. 2001 May;111(5):747–58.

156. Hertegård S, Dahlqvist A, Laurent C, Borzacchiello A, Ambrosio L. Viscoelastic properties of rabbit vocal folds after augmentation. Otolaryngol Head Neck Surg. 2003 Mar;128(3):401–6.

157. Dahlqvist A, Gärskog O, Laurent C, Hertegård S, Ambrosio L, Borzacchiello A. Viscoelasticity of rabbit vocal folds after injection augmentation. Laryngoscope. 2004 Jan;114(1):138–42.

158. Sataloff RT. Autologous fat implantation for vocal fold scar. Curr Opin Otolaryngol Head Neck Surg. 2010 Dec;18(6):503–6.

159. Neuenschwander MC, Sataloff RT, Abaza MM, Hawkshaw MJ, Reiter D, Spiegel JR. Management of vocal fold scar with autologous fat implantation: perceptual results. J Voice. 2001 Jun;15(2):295–304.

160. Cantarella G, Mazzola RF, Domenichini E, Arnone F, Maraschi B. Vocal fold augmentation by autologous fat injection with lipostructure procedure. Otolaryngol Head Neck Surg. 2005 Feb;132(2):239–43.

161. Hertegård S, Dahlqvist A, Goodyer E. Viscoelastic measurements after vocal fold scarring in rabbits--short-term results after hyaluronan injection. Acta Otolaryngol. 2006 Jul;126(7):758–63.

162. Chhetri DK, Mendelsohn AH. Hyaluronic acid for the treatment of vocal fold scars. Curr Opin Otolaryngol Head Neck Surg. 2010 Dec;18(6):498–502.

163. Fraser JR, Laurent TC, Laurent UB. Hyaluronan: its nature, distribution, functions and turnover. J Intern Med. 1997 Jul;242(1):27–33.

164. Thibeault SL, Klemuk SA, Chen X, Quinchia Johnson BH. In Vivo engineering of the vocal fold ECM with injectable HA hydrogels-late effects on tissue repair and biomechanics in a rabbit model. J Voice. 2011 Mar;25(2):249–53.

165. Hallén L, Johansson C, Laurent C. Cross-linked hyaluronan (Hylan B gel): a new injectable remedy for treatment of vocal fold insufficiency--an animal study. Acta Otolaryngol. 1999 Jan;119(1):107–11.

166. Shu XZ, Liu Y, Luo Y, Roberts MC, Prestwich GD. Disulfide cross-linked hyaluronan hydrogels. Biomacromolecules. 2002 Dec;3(6):1304–11.

167. Liu Y, Zheng Shu X, Prestwich GD. Biocompatibility and stability of disulfide-crosslinked hyaluronan films. Biomaterials. 2005 Aug;26(23):4737–46.

168. Zheng Shu X, Liu Y, Palumbo FS, Luo Y, Prestwich GD. In situ crosslinkable hyaluronan hydrogels for tissue engineering. Biomaterials. 2004 Apr;25(7–8):1339–48.

169. Liao H, Munoz-Pinto D, Qu X, Hou Y, Grunlan MA, Hahn MS. Influence of hydrogel mechanical properties and mesh size on vocal fold fibroblast extracellular matrix production and phenotype. Acta Biomater. 2008 Sep;4(5):1161–71.

170. Hansen JK, Thibeault SL, Walsh JF, Shu XZ, Prestwich GD. In vivo engineering of the vocal fold extracellular matrix with injectable hyaluronic acid hydrogels: early effects on tissue repair and biomechanics in a rabbit model. Ann Otol Rhinol Laryngol. 2005 Sep;114(9):662–70.

171. Chen X, Thibeault SL. Role of tumor necrosis factor-alpha in wound repair in human vocal fold fibroblasts. Laryngoscope. 2010 Sep;120(9):1819–25.

172. Duflo S, Thibeault SL, Li W, Shu XZ, Prestwich G. Effect of a synthetic extracellular matrix on vocal fold lamina propria gene expression in early wound healing. Tissue Eng. 2006 Nov;12(11):3201–7.

173. Khademhosseini A, Langer R. Microengineered hydrogels for tissue engineering. Biomaterials. 2007 Dec;28(34):5087–92.

174. Zhou W, Stukel JM, Cebull HL, Willits RK. Tuning the Mechanical Properties of Poly(Ethylene Glycol) Microgel-Based Scaffolds to Increase 3D Schwann Cell Proliferation. Macromol Biosci. 2016 Apr;16(4):535–44.

175. Jia X, Yeo Y, Clifton RJ, Jiao T, Kohane DS, Kobler JB, et al. Hyaluronic acid-based microgels and microgel networks for vocal fold regeneration. Biomacromolecules. 2006 Dec;7(12):3336–44.

176. Coppoolse JMS, Van Kooten TG, Heris HK, Mongeau L, Li NYK, Thibeault SL, et al. An in vivo study of composite microgels based on hyaluronic acid and gelatin for the reconstruction of surgically injured rat vocal folds. J Speech Lang Hear Res. 2014 Apr 1;57(2):S658-673.

177. Karajanagi SS, Lopez-Guerra G, Park H, Kobler JB, Galindo M, Aanestad J, et al. Assessment of canine vocal fold function after injection of a new biomaterial designed to treat phonatory mucosal scarring. Ann Otol Rhinol Laryngol. 2011 Mar;120(3):175–84.

178. Kwon SK, Song J-J, Cho CG, Park S-W, Choi SJ, Oh SH, et al. Polycaprolactone spheres and theromosensitive Pluronic F127 hydrogel for vocal fold

augmentation: in vivo animal study for the treatment of unilateral vocal fold palsy. Laryngoscope. 2013 Jul;123(7):1694–703.

179. Lee JH, Kim DW, Kim EN, Park S-W, Kim H-B, Oh SH, et al. Evaluation of the poly(lactic-co-glycolic acid)/pluronic F127 for injection laryngoplasty in rabbits. Otolaryngol Head Neck Surg. 2014 Nov;151(5):830–5.

180. Hirano S, Bless DM, Rousseau B, Welham N, Montequin D, Chan RW, et al. Prevention of vocal fold scarring by topical injection of hepatocyte growth factor in a rabbit model. Laryngoscope. 2004 Mar;114(3):548–56.

181. Hirano S, Bless D, Heisey D, Ford C. Roles of hepatocyte growth factor and transforming growth factor beta1 in production of extracellular matrix by canine vocal fold fibroblasts. Laryngoscope. 2003 Jan;113(1):144–8.

182. Graupp M, Rinner B, Frisch MT, Weiss G, Fuchs J, Sundl M, et al. Towards an in vitro fibrogenesis model of human vocal fold scarring. Eur Arch Otorhinolaryngol. 2018 May;275(5):1211–8.

183. Suzuki R, Kawai Y, Tsuji T, Hiwatashi N, Kishimoto Y, Tateya I, et al. Prevention of vocal fold scarring by local application of basic fibroblast growth factor in a rat vocal fold injury model. Laryngoscope. 2017;127(2):E67–74.

184. Hirano S, Nagai H, Tateya I, Tateya T, Ford CN, Bless DM. Regeneration of aged vocal folds with basic fibroblast growth factor in a rat model: a preliminary report. Ann Otol Rhinol Laryngol. 2005 Apr;114(4):304–8.

185. Hiwatashi N, Hirano S, Mizuta M, Kobayashi T, Kawai Y, Kanemaru S-I, et al. The efficacy of a novel collagen-gelatin scaffold with basic fibroblast growth factor for the treatment of vocal fold scar. J Tissue Eng Regen Med. 2017;11(5):1598–609.

186. Hirano S, Kawamoto A, Tateya I, Mizuta M, Kishimoto Y, Hiwatashi N, et al. A phase I/II exploratory clinical trial for intracordal injection of recombinant hepatocyte growth factor for vocal fold scar and sulcus. J Tissue Eng Regen Med. 2018;12(4):1031–8.

187. Ban MJ, Park JH, Kim JW, Park KN, Lee JY, Kim HK, et al. The Efficacy of Fibroblast Growth Factor for the Treatment of Chronic Vocal Fold Scarring: From Animal Model to Clinical Application. Clin Exp Otorhinolaryngol. 2017 Dec;10(4):349–56.

188. Svensson B, Nagubothu SR, Cedervall J, Chan RW, Le Blanc K, Kimura M, et al. Injection of human mesenchymal stem cells improves healing of vocal folds after scar excision--a xenograft analysis. Laryngoscope. 2011 Oct;121(10):2185–90.

189. Nagubothu SR, Sugars RV, Tudzarovski N, Andrén AT, Bottai M, Davies LC, et al. Mesenchymal stromal cells modulate tissue repair responses within the injured vocal fold. Laryngoscope. 2020 Jan;130(1):E21–9.

190. Hiwatashi N, Bing R, Kraja I, Branski RC. Mesenchymal stem cells have antifibrotic effects on transforming growth factor-β1-stimulated vocal fold fibroblasts. Laryngoscope. 2017 Jan;127(1):E35–41.

191. Hiwatashi N, Hirano S, Suzuki R, Kawai Y, Mizuta M, Kishimoto Y, et al. Comparison of ASCs and BMSCs combined with atelocollagen for vocal fold scar regeneration. Laryngoscope. 2016;126(5):1143–50.

192. Lee BJ, Wang SG, Lee JC, Jung JS, Bae YC, Jeong HJ, et al. The prevention of vocal fold scarring using autologous adipose tissue-derived stromal cells. Cells Tissues Organs (Print). 2006;184(3–4):198–204.

193. Long JL. Repairing the vibratory vocal fold. Laryngoscope. 2018;128(1):153–9.

194. Mattei A, Bertrand B, Jouve E, Blaise T, Philandrianos C, Grimaud F, et al. Feasibility of First Injection of Autologous Adipose Tissue-Derived Stromal Vascular Fraction in Human Scarred Vocal Folds: A Nonrandomized Controlled Trial. JAMA Otolaryngol Head Neck Surg. 2020 Feb 13;

195. Magalon J, Velier M, Simoncini S, François P, Bertrand B, Daumas A, et al. Molecular profile and proangiogenic activity of the adipose-derived stromal vascular fraction used as an autologous innovative medicinal product in patients with systemic sclerosis. Ann Rheum Dis. 2019;78(3):391–8.

196. Paul BC, Rafii BY, Gandonu S, Bing R, Born H, Amin MR, et al. Smad3: an emerging target for vocal fold fibrosis. Laryngoscope. 2014 Oct;124(10):2327–31.

197. Branski RC, Bing R, Kraja I, Amin MR. The role of Smad3 in the fibrotic phenotype in human vocal fold fibroblasts. Laryngoscope. 2016;126(5):1151–6.

198. Kraja I, Bing R, Hiwatashi N, Rousseau B, Nalband D, Kirshenbaum K, et al. Preliminary study of a novel transfection modality for in vivo siRNA delivery to vocal fold fibroblasts. Laryngoscope. 2017;127(7):E231–7.

199. Hiwatashi N, Kraja I, Benedict PA, Dion GR, Bing R, Rousseau B, et al. Nanoparticle delivery of RNA-based therapeutics to alter the vocal fold tissue response to injury. Laryngoscope. 2018;128(5):E178–83.

200. Bless DM, Welham NV. Characterization of vocal fold scar formation, prophylaxis, and treatment using animal models. Curr Opin Otolaryngol Head Neck Surg. 2010 Dec;18(6):481–6.

201. Zealear DL, Billante CR, Chongkolwatana C, Rho YS, Hamdan AL, Herzon GD. The effects of chronic electrical stimulation on laryngeal muscle physiology and histochemistry. ORL J Otorhinolaryngol Relat Spec. 2000 Apr;62(2):81–6.

202. Zealear DL, Billante CL, Chongkolwatana C, Herzon GD. The effects of chronic electrical stimulation on laryngeal muscle reinnervation. ORL J Otorhinolaryngol Relat Spec. 2000 Apr;62(2):87–95.

203. Jacobs IN, Sanders I, Wu BL, Biller HF. Reinnervation of the canine posterior cricoarytenoid muscle with sympathetic preganglionic neurons. Ann Otol Rhinol Laryngol. 1990 Mar;99(3 Pt 1):167–74.

204. Shindo ML, Herzon GD, Hanson DG, Cain DJ, Sahgal V. Effects of denervation on laryngeal muscles: a canine model. Laryngoscope. 1992 Jun;102(6):663–9.

205. Brondbo K, Hall C, Dahl HA, Teig E, Gujord KM. A histochemical evaluation of experimentally reinnervated canine laryngeal muscles. J Otolaryngol. 1986 Oct;15(5):265–72.

206. Zealear DL, Mainthia R, Li Y, Kunibe I, Katada A, Billante C, et al. Stimulation of denervated muscle promotes selective reinnervation, prevents synkinesis, and restores function. Laryngoscope. 2014 May;124(5):E180-187.

207. Hoffman HT, Dailey SH, Bock JM, Thibeault SL, McCulloch TM. Transillumination for needle localization in the larynx. Laryngoscope. 2015 Oct;125(10):2341–8.

208. Cha W, Ro JH, Yang SC, Choi CJ, Yang I, Kang H, et al. Real-Time Light-Guided Vocal Fold Injection: Ex Vivo Feasibility Study in a Canine Model. Laryngoscope. 2019;129(4):935–42.

209. Wang S-G, Park H-J, Cho JK, Jang JY, Lee WY, Lee B-J, et al. The First Application of the Two-Dimensional Scanning Videokymography in Excised Canine Larynx Model. J Voice. 2016 Jan;30(1):1–4.

210. Gulka CP, Brown JE, Giordano JEM, Hickey JE, Montero MP, Hoang A, et al. A novel silk-based vocal fold augmentation material: 6-month evaluation in a canine model. Laryngoscope. 2019;129(8):1856–62.

211. Herrera VLM, Viereck JC, Lopez-Guerra G, Kumai Y, Kobler J, Karajanagi S, et al. 11.7 Tesla magnetic resonance microimaging of laryngeal tissue architecture. Laryngoscope. 2009 Nov;119(11):2187–94.

212. Suehiro A, Hirano S, Kishimoto Y, Rousseau B, Nakamura T, Ito J. Treatment of acute vocal fold scar with local injection of basic fibroblast growth factor: a canine study. Acta Otolaryngol. 2010 Jul;130(7):844–50.

213. Kishimoto Y, Hirano S, Kitani Y, Suehiro A, Umeda H, Tateya I, et al. Chronic vocal fold scar restoration with hepatocyte growth factor hydrogel. Laryngoscope. 2010 Jan;120(1):108–13.

214. Chhetri DK, Head C, Revazova E, Hart S, Bhuta S, Berke GS. Lamina propria replacement therapy with cultured autologous fibroblasts for vocal fold scars. Otolaryngol Head Neck Surg. 2004 Dec;131(6):864–70.

215. Rousseau B, Hirano S, Scheidt TD, Welham NV, Thibeault SL, Chan RW, et al. Characterization of vocal fold scarring in a canine model. Laryngoscope. 2003 Apr;113(4):620–7.

216. Regner MF, Robitaille MJ, Jiang JJ. Interspecies comparison of mucosal wave properties using high-speed digital imaging. Laryngoscope. 2010 Jun;120(6):1188–94.

217. Alipour F, Finnegan EM, Jaiswal S. Phonatory characteristics of the excised human larynx in comparison to other species. J Voice. 2013 Jul;27(4):441–7.

218. Garrett CG, Coleman JR, Reinisch L. Comparative histology and vibration of the vocal folds: implications for experimental studies in microlaryngeal surgery. Laryngoscope. 2000 May;110(5 Pt 1):814–24.

219. Rousseau B, Tateya I, Lim X, Munoz-del-Rio A, Bless DM. Investigation of anti-hyaluronidase treatment on vocal fold wound healing. J Voice. 2006 Sep;20(3):443–51.

220. Woodson G. Developing a porcine model for study of vocal fold scar. J Voice. 2012 Nov;26(6):706–10.

221. Gill GA, Buda A, Moorghen M, Dettmar PW, Pignatelli M. Characterisation of adherens and tight junctional molecules in normal animal larynx; determining a suitable model for studying molecular abnormalities in human laryngopharyngeal reflux. J Clin Pathol. 2005 Dec;58(12):1265–70.

222. Gugatschka M, Jarvis JC, Perkins JD, Bubalo V, Wiederstein-Grasser I, Lanmüller H, et al. Functional Electrical Stimulation Leads to Increased Volume of the Aged Thyroarytenoid Muscle. Laryngoscope. 2018;128(12):2852–7.

223. Karbiener M, Jarvis JC, Perkins JD, Lanmüller H, Schmoll M, Rode HS, et al. Reversing Age Related Changes of the Laryngeal Muscles by Chronic Electrostimulation of the Recurrent Laryngeal Nerve. PLoS ONE. 2016;11(11):e0167367.

224. Maunsell RCK, de Freitas LL, Altemani A, Crespo AN. Histologic comparison of vocal fold microflap healing with sutures and glue. Laryngoscope. 2013 Jul;123(7):1709–16.

225. Thibeault SL, Klemuk SA, Smith ME, Leugers C, Prestwich G. In vivo comparison of biomimetic approaches for tissue regeneration of the scarred vocal fold. Tissue Eng Part A. 2009 Jul;15(7):1481–7.

226. Hertegård S, Cedervall J, Svensson B, Forsberg K, Maurer FHJ, Vidovska D, et al. Viscoelastic and histologic properties in scarred rabbit vocal folds after mesenchymal stem cell injection. Laryngoscope. 2006 Jul;116(7):1248–54.

227. Leydon C, Imaizumi M, Bartlett RS, Wang SF, Thibeault SL. Epithelial cells are active participants in vocal fold wound healing: an in vivo animal model of injury. PLoS ONE. 2014;9(12):e115389.

228. Ling C, Yamashita M, Waselchuk EA, Raasch JL, Bless DM, Welham NV. Alteration in cellular morphology, density and distribution in rat vocal fold mucosa following injury. Wound Repair Regen. 2010 Feb;18(1):89–97.

229. Li L, Stiadle JM, Levendoski EE, Lau HK, Thibeault SL, Kiick KL. Biocompatibility of injectable resilin-based hydrogels. J Biomed Mater Res A. 2018;106(8):2229–42.

230. Erickson-Levendoski E, Sivasankar MP. Role for ion transport in porcine vocal fold epithelial defense to acid challenge. Otolaryngol Head Neck Surg. 2012 Feb;146(2):272–8.

231. Gray SD. Cellular physiology of the vocal folds. Otolaryngol Clin North Am. 2000 Aug;33(4):679–98.

232. Branco A, Bartley SM, King SN, Jetté ME, Thibeault SL. Vocal fold myofibroblast profile of scarring. Laryngoscope. 2016 Mar;126(3):E110-117.

233. Walimbe T, Panitch A, Sivasankar MP. An in vitro scaffold-free epithelial-fibroblast coculture model for the larynx. Laryngoscope. 2017 Jun;127(6):E185–92.

234. Yamaguchi T, Shin T, Sugihara H. Reconstruction of the laryngeal mucosa. A three-dimensional collagen gel matrix culture. Arch Otolaryngol Head Neck Surg. 1996 Jun;122(6):649–54.

235. Leydon C, Selekman JA, Palecek S, Thibeault SL. Human embryonic stem cell-derived epithelial cells in a novel in vitro model of vocal mucosa. Tissue Eng Part A. 2013 Oct;19(19–20):2233–41.

236. Lungova V, Leydon C, Thibeault S. Derivation of Epithelial Cells from Human Embryonic Stem Cells as an In Vitro Model of Vocal Mucosa. Methods Mol Biol. 2016;1307:237–43.

237. Mizuta M, Kurita T, Kimball EE, Rousseau B. Structurally and functionally characterized in vitro model of rabbit vocal fold epithelium. Tissue Cell. 2017 Jun;49(3):427–34.

238. Ling C, Li Q, Brown ME, Kishimoto Y, Toya Y, Devine EE, et al. Bioengineered vocal fold mucosa for voice restoration. Sci Transl Med. 2015 Nov 18;7(314):314ra187.

239. Fukahori M, Chitose S-I, Sato K, Sueyoshi S, Kurita T, Umeno H, et al. Regeneration of Vocal Fold Mucosa Using Tissue-Engineered Structures with Oral Mucosal Cells. PLoS ONE. 2016;11(1):e0146151.

240. Wolchok JC, Brokopp C, Underwood CJ, Tresco PA. The effect of bioreactor induced vibrational stimulation on extracellular matrix production from human derived fibroblasts. Biomaterials. 2009 Jan;30(3):327–35.

241. Titze IR, Hitchcock RW, Broadhead K, Webb K, Li W, Gray SD, et al. Design and validation of a bioreactor for engineering vocal fold tissues under combined tensile and vibrational stresses. J Biomech. 2004 Oct;37(10):1521–9.

242. Farran AJE, Teller SS, Jia F, Clifton RJ, Duncan RL, Jia X. Design and characterization of a dynamic vibrational culture system. J Tissue Eng Regen Med. 2013 Mar;7(3):213–25.

243. Gaston J, Quinchia Rios B, Bartlett R, Berchtold C, Thibeault SL. The response of vocal fold fibroblasts and mesenchymal stromal cells to vibration. PLoS ONE. 2012;7(2):e30965.

244. Zerdoum AB, Tong Z, Bachman B, Jia X. Construction and characterization of a novel vocal fold bioreactor. J Vis Exp. 2014 Aug 1;(90):e51594.

245. Kim D, Lim J-Y, Kwon S. Development of Vibrational Culture Model Mimicking Vocal Fold Tissues. Ann Biomed Eng. 2016;44(10):3136–43.

246. Kirsch A, Hortobagyi D, Stachl T, Karbiener M, Grossmann T, Gerstenberger C, et al. Development and validation of a novel phonomimetic bioreactor. PLoS ONE. 2019;14(3):e0213788.

247. Thibeault SL, Li W, Bartley S. A method for identification of vocal fold lamina propria fibroblasts in culture. Otolaryngol Head Neck Surg. 2008 Dec;139(6):816–22.

248. Luo Y, Kobler JB, Zeitels SM, Langer R. Effects of growth factors on extracellular matrix production by vocal fold fibroblasts in 3-dimensional culture. Tissue Eng. 2006 Dec;12(12):3365–74.

249. Hirano S, Bless DM, Heisey D, Ford CN. Effect of growth factors on hyaluronan production by canine vocal fold fibroblasts. Ann Otol Rhinol Laryngol. 2003 Jul;112(7):617–24.

250. Suehiro A, Hirano S, Kishimoto Y, Tateya I, Rousseau B, Ito J. Effects of basic fibroblast growth factor on rat vocal fold fibroblasts. Ann Otol Rhinol Laryngol. 2010 Oct;119(10):690–6.

251. Krishna P, Rosen CA, Branski RC, Wells A, Hebda PA. Primed fibroblasts and exogenous decorin: potential treatments for subacute vocal fold scar. Otolaryngol Head Neck Surg. 2006 Dec;135(6):937–45.

252. Chen X, Thibeault SL. Novel isolation and biochemical characterization of immortalized fibroblasts for tissue engineering vocal fold lamina propria. Tissue Eng Part C Methods. 2009 Jun;15(2):201–12.

253. Farran AJE, Teller SS, Jha AK, Jiao T, Hule RA, Clifton RJ, et al. Effects of matrix composition, microstructure, and viscoelasticity on the behaviors of vocal fold fibroblasts cultured in three-dimensional hydrogel networks. Tissue Eng Part A. 2010 Apr;16(4):1247–61.

254. Karbiener M, Darnhofer B, Frisch M-T, Rinner B, Birner-Gruenberger R, Gugatschka M. Comparative proteomics of paired vocal fold and oral mucosa fibroblasts. J Proteomics. 2017 Feb 23;155:11–21.

255. Bonet M, Basterra J, Pérez A, Zapater E. A novel method for culturing human glottic cells. Laryngoscope. 2013 Dec;123(12):E104-108.

256. Izumi K, Marcelo CL, Feinberg SE. Enrichment of Oral Mucosa and Skin Keratinocyte Progenitor/Stem Cells. In: Turksen K, editor. Skin Stem Cells [Internet]. Totowa, NJ: Humana Press; 2013 [cited 2019 May 21]. p. 293–303. Available from: http://link.springer.com/10.1007/978-1-62703-330-5_23

257. You J, Munoz-Erazo L, Wen L, Hodge C, Madigan MC, Sutton G. In-Vitro Effects of Secreted Frizzled-Related Protein 1 (SFRP1) On Human Corneal Epithelial Cells. Curr Eye Res. 2018;43(4):455–9.

258. González S, Chen L, Deng SX. Comparative Study of Xenobiotic-Free Media for the Cultivation of Human Limbal Epithelial Stem/Progenitor Cells. Tissue Eng Part C Methods. 2017;23(4):219–27.

259. Rao X, Huang X, Zhou Z, Lin X. An improvement of the 2ˆ(-delta delta CT) method for quantitative real-time polymerase chain reaction data analysis. Biostat Bioinforma Biomath. 2013 Aug;3(3):71–85.

260. Wiśniewski JR, Zougman A, Nagaraj N, Mann M. Universal sample preparation method for proteome analysis. Nat Methods. 2009 May;6(5):359–62.

261. Cox J, Hein MY, Luber CA, Paron I, Nagaraj N, Mann M. Accurate proteome-wide label-free quantification by delayed normalization and maximal peptide ratio extraction, termed MaxLFQ. Mol Cell Proteomics. 2014 Sep;13(9):2513–26.

262. Grossmann T, Steffan B, Kirsch A, Grill M, Gerstenberger C, Gugatschka M. Exploring the pathophysiology of Reinke´s edema: The cellular impact of cigarette smoke and vibration. Laryngoscope. 2020; doi:10.1002/lary.28855.

263. Samuels TL, Handler E, Syring ML, Pajewski NM, Blumin JH, Kerschner JE, et al. Mucin gene expression in human laryngeal epithelia: effect of laryngopharyngeal reflux. Ann Otol Rhinol Laryngol. 2008 Sep;117(9):688–95.

264. Rousseau B, Suehiro A, Echemendia N, Sivasankar M. Raised intensity phonation compromises vocal fold epithelial barrier integrity. Laryngoscope. 2011 Feb;121(2):346–51.

265. Gill GA, Johnston N, Buda A, Pignatelli M, Pearson J, Dettmar PW, et al. Laryngeal epithelial defenses against laryngopharyngeal reflux: investigations of E-cadherin, carbonic anhydrase isoenzyme III, and pepsin. Ann Otol Rhinol Laryngol. 2005 Dec;114(12):913–21.

266. Dworkin JP. Laryngitis: types, causes, and treatments. Otolaryngol Clin North Am. 2008 Apr;41(2):419–36, ix.

267. Arens C, Glanz H, Wönckhaus J, Hersemeyer K, Kraft M. Histologic assessment of epithelial thickness in early laryngeal cancer or precursor lesions and its impact on endoscopic imaging. Eur Arch Otorhinolaryngol. 2007 Jun;264(6):645–9.

268. Squier CA, Kremer MJ. Biology of oral mucosa and esophagus. J Natl Cancer Inst Monographs. 2001;(29):7–15.

269. Houghton O, McCluggage WG. The expression and diagnostic utility of p63 in the female genital tract. Adv Anat Pathol. 2009 Sep;16(5):316–21.

270. Kinoshita S, Adachi W, Sotozono C, Nishida K, Yokoi N, Quantock AJ, et al. Characteristics of the human ocular surface epithelium. Prog Retin Eye Res. 2001 Sep;20(5):639–73.

271. Morino T, Takagi R, Yamamoto K, Kojima H, Yamato M. Explant culture of oral mucosal epithelial cells for fabricating transplantable epithelial cell sheet. Regen Ther. 2019 Jun;10:36–45.

272. Erickson-DiRenzo E, Leydon C, Thibeault SL. Methodology for the establishment of primary porcine vocal fold epithelial cell cultures. Laryngoscope. 2019;129(10):E355–64.

273. Johnston N, Yan JC, Hoekzema CR, Samuels TL, Stoner GD, Blumin JH, et al. Pepsin promotes proliferation of laryngeal and pharyngeal epithelial cells. Laryngoscope. 2012 Jun;122(6):1317–25.

274. Southgate J, Williams HK, Trejdosiewicz LK, Hodges GM. Primary culture of human oral epithelial cells. Growth requirements and expression of differentiated characteristics. Lab Invest. 1987 Feb;56(2):211–23.

275. Kaeffer B. Mammalian intestinal epithelial cells in primary culture: a mini-review. In Vitro Cell Dev Biol Anim. 2002 Mar;38(3):123–34.

276. Loret S, Rusu D, El Moualij B, Taminiau B, Heinen E, Dandrifosse G, et al. Preliminary characterization of jejunocyte and colonocyte cell lines isolated by enzymatic digestion from adult and young cattle. Res Vet Sci. 2009 Aug;87(1):123–32.

277. Wolbank S, Stadler G, Peterbauer A, Gillich A, Karbiener M, Streubel B, et al. Telomerase immortalized human amnion- and adipose-derived mesenchymal stem cells: maintenance of differentiation and immunomodulatory characteristics. Tissue Eng Part A. 2009 Jul;15(7):1843–54.

278. Bodnar AG, Ouellette M, Frolkis M, Holt SE, Chiu CP, Morin GB, et al. Extension of life-span by introduction of telomerase into normal human cells. Science. 1998 Jan 16;279(5349):349–52.

279. Yasunaga Y, Nakamura K, Ewing CM, Isaacs WB, Hukku B, Rhim JS. A novel human cell culture model for the study of familial prostate cancer. Cancer Res. 2001 Aug 15;61(16):5969–73.

280. Carney SA, Tahara H, Swartz CD, Risinger JI, He H, Moore AB, et al. Immortalization of human uterine leiomyoma and myometrial cell lines after induction of telomerase activity: molecular and phenotypic characteristics. Lab Invest. 2002 Jun;82(6):719–28.

281. Kang MK, Park N-H. Extension of cell life span using exogenous telomerase. Methods Mol Biol. 2007;371:151–65.

282. Katwal P, Thomas M, Uprety T, Hildreth MB, Kaushik RS. Development and biochemical and immunological characterization of early passage and immortalized bovine intestinal epithelial cell lines from the ileum of a young calf. Cytotechnology. 2019 Feb;71(1):127–48.

283. Wen L, Yuan Q, Sun M, Niu M, Wang H, Fu H, et al. Generation and characteristics of human Sertoli cell line immortalized by overexpression of human telomerase. Oncotarget. 2017 Mar 7;8(10):16553–70.

284. Sidney LE, McIntosh OD, Hopkinson A. Phenotypic Change and Induction of Cytokeratin Expression During In Vitro Culture of Corneal Stromal Cells. Invest Ophthalmol Vis Sci. 2015 Nov;56(12):7225–35.

285. Omary MB, Ku NO, Liao J, Price D. Keratin modifications and solubility properties in epithelial cells and in vitro. Subcell Biochem. 1998;31:105–40.

286. Gibbs S, Ponec M. Intrinsic regulation of differentiation markers in human epidermis, hard palate and buccal mucosa. Arch Oral Biol. 2000 Feb;45(2):149–58.

287. Barallon R, Bauer SR, Butler J, Capes-Davis A, Dirks WG, Elmore E, et al. Recommendation of short tandem repeat profiling for authenticating human cell lines, stem cells, and tissues. In Vitro Cell Dev Biol Anim. 2010 Oct;46(9):727–32.

288. Dirks WG, Faehnrich S, Estella IAJ, Drexler HG. Short tandem repeat DNA typing provides an international reference standard for authentication of human cell lines. ALTEX. 2005;22(2):103–9.

289. Buehring GC, Eby EA, Eby MJ. Cell line cross-contamination: how aware are Mammalian cell culturists of the problem and how to monitor it? In Vitro Cell Dev Biol Anim. 2004 Aug;40(7):211–5.

290. Nims RW, Sykes G, Cottrill K, Ikonomi P, Elmore E. Short tandem repeat profiling: part of an overall strategy for reducing the frequency of cell misidentification. In Vitro Cell Dev Biol Anim. 2010 Dec;46(10):811–9.

291. Hasegawa H, Fujita H, Katoh H, Aoki J, Nakamura K, Ichikawa A, et al. Opposite regulation of transepithelial electrical resistance and paracellular permeability by Rho in Madin-Darby canine kidney cells. J Biol Chem. 1999 Jul 23;274(30):20982–8.

292. Bierbaumer L, Schwarze UY, Gruber R, Neuhaus W. Cell culture models of oral mucosal barriers: A review with a focus on applications, culture conditions and barrier properties. Tissue Barriers. 2018;6(3):1479568.

293. Palencia L, Das A, Palecek SP, Thibeault SL, Leydon C. Epidermal growth factor mediated healing in stem cell-derived vocal fold mucosa. J Surg Res. 2015 Jul;197(1):32–8.

294. Sivasankar M, Erickson E, Rosenblatt M, Branski RC. Hypertonic challenge to porcine vocal folds: effects on epithelial barrier function. Otolaryngol Head Neck Surg. 2010 Jan;142(1):79–84.

295. Suzuki S, Sato M, Senoo H, Ishikawa K. Direct cell-cell interaction enhances pro-MMP-2 production and activation in co-culture of laryngeal cancer cells and fibroblasts: involvement of EMMPRIN and MT1-MMP. Exp Cell Res. 2004 Feb 15;293(2):259–66.

296. Lombardo Bedran TB, Palomari Spolidorio D, Grenier D. Green tea polyphenol epigallocatechin-3-gallate and cranberry proanthocyanidins act in synergy with cathelicidin (LL-37) to reduce the LPS-induced inflammatory response in a three-dimensional co-culture model of gingival epithelial cells and fibroblasts. Arch Oral Biol. 2015 Jun;60(6):845–53.

297. Papazian D, Wagtmann VR, Hansen S, Würtzen PA. Direct contact between dendritic cells and bronchial epithelial cells inhibits T cell recall responses towards mite and pollen allergen extracts in vitro. Clin Exp Immunol. 2015 Aug;181(2):207–18.

298. Krishna P, Regner M, Palko J, Liu F, Abramowitch S, Jiang J, et al. The effects of decorin and HGF-primed vocal fold fibroblasts in vitro and ex vivo in a porcine model of vocal fold scarring. Laryngoscope. 2010 Nov;120(11):2247–57.

299. Hahn MS, Teply BA, Stevens MM, Zeitels SM, Langer R. Collagen composite hydrogels for vocal fold lamina propria restoration. Biomaterials. 2006 Mar;27(7):1104–9.

300. Hiwatashi N, Hirano S, Mizuta M, Tateya I, Kanemaru S-I, Nakamura T, et al. Biocompatibility and efficacy of collagen/gelatin sponge scaffold with sustained release of basic fibroblast growth factor on vocal fold fibroblasts in 3-dimensional culture. Ann Otol Rhinol Laryngol. 2015 Feb;124(2):116–25.

301. Chen X, Thibeault SL. Biocompatibility of a synthetic extracellular matrix on immortalized vocal fold fibroblasts in 3-D culture. Acta Biomater. 2010 Aug;6(8):2940–8.

302. Lawrenson K, Notaridou M, Lee N, Benjamin E, Jacobs IJ, Jones C, et al. In vitro three-dimensional modeling of fallopian tube secretory epithelial cells. BMC Cell Biol. 2013 Sep 27;14:43.

303. Kutty JK, Webb K. Vibration stimulates vocal mucosa-like matrix expression by hydrogel-encapsulated fibroblasts. J Tissue Eng Regen Med. 2010 Jan;4(1):62–72.

304. Imaizumi M, Sato Y, Yang DT, Thibeault SL. In vitro epithelial differentiation of human induced pluripotent stem cells for vocal fold tissue engineering. Ann Otol Rhinol Laryngol. 2013 Dec;122(12):737–47.

305. Gangatirkar P, Paquet-Fifield S, Li A, Rossi R, Kaur P. Establishment of 3D organotypic cultures using human neonatal epidermal cells. Nat Protoc. 2007;2(1):178–86.

306. Dongari-Bagtzoglou A, Kashleva H. Development of a highly reproducible three-dimensional organotypic model of the oral mucosa. Nat Protoc. 2006;1(4):2012–8.

307. Hahn MS, Kobler JB, Zeitels SM, Langer R. Quantitative and comparative studies of the vocal fold extracellular matrix II: collagen. Ann Otol Rhinol Laryngol. 2006 Mar;115(3):225–32.

308. Mostefaoui Y, Bart C, Frenette M, Rouabhia M. Candida albicans and Streptococcus salivarius modulate IL-6, IL-8, and TNF-alpha expression and secretion by engineered human oral mucosa cells. Cell Microbiol. 2004 Nov;6(11):1085–96.

309. Hartnick CJ, Rehbar R, Prasad V. Development and maturation of the pediatric human vocal fold lamina propria. Laryngoscope. 2005 Jan;115(1):4–15.

310. Hirano M, Sato K, Nakashima T. Fibroblasts in human vocal fold mucosa. Acta Otolaryngol. 1999 Mar;119(2):271–6.

311. Mochitate K, Pawelek P, Grinnell F. Stress relaxation of contracted collagen gels: disruption of actin filament bundles, release of cell surface fibronectin, and down-regulation of DNA and protein synthesis. Exp Cell Res. 1991 Mar;193(1):198–207.

312. Swift J, Ivanovska IL, Buxboim A, Harada T, Dingal PCDP, Pinter J, et al. Nuclear lamin-A scales with tissue stiffness and enhances matrix-directed differentiation. Science. 2013 Aug 30;341(6149):1240104.

313. Gray SD, Titze IR, Chan R, Hammond TH. Vocal fold proteoglycans and their influence on biomechanics. Laryngoscope. 1999 Jun;109(6):845–54.

314. Itano N, Sawai T, Yoshida M, Lenas P, Yamada Y, Imagawa M, et al. Three isoforms of mammalian hyaluronan synthases have distinct enzymatic properties. J Biol Chem. 1999 Aug 27;274(35):25085–92.

315. D'Ardenne AJ, Burns J, Sykes BC, Kirkpatrick P. Comparative distribution of fibronectin and type III collagen in normal human tissues. J Pathol. 1983 Sep;141(1):55–69.

316. Ruoslahti E. Fibronectin and its receptors. Annu Rev Biochem. 1988;57:375–413.

317. Singh P, Carraher C, Schwarzbauer JE. Assembly of fibronectin extracellular matrix. Annu Rev Cell Dev Biol. 2010;26:397–419.

318. Saed GM, Zhang W, Diamond MP. Molecular characterization of fibroblasts isolated from human peritoneum and adhesions. Fertil Steril. 2001 Apr;75(4):763–8.

319. Ehrlich HP, Desmoulière A, Diegelmann RF, Cohen IK, Compton CC, Garner WL, et al. Morphological and immunochemical differences between keloid and hypertrophic scar. Am J Pathol. 1994 Jul;145(1):105–13.

320. McQuibban GA, Gong J-H, Wong JP, Wallace JL, Clark-Lewis I, Overall CM. Matrix metalloproteinase processing of monocyte chemoattractant proteins generates CC chemokine receptor antagonists with anti-inflammatory properties in vivo. Blood. 2002 Aug 15;100(4):1160–7.

321. Welham NV, Chang Z, Smith LM, Frey BL. Proteomic analysis of a decellularized human vocal fold mucosa scaffold using 2D electrophoresis and high-resolution mass spectrometry. Biomaterials. 2013 Jan;34(3):669–76.

322. Tse JR, Long JL. Microstructure characterization of a decellularized vocal fold scaffold for laryngeal tissue engineering. Laryngoscope. 2014 Aug;124(8):E326-331.

323. Fisher KV, Telser A, Phillips JE, Yeates DB. Regulation of vocal fold transepithelial water fluxes. J Appl Physiol. 2001 Sep;91(3):1401–11.

324. Schneider B, Teschner M, Sudermann T, Pikula B, Lautermann J. Expression of gap junction proteins (connexin 26, 30, 32, 43) in normal mucosa, hyperkeratosis and carcinoma of the human larynx. ORL J Otorhinolaryngol Relat Spec. 2002 Oct;64(5):324–9.

325. Kalluri R, Weinberg RA. The basics of epithelial-mesenchymal transition. J Clin Invest. 2009 Jun;119(6):1420–8.

326. Zavadil J, Böttinger EP. TGF-beta and epithelial-to-mesenchymal transitions. Oncogene. 2005 Aug 29;24(37):5764–74.

327. Long JL, Zuk P, Berke GS, Chhetri DK. Epithelial differentiation of adipose-derived stem cells for laryngeal tissue engineering. Laryngoscope. 2010 Jan;120(1):125–31.

328. Erickson AC, Couchman JR. Still more complexity in mammalian basement membranes. J Histochem Cytochem. 2000 Oct;48(10):1291–306.

329. Streuli CH, Bailey N, Bissell MJ. Control of mammary epithelial differentiation: basement membrane induces tissue-specific gene expression in the absence of cell-cell interaction and morphological polarity. J Cell Biol. 1991 Dec;115(5):1383–95.

330. Hynes RO. The extracellular matrix: not just pretty fibrils. Science. 2009 Nov 27;326(5957):1216–9.

331. Berchtold CM, Coughlin A, Kasper Z, Thibeault SL. Paracrine potential of fibroblasts exposed to cigarette smoke extract with vascular growth factor induction. Laryngoscope. 2013 Sep;123(9):2228–36.

332. Branski RC, Saltman B, Sulica L, Szeto H, Duflo S, Felsen D, et al. Cigarette smoke and reactive oxygen species metabolism: implications for the pathophysiology of Reinke's edema. Laryngoscope. 2009 Oct;119(10):2014–8.

333. Wang J, Fang R, Peterson A, Jiang JJ. The Protective Role of Autophagy in Human Vocal Fold Fibroblasts under Cigarette Smoke Extract Exposure: A New Insight into the Study of Reinke's Edema. ORL J Otorhinolaryngol Relat Spec. 2016;78(1):26–35.

334. Gugatschka M, Darnhofer B, Grossmann T, Schittmayer M, Hortobagyi D, Kirsch A, et al. Proteomic Analysis of Vocal Fold Fibroblasts Exposed to Cigarette Smoke Extract: Exploring the Pathophysiology of Reinke's Edema. Mol Cell Proteomics. 2019;18(8):1511–25.

335. Ishii K, Yamashita K, Akita M, Hirose H. Age-related development of the arrangement of connective tissue fibers in the lamina propria of the human vocal fold. Ann Otol Rhinol Laryngol. 2000 Nov;109(11):1055–64.

6. Supplementary data

Table S 1. List of proteins identified in LC-MS/MS analysis of hVFF without collagen matrix, analyzed by MaxQuant by searching the public SwissProt human database plus rat collagens, based on a 1 % FDR. Proteins are listed in order of descending intensities.

Majority protein IDs	Protein names	Gene names	Intensity
P08670	Vimentin	VIM	587100000
P63261;P60709	Actin, cytoplasmic 2;Actin, cytoplasmic 2, N-terminally processed;Actin, cytoplasmic 1;Actin, cytoplasmic 1, N-terminally processed	ACTG1;ACTB	244220000
P12111	Collagen alpha-3(VI) chain	COL6A3	144020000
P02545	Prelamin-A/C;Lamin-A/C	LMNA	93987000
Q71U36;P68363;P0DPH8;P0DPH7;Q6PEY2	Tubulin alpha-1A chain;Tubulin alpha-1B chain;Tubulin alpha-3E chain	TUBA1A;TUBA1B;TUBA3E	93978000
P07355;A6NMY6	Annexin A2;Putative annexin A2-like protein	ANXA2;ANXA2P2	87150000
P09382	Galectin-1	LGALS1	86551000
P35579	Myosin-9	MYH9	73286000
P06703	Protein S100-A6	S100A6	69979000
Q15149	Plectin	PLEC	61374000
Q5VTE0;P68104;Q05639	Putative elongation factor 1-alpha-like 3;Elongation factor 1-alpha 1;Elongation factor 1-alpha 2	EEF1A1P5;EEF1A1;EEF1A2	59721000
P21333	Filamin-A	FLNA	58959000
P68371;P04350	Tubulin beta-4B chain;Tubulin beta-4A chain	TUBB4B;TUBB4A	58886000
Q09666	Neuroblast differentiation-associated protein AHNAK	AHNAK	50918000
P14618	Pyruvate kinase PKM	PKM	46622000
P08238	Heat shock protein HSP 90-beta	HSP90AB1	45793000
P62805	Histone H4	HIST1H4A	45789000
P07858	Cathepsin B;Cathepsin B light chain;Cathepsin B heavy chain	CTSB	45530000
Q16778;P33778;P23527;P06899;Q8N257	Histone H2B type 2-E;Histone H2B type 1-B;Histone H2B type 1-O;Histone H2B type 1-J;Histone H2B type 3-B	HIST2H2BE;HIST1H2BB;HIST1H2BO;HIST1H2BJ;HIST3H2BB	43459000
P18206	Vinculin	VCL	42634000
P15121	Aldose reductase	AKR1B1	41516000
P08758	Annexin A5	ANXA5	41194000
P06733	Alpha-enolase	ENO1	40058000
P11142	Heat shock cognate 71 kDa protein	HSPA8	38513000
Q06830	Peroxiredoxin-1	PRDX1	37906000
P60174	Triosephosphate isomerase	TPI1	35146000
P23528;Q9Y281	Cofilin-1;Cofilin-2	CFL1;CFL2	33506000
P08962	CD63 antigen	CD63	33337000
P04179	Superoxide dismutase [Mn], mitochondrial	SOD2	32931000
P00338	L-lactate dehydrogenase A chain	LDHA	32119000
P63104	14-3-3 protein zeta/delta	YWHAZ	30960000
P13639	Elongation factor 2	EEF2	30761000
P04083	Annexin A1	ANXA1	29639000
P04792	Heat shock protein beta-1	HSPB1	26673000
P16401	Histone H1.5	HIST1H1B	25890000
P04406	Glyceraldehyde-3-phosphate dehydrogenase	GAPDH	24326000
P27797	Calreticulin	CALR	23306000
P12110	Collagen alpha-2(VI) chain	COL6A2	22131000
P07900	Heat shock protein HSP 90-alpha	HSP90AA1	20982000

Q9H299	SH3 domain-binding glutamic acid-rich-like protein 3	SH3BGRL3	20973000
P06748	Nucleophosmin	NPM1	20618000
P67936	Tropomyosin alpha-4 chain	TPM4	20435000
P06396;CON__Q3SX14	Gelsolin	GSN	20116000
P16403;P10412;P16402;P22492;Q02539	Histone H1.2;Histone H1.4;Histone H1.3;Histone H1t;Histone H1.1	HIST1H1C;HIST1H1E;HIST1H1D;HIST1H1T;HIST1H1A	19915000
P00558	Phosphoglycerate kinase 1	PGK1	19270000
P11021	78 kDa glucose-regulated protein	HSPA5	19091000
Q14315	Filamin-C	FLNC	19074000
P30101	Protein disulfide-isomerase A3	PDIA3	18972000
P12109	Collagen alpha-1(VI) chain	COL6A1	18691000
P22626	Heterogeneous nuclear ribonucleoproteins A2/B1	HNRNPA2B1	18635000
P29401	Transketolase	TKT	18558000
P07737	Profilin-1	PFN1	18441000
P14625	Endoplasmin	HSP90B1	18440000
Q01995	Transgelin	TAGLN	18127000
P37802	Transgelin-2	TAGLN2	17773000
P05556	Integrin beta-1	ITGB1	17275000
Q00610	Clathrin heavy chain 1	CLTC	17013000
P80297;P02795;P13640;P80294;P04731	Metallothionein-1X;Metallothionein-2;Metallothionein-1G;Metallothionein-1H;Metallothionein-1A	MT1X;MT2A;MT1G;MT1H;MT1A	16484000
P07237	Protein disulfide-isomerase	P4HB	15321000
P60660	Myosin light polypeptide 6	MYL6	14745000
P09936	Ubiquitin carboxyl-terminal hydrolase isozyme L1	UCHL1	14358000
O43707	Alpha-actinin-4	ACTN4	13875000
P10809	60 kDa heat shock protein, mitochondrial	HSPD1	13740000
P19338	Nucleolin	NCL	13397000
P08133	Annexin A6	ANXA6	13388000
Q07065	Cytoskeleton-associated protein 4	CKAP4	12949000
Q9Y490	Talin-1	TLN1	12878000
P00761;CON__P00761			12612000
P15144	Aminopeptidase N	ANPEP	12274000
P10599	Thioredoxin	TXN	12208000
P04075;P00883	Fructose-bisphosphate aldolase A	ALDOA	12093000
Q14764	Major vault protein	MVP	11896000
P62820;Q9H0U4	Ras-related protein Rab-1A;Ras-related protein Rab-1B	RAB1A;RAB1B	11850000
P26038	Moesin	MSN	11799000
O00299	Chloride intracellular channel protein 1	CLIC1	11673000
O75083	WD repeat-containing protein 1	WDR1	11240000
CON__P21752;P63313;P62328	Thymosin beta-10;Thymosin beta-4;Hematopoietic system regulatory peptide	TMSB10;TMSB4X	11074000
P46781	40S ribosomal protein S9	RPS9	11023000
P17096	High mobility group protein HMG-I/HMG-Y	HMGA1	10946000
Q8IYM0	Protein FAM186B	FAM186B	10914000
P11413	Glucose-6-phosphate 1-dehydrogenase	G6PD	10846000
P12236;P05141;P12235	ADP/ATP translocase 3;ADP/ATP translocase 3, N-terminally processed;ADP/ATP translocase 2;ADP/ATP translocase 2, N-terminally processed;ADP/ATP translocase 1	SLC25A6;SLC25A5;SLC25A4	10657000
P62826	GTP-binding nuclear protein Ran	RAN	10264000
P63244	Guanine nucleotide-binding protein subunit beta-2-like 1;Guanine nucleotide-binding protein subunit beta-2-like 1, N-terminally processed	GNB2L1	10246000
P38646	Stress-70 protein, mitochondrial	HSPA9	10106000

P62258	14-3-3 protein epsilon	YWHAE	10030000
P15880	40S ribosomal protein S2	RPS2	10017000
P62851	40S ribosomal protein S25	RPS25	9982000
P23396	40S ribosomal protein S3	RPS3	9868500
P21796	Voltage-dependent anion-selective channel protein 1	VDAC1	9634000
P24821	Tenascin	TNC	9616800
P36578	60S ribosomal protein L4	RPL4	9187100
P62937	Peptidyl-prolyl cis-trans isomerase A;Peptidyl-prolyl cis-trans isomerase A, N-terminally processed	PPIA	9138200
P61978	Heterogeneous nuclear ribonucleoprotein K	HNRNPK	9066800
P26641	Elongation factor 1-gamma	EEF1G	8765600
P23284	Peptidyl-prolyl cis-trans isomerase B	PPIB	8712400
P17066;P48741	Heat shock 70 kDa protein 6;Putative heat shock 70 kDa protein 7	HSPA6;HSPA7	8653900
CON__P13645;P13645;CON__P02535-1	Keratin, type I cytoskeletal 10	KRT10	8526800
P31949	Protein S100-A11;Protein S100-A11, N-terminally processed	S100A11	8450700
P63267;P68032;P62736;P68133	Actin, gamma-enteric smooth muscle;Actin, alpha cardiac muscle 1;Actin, aortic smooth muscle;Actin, alpha skeletal muscle	ACTG2;ACTC1;ACTA2;ACTA1	8436000
P13667	Protein disulfide-isomerase A4	PDIA4	8412500
Q14195	Dihydropyrimidinase-related protein 3	DPYSL3	8338600
P11766	Alcohol dehydrogenase class-3	ADH5	8230800
P46821	Microtubule-associated protein 1B;MAP1B heavy chain;MAP1 light chain LC1	MAP1B	8179600
P25705	ATP synthase subunit alpha, mitochondrial	ATP5A1	8178100
P39019	40S ribosomal protein S19	RPS19	8156900
P30086	Phosphatidylethanolamine-binding protein 1;Hippocampal cholinergic neurostimulating peptide	PEBP1	8093100
P02769;CON__P02769			8065700
P11279	Lysosome-associated membrane glycoprotein 1	LAMP1	8044300
Q14956	Transmembrane glycoprotein NMB	GPNMB	7887400
P45880	Voltage-dependent anion-selective channel protein 2	VDAC2	7694000
P60842	Eukaryotic initiation factor 4A-I	EIF4A1	7685800
P26447	Protein S100-A4	S100A4	7656300
P20700	Lamin-B1	LMNB1	7404800
P17655	Calpain-2 catalytic subunit	CAPN2	7351800
P07195	L-lactate dehydrogenase B chain	LDHB	7299800
Q14204	Cytoplasmic dynein 1 heavy chain 1	DYNC1H1	7100600
Q9P2E9	Ribosome-binding protein 1	RRBP1	7065900
P32119	Peroxiredoxin-2	PRDX2	7023400
Q9Y696	Chloride intracellular channel protein 4	CLIC4	6656400
Q99878;Q96KK5;Q9BTM1;Q93077;Q7L7L0;P20671;P0C0S8;P04908;Q16777;Q6FI13;Q8IUE6;P16104;Q96QV6	Histone H2A type 1-J;Histone H2A type 1-H;Histone H2A.J;Histone H2A type 1-C;Histone H2A type 3;Histone H2A type 1-D;Histone H2A type 1;Histone H2A type 1-B/E;Histone H2A type 2-C;Histone H2A type 2-A;Histone H2A type 2-B;Histone H2AX;Histone H2A type 1-A	HIST1H2AJ;HIST1H2AH;H2AFJ;HIST1H2AC;HIST3H2A;HIST1H2AD;HIST1H2AG;HIST1H2AB;HIST2H2AC;HIST2H2AA3;HIST2H2AB;H2AFX;HIST1H2AA	6622300
O60664	Perilipin-3	PLIN3	6597100
Q6BDS2	UHRF1-binding protein 1	UHRF1BP1	6562400
Q9UNX3;P61254	60S ribosomal protein L26-like 1;60S ribosomal protein L26	RPL26L1;RPL26	6547100
P09211	Glutathione S-transferase P	GSTP1	6404100
Q9GZV4;P63241;Q6IS14	Eukaryotic translation initiation factor 5A-2;Eukaryotic translation initiation factor 5A-1;Eukaryotic translation initiation factor 5A-1-like	EIF5A2;EIF5A;EIF5AL1	6389000

P61604	10 kDa heat shock protein, mitochondrial	HSPE1	6331700
P05120	Plasminogen activator inhibitor 2	SERPINB2	6326700
Q01518	Adenylyl cyclase-associated protein 1	CAP1	6309100
P18669	Phosphoglycerate mutase 1	PGAM1	6021100
P17301	Integrin alpha-2	ITGA2	6000100
P37837	Transaldolase	TALDO1	5989500
P61247	40S ribosomal protein S3a	RPS3A	5908100
Q14108	Lysosome membrane protein 2	SCARB2	5839600
P13987	CD59 glycoprotein	CD59	5805900
P30041	Peroxiredoxin-6	PRDX6	5747800
P61158	Actin-related protein 3	ACTR3	5627100
O43852	Calumenin	CALU	5610200
Q16658	Fascin	FSCN1	5580300
P46940	Ras GTPase-activating-like protein IQGAP1	IQGAP1	5521000
P61586	Transforming protein RhoA	RHOA	5429800
P61981	14-3-3 protein gamma;14-3-3 protein gamma, N-terminally processed	YWHAG	5259200
Q7KZF4	Staphylococcal nuclease domain-containing protein 1	SND1	5253200
Q96TA1	Niban-like protein 1	FAM129B	5234900
P08865	40S ribosomal protein SA	RPSA	5204000
CON__ENSEMBL:ENSBTAP00000025008			5196500
P52272	Heterogeneous nuclear ribonucleoprotein M	HNRNPM	5196500
P09525	Annexin A4	ANXA4	5147500
P13797	Plastin-3	PLS3	5134900
P49207	60S ribosomal protein L34	RPL34	5088300
REV__P48681			5088300
P31150	Rab GDP dissociation inhibitor alpha	GDI1	5070600
P46782	40S ribosomal protein S5;40S ribosomal protein S5, N-terminally processed	RPS5	5057500
P62424	60S ribosomal protein L7a	RPL7A	5026000
Q15582	Transforming growth factor-beta-induced protein ig-h3	TGFBI	5022700
P40925	Malate dehydrogenase, cytoplasmic	MDH1	5015400
P52565	Rho GDP-dissociation inhibitor 1	ARHGDIA	4981300
Q99439	Calponin-2	CNN2	4955100
P07951;CON__Q3SX28	Tropomyosin beta chain	TPM2	4931600
P21399	Cytoplasmic aconitate hydratase	ACO1	4917700
P06744	Glucose-6-phosphate isomerase	GPI	4860800
P04264;CON__P04264	Keratin, type II cytoskeletal 1	KRT1	4833200
P61313	60S ribosomal protein L15	RPL15	4827700
P62269	40S ribosomal protein S18	RPS18	4826400
Q02878	60S ribosomal protein L6	RPL6	4782400
Q15365;Q15366	Poly(rC)-binding protein 1;Poly(rC)-binding protein 2	PCBP1;PCBP2	4749700
P55072	Transitional endoplasmic reticulum ATPase	VCP	4740000
P13489	Ribonuclease inhibitor	RNH1	4670200
Q07954	Prolow-density lipoprotein receptor-related protein 1;Low-density lipoprotein receptor-related protein 1 85 kDa subunit;Low-density lipoprotein receptor-related protein 1 515 kDa subunit;Low-density lipoprotein receptor-related protein 1 intracellular domain	LRP1	4613200
P06576	ATP synthase subunit beta, mitochondrial	ATP5B	4516900
REV__Q7Z5W3			4487000
Q14847	LIM and SH3 domain protein 1	LASP1	4462500
P54727	UV excision repair protein RAD23 homolog B	RAD23B	4418500
Q16555	Dihydropyrimidinase-related protein 2	DPYSL2	4401500

P07339	Cathepsin D;Cathepsin D light chain;Cathepsin D heavy chain	CTSD	4388900
P29373	Cellular retinoic acid-binding protein 2	CRABP2	4351300
P62241	40S ribosomal protein S8	RPS8	4349300
Q14697	Neutral alpha-glucosidase AB	GANAB	4331600
P09651;Q32P51	Heterogeneous nuclear ribonucleoprotein A1;Heterogeneous nuclear ribonucleoprotein A1, N-terminally processed;Heterogeneous nuclear ribonucleoprotein A1-like 2	HNRNPA1;HNRNPA1L2	4329500
Q969G5	Protein kinase C delta-binding protein	PRKCDBP	4302900
P40926	Malate dehydrogenase, mitochondrial	MDH2	4263800
O60361;P22392;P15531	Putative nucleoside diphosphate kinase;Nucleoside diphosphate kinase B;Nucleoside diphosphate kinase A	NME2P1;NME2;NME1	4258500
P51149	Ras-related protein Rab-7a	RAB7A	4250400
O75396	Vesicle-trafficking protein SEC22b	SEC22B	4193800
Q07020	60S ribosomal protein L18	RPL18	4185400
P31948	Stress-induced-phosphoprotein 1	STIP1	4068300
P48681	Nestin	NES	4065400
P27348	14-3-3 protein theta	YWHAQ	4063900
P39023;Q92901	60S ribosomal protein L3;60S ribosomal protein L3-like	RPL3;RPL3L	4063700
P31946	14-3-3 protein beta/alpha;14-3-3 protein beta/alpha, N-terminally processed	YWHAB	4048700
P24534	Elongation factor 1-beta	EEF1B2	4025800
P21980	Protein-glutamine gamma-glutamyltransferase 2	TGM2	4005900
P00387	NADH-cytochrome b5 reductase 3;NADH-cytochrome b5 reductase 3 membrane-bound form;NADH-cytochrome b5 reductase 3 soluble form	CYB5R3	3999700
Q99497	Protein deglycase DJ-1	PARK7	3975600
Q99584	Protein S100-A13	S100A13	3964200
P00441	Superoxide dismutase [Cu-Zn]	SOD1	3963900
P40121	Macrophage-capping protein	CAPG	3923500
P62081	40S ribosomal protein S7	RPS7	3915200
P04843	Dolichyl-diphosphooligosaccharide--protein glycosyltransferase subunit 1	RPN1	3901400
Q14247	Src substrate cortactin	CTTN	3889900
O60701	UDP-glucose 6-dehydrogenase	UGDH	3889400
P19105;O14950	Myosin regulatory light chain 12A;Myosin regulatory light chain 12B	MYL12A;MYL12B	3883200
P00325;P00326;P07327	Alcohol dehydrogenase 1B;Alcohol dehydrogenase 1C;Alcohol dehydrogenase 1A	ADH1B;ADH1C;ADH1A	3752100
Q8TF72	Protein Shroom3	SHROOM3	3687600
P23219	Prostaglandin G/H synthase 1	PTGS1	3676500
P17931	Galectin-3	LGALS3	3659100
Q15942	Zyxin	ZYX	3646400
P26639	Threonine--tRNA ligase, cytoplasmic	TARS	3618100
P47756	F-actin-capping protein subunit beta	CAPZB	3617500
Q6NZI2	Polymerase I and transcript release factor	PTRF	3613200
P16152	Carbonyl reductase [NADPH] 1	CBR1	3609500
P06865	Beta-hexosaminidase subunit alpha	HEXA	3526000
P10316;P01892;P01891	HLA class I histocompatibility antigen, A-69 alpha chain;HLA class I histocompatibility antigen, A-2 alpha chain;HLA class I histocompatibility antigen, A-68 alpha chain	HLA-A	3512100
P07910	Heterogeneous nuclear ribonucleoproteins C1/C2	HNRNPC	3479200
P62913	60S ribosomal protein L11	RPL11	3477200
P12814	Alpha-actinin-1	ACTN1	3418900
P78527	DNA-dependent protein kinase catalytic subunit	PRKDC	3394800
Q9UL46	Proteasome activator complex subunit 2	PSME2	3390700
Q8WUM4	Programmed cell death 6-interacting protein	PDCD6IP	3315800
Q9NZM1	Myoferlin	MYOF	3299100
P0DMV9;P0DMV8	Heat shock 70 kDa protein 1B;Heat shock 70 kDa protein 1A	HSPA1B;HSPA1A	3282400

P61224;A6NIZ1	Ras-related protein Rap-1b;Ras-related protein Rap-1b-like protein	RAP1B	3266300
Q9Y6N5	Sulfide:quinone oxidoreductase, mitochondrial	SQRDL	3258600
P84077;P61204;P84085	ADP-ribosylation factor 1;ADP-ribosylation factor 3;ADP-ribosylation factor 5	ARF1;ARF3;ARF5	3256800
Q00325	Phosphate carrier protein, mitochondrial	SLC25A3	3226800
P40227	T-complex protein 1 subunit zeta	CCT6A	3219200
P17987	T-complex protein 1 subunit alpha	TCP1	3214100
Q14974	Importin subunit beta-1	KPNB1	3205800
P50990	T-complex protein 1 subunit theta	CCT8	3204100
P25788	Proteasome subunit alpha type-3	PSMA3	3200900
P07384	Calpain-1 catalytic subunit	CAPN1	3175200
P18124	60S ribosomal protein L7	RPL7	3155300
P62857	40S ribosomal protein S28	RPS28	3155000
P62753	40S ribosomal protein S6	RPS6	3132500
P83731	60S ribosomal protein L24	RPL24	3132000
P62942	Peptidyl-prolyl cis-trans isomerase FKBP1A	FKBP1A	3126000
P27816	Microtubule-associated protein 4	MAP4	3125600
P31939	Bifunctional purine biosynthesis protein PURH;Phosphoribosylaminoimidazolecarboxamide formyltransferase;IMP cyclohydrolase	ATIC	3121600
Q05682	Caldesmon	CALD1	3119400
P60981	Destrin	DSTN	3088600
P62899	60S ribosomal protein L31	RPL31	3066100
Q16181	Septin-7	07.Sep	3062600
P16070	CD44 antigen	CD44	3007900
P63010	AP-2 complex subunit beta	AP2B1	2976400
P35268	60S ribosomal protein L22	RPL22	2955800
P04632	Calpain small subunit 1	CAPNS1	2914900
P29692	Elongation factor 1-delta	EEF1D	2912400
P35555	Fibrillin-1	FBN1	2905300
P46776	60S ribosomal protein L27a	RPL27A	2882900
P49448;P00367	Glutamate dehydrogenase 2, mitochondrial;Glutamate dehydrogenase 1, mitochondrial	GLUD2;GLUD1	2838400
P62491;Q15907	Ras-related protein Rab-11A;Ras-related protein Rab-11B	RAB11A;RAB11B	2826500
P0DP25;P0DP24;P0DP23			2800800
P47755	F-actin-capping protein subunit alpha-2	CAPZA2	2793400
P62701;Q8TD47;P22090	40S ribosomal protein S4, X isoform;40S ribosomal protein S4, Y isoform 2;40S ribosomal protein S4, Y isoform 1	RPS4X;RPS4Y2;RPS4Y1	2789700
Q12797	Aspartyl/asparaginyl beta-hydroxylase	ASPH	2779500
P38159;Q96E39	RNA-binding motif protein, X chromosome;RNA-binding motif protein, X chromosome, N-terminally processed;RNA binding motif protein, X-linked-like-1	RBMX;RBMXL1	2738900
P11940	Polyadenylate-binding protein 1	PABPC1	2729700
P60468	Protein transport protein Sec61 subunit beta	SEC61B	2718700
Q02543	60S ribosomal protein L18a	RPL18A	2697700

P30464;P30484;Q95365;P30466;Q29940;P30685;P30491;P30490;P18464;P30481;P18463;P30498;P30495;P30493;P30492;P18465;P10319;Q29960	HLA class I histocompatibility antigen, B-15 alpha chain;HLA class I histocompatibility antigen, B-46 alpha chain;HLA class I histocompatibility antigen, B-38 alpha chain;HLA class I histocompatibility antigen, B-18 alpha chain;HLA class I histocompatibility antigen, B-59 alpha chain;HLA class I histocompatibility antigen, B-35 alpha chain;HLA class I histocompatibility antigen, B-53 alpha chain;HLA class I histocompatibility antigen, B-52 alpha chain;HLA class I histocompatibility antigen, B-51 alpha chain;HLA class I histocompatibility antigen, B-44 alpha chain;HLA class I histocompatibility antigen, B-37 alpha chain;HLA class I histocompatibility antigen, B-78 alpha chain;HLA class I histocompatibility antigen, B-56 alpha chain;HLA class I histocompatibility antigen, B-55 alpha chain;HLA class I histocompatibility antigen, B-54 alpha chain;HLA class I histocompatibility antigen, B-57 alpha chain;HLA class I histocompatibility antigen, B-58 alpha chain;HLA class I histocompatibility antigen, Cw-16 alpha chain	HLA-B;HLA-C	2682300
Q5JNZ5;P62854	Putative 40S ribosomal protein S26-like 1;40S ribosomal protein S26	RPS26P11;RPS26	2662500
P07437	Tubulin beta chain	TUBB	2652900
P18621	60S ribosomal protein L17	RPL17	2633700
P27105	Erythrocyte band 7 integral membrane protein	STOM	2603900
O15143	Actin-related protein 2/3 complex subunit 1B	ARPC1B	2602700
P62263	40S ribosomal protein S14	RPS14	2595700
P14866	Heterogeneous nuclear ribonucleoprotein L	HNRNPL	2578600
P55084	Trifunctional enzyme subunit beta, mitochondrial;3-ketoacyl-CoA thiolase	HADHB	2568200
Q16881	Thioredoxin reductase 1, cytoplasmic	TXNRD1	2547700
P48444	Coatomer subunit delta	ARCN1	2533100
P07686	Beta-hexosaminidase subunit beta;Beta-hexosaminidase subunit beta chain B;Beta-hexosaminidase subunit beta chain A	HEXB	2530300
P50995	Annexin A11	ANXA11	2506100
P84098	60S ribosomal protein L19	RPL19	2498000
P40939	Trifunctional enzyme subunit alpha, mitochondrial;Long-chain enoyl-CoA hydratase;Long chain 3-hydroxyacyl-CoA dehydrogenase	HADHA	2486000
Q15185	Prostaglandin E synthase 3	PTGES3	2485600
P14314	Glucosidase 2 subunit beta	PRKCSH	2470300
P62879;P62873;P16520	Guanine nucleotide-binding protein G(I)/G(S)/G(T) subunit beta-2;Guanine nucleotide-binding protein G(I)/G(S)/G(T) subunit beta-1;Guanine nucleotide-binding protein G(I)/G(S)/G(T) subunit beta-3	GNB2;GNB1;GNB3	2462900
O60506;O43390	Heterogeneous nuclear ribonucleoprotein Q;Heterogeneous nuclear ribonucleoprotein R	SYNCRIP;HNRNPR	2434200
P07108	Acyl-CoA-binding protein	DBI	2422600
Q15084	Protein disulfide-isomerase A6	PDIA6	2391400
P24752	Acetyl-CoA acetyltransferase, mitochondrial	ACAT1	2384300
Q9NRW1;P20340;Q14964	Ras-related protein Rab-6B;Ras-related protein Rab-6A;Ras-related protein Rab-39A	RAB6B;RAB6A;RAB39A	2380500
P52209	6-phosphogluconate dehydrogenase, decarboxylating	PGD	2374200
P26373	60S ribosomal protein L13	RPL13	2340800
P67809	Nuclease-sensitive element-binding protein 1	YBX1	2334100
P62906	60S ribosomal protein L10a	RPL10A	2322000
O14818;Q8TAA3	Proteasome subunit alpha type-7;Proteasome subunit alpha type-7-like	PSMA7;PSMA8	2314200
P62249	40S ribosomal protein S16	RPS16	2305400
P50991	T-complex protein 1 subunit delta	CCT4	2303800
P61088;Q5JXB2	Ubiquitin-conjugating enzyme E2 N;Putative ubiquitin-conjugating enzyme E2 N-like	UBE2N;UBE2NL	2299900
Q99832	T-complex protein 1 subunit eta	CCT7	2295600

O43399	Tumor protein D54	TPD52L2	2245100
P43490	Nicotinamide phosphoribosyltransferase	NAMPT	2243100
Q13404	Ubiquitin-conjugating enzyme E2 variant 1	UBE2V1	2231400
P09622	Dihydrolipoyl dehydrogenase, mitochondrial	DLD	2200100
Q12792	Twinfilin-1	TWF1	2198800
Q9BVK6	Transmembrane emp24 domain-containing protein 9	TMED9	2189700
P25398	40S ribosomal protein S12	RPS12	2183900
P50454	Serpin H1	SERPINH1	2161100
P21926	CD9 antigen	CD9	2153400
P60900	Proteasome subunit alpha type-6	PSMA6	2142100
P30040	Endoplasmic reticulum resident protein 29	ERP29	2132700
P07305	Histone H1.0;Histone H1.0, N-terminally processed	H1F0	2100200
P35232	Prohibitin	PHB	2095600
P40429;Q6NVV1	60S ribosomal protein L13a;Putative 60S ribosomal protein L13a protein RPL13AP3	RPL13A;RPL13AP3	2076300
Q01130;Q9BRL6	Serine/arginine-rich splicing factor 2;Serine/arginine-rich splicing factor 8	SRSF2;SRSF8	2016000
Q7L1Q6	Basic leucine zipper and W2 domain-containing protein 1	BZW1	1996800
P35237	Serpin B6	SERPINB6	1967100
Q03252	Lamin-B2	LMNB2	1964400
CON__Q3SZV7			1955000
Q00839	Heterogeneous nuclear ribonucleoprotein U	HNRNPU	1951800
P06753	Tropomyosin alpha-3 chain	TPM3	1939900
Q14103	Heterogeneous nuclear ribonucleoprotein D0	HNRNPD	1939300
Q16851	UTP--glucose-1-phosphate uridylyltransferase	UGP2	1927900
Q9UBR2	Cathepsin Z	CTSZ	1925400
Q92945	Far upstream element-binding protein 2	KHSRP	1916000
P46779	60S ribosomal protein L28	RPL28	1910300
Q92804	TATA-binding protein-associated factor 2N	TAF15	1893400
P21291	Cysteine and glycine-rich protein 1	CSRP1	1885000
P07814	Bifunctional glutamate/proline--tRNA ligase;Glutamate--tRNA ligase;Proline--tRNA ligase	EPRS	1884600
P28482	Mitogen-activated protein kinase 1	MAPK1	1878600
P62244	40S ribosomal protein S15a	RPS15A	1844100
Q12884	Prolyl endopeptidase FAP;Antiplasmin-cleaving enzyme FAP, soluble form	FAP	1830200
Q07960	Rho GTPase-activating protein 1	ARHGAP1	1823600
P53621	Coatomer subunit alpha;Xenin;Proxenin	COPA	1817500
P27635;Q96L21	60S ribosomal protein L10;60S ribosomal protein L10-like	RPL10;RPL10L	1813600
Q70UQ0	Inhibitor of nuclear factor kappa-B kinase-interacting protein	IKBIP	1772600
P13010	X-ray repair cross-complementing protein 5	XRCC5	1769000
P28066	Proteasome subunit alpha type-5	PSMA5	1768200
Q01813;P17858	ATP-dependent 6-phosphofructokinase, platelet type;ATP-dependent 6-phosphofructokinase, liver type	PFKP;PFKL	1767000
Q8NHW5;P05388	60S acidic ribosomal protein P0-like;60S acidic ribosomal protein P0	RPLP0P6;RPLP0	1747100
P30044	Peroxiredoxin-5, mitochondrial	PRDX5	1733800
Q08211	ATP-dependent RNA helicase A	DHX9	1728800
P35606	Coatomer subunit beta	COPB2	1728000
P62917	60S ribosomal protein L8	RPL8	1702200
Q15075	Early endosome antigen 1	EEA1	1699000
P84090	Enhancer of rudimentary homolog	ERH	1692000
P51572	B-cell receptor-associated protein 31	BCAP31	1663000
O00151	PDZ and LIM domain protein 1	PDLIM1	1656800
P02751	Fibronectin;Anastellin;Ugl-Y1;Ugl-Y2;Ugl-Y3	FN1	1654800
P63220	40S ribosomal protein S21	RPS21	1652400
P52926	High mobility group protein HMGI-C	HMGA2	1650900
P78371	T-complex protein 1 subunit beta	CCT2	1630100
P62633	Cellular nucleic acid-binding protein	CNBP	1619800

O75947	ATP synthase subunit d, mitochondrial	ATP5H	1610100
P26022	Pentraxin-related protein PTX3	PTX3	1601300
Q15233	Non-POU domain-containing octamer-binding protein	NONO	1581300
P25786	Proteasome subunit alpha type-1	PSMA1	1573400
Q8NBS9	Thioredoxin domain-containing protein 5	TXNDC5	1569100
P30626	Sorcin	SRI	1566800
P00505	Aspartate aminotransferase, mitochondrial	GOT2	1560600
O75390	Citrate synthase, mitochondrial	CS	1560500
Q04837	Single-stranded DNA-binding protein, mitochondrial	SSBP1	1558700
P51858	Hepatoma-derived growth factor	HDGF	1555700
Q13247	Serine/arginine-rich splicing factor 6	SRSF6	1540600
P49327	Fatty acid synthase;[Acyl-carrier-protein] S-acetyltransferase;[Acyl-carrier-protein] S-malonyltransferase;3-oxoacyl-[acyl-carrier-protein] synthase;3-oxoacyl-[acyl-carrier-protein] reductase;3-hydroxyacyl-[acyl-carrier-protein] dehydratase;Enoyl-[acyl-carrier-protein] reductase;Oleoyl-[acyl-carrier-protein] hydrolase	FASN	1537200
P10768	S-formylglutathione hydrolase	ESD	1524000
P25789	Proteasome subunit alpha type-4	PSMA4	1524000
O95302	Peptidyl-prolyl cis-trans isomerase FKBP9	FKBP9	1520500
Q99623	Prohibitin-2	PHB2	1517400
P05387	60S acidic ribosomal protein P2	RPLP2	1510700
Q16629	Serine/arginine-rich splicing factor 7	SRSF7	1504000
P32969	60S ribosomal protein L9	RPL9	1499700
P49368	T-complex protein 1 subunit gamma	CCT3	1497000
P62277	40S ribosomal protein S13	RPS13	1489000
P16435	NADPH--cytochrome P450 reductase	POR	1478100
Q9UBG0	C-type mannose receptor 2	MRC2	1470100
P55786;A6NEC2	Puromycin-sensitive aminopeptidase;Puromycin-sensitive aminopeptidase-like protein	NPEPPS;NPEPPSL1	1460400
Q9BR76	Coronin-1B	CORO1B	1436900
Q13813	Spectrin alpha chain, non-erythrocytic 1	SPTAN1	1434300
Q9UHD8	Septin-9	09.Sep	1415200
Q99536	Synaptic vesicle membrane protein VAT-1 homolog	VAT1	1402200
P50395	Rab GDP dissociation inhibitor beta	GDI2	1354100
Q13162	Peroxiredoxin-4	PRDX4	1344100
Q13557	Calcium/calmodulin-dependent protein kinase type II subunit delta	CAMK2D	1340800
P41250	Glycine--tRNA ligase	GARS	1323500
Q9UHB6	LIM domain and actin-binding protein 1	LIMA1	1319000
P48643	T-complex protein 1 subunit epsilon	CCT5	1312900
P20962	Parathymosin	PTMS	1309100
Q8IWE2	Protein NOXP20	FAM114A1	1308300
P55735	Protein SEC13 homolog	SEC13	1306500
Q13200	26S proteasome non-ATPase regulatory subunit 2	PSMD2	1296700
Q01082	Spectrin beta chain, non-erythrocytic 1	SPTBN1	1291700
Q03135	Caveolin-1	CAV1	1283400
P45974	Ubiquitin carboxyl-terminal hydrolase 5	USP5	1281700
P35998	26S protease regulatory subunit 7	PSMC2	1256000
Q9C0C2	182 kDa tankyrase-1-binding protein	TNKS1BP1	1247900
P62829	60S ribosomal protein L23	RPL23	1245100
Q9NQC3	Reticulon-4	RTN4	1242500
Q9NYU2	UDP-glucose:glycoprotein glucosyltransferase 1	UGGT1	1240800
P46439;P28161;P21266	Glutathione S-transferase Mu 5;Glutathione S-transferase Mu 2;Glutathione S-transferase Mu 3	GSTM5;GSTM2;GSTM3	1231400
Q15019	Septin-2	02.Sep	1227500
P61619;Q9H9S3	Protein transport protein Sec61 subunit alpha isoform 1;Protein transport protein Sec61 subunit alpha isoform 2	SEC61A1;SEC61A2	1218600
P08473	Neprilysin	MME	1211400
P35613	Basigin	BSG	1209900

Q9UNH7	Sorting nexin-6;Sorting nexin-6, N-terminally processed	SNX6	1200200
P62280	40S ribosomal protein S11	RPS11	1192100
Q96PK6	RNA-binding protein 14	RBM14	1186700
P42766	60S ribosomal protein L35	RPL35	1157300
Q5SSJ5	Heterochromatin protein 1-binding protein 3	HP1BP3	1155800
P10253	Lysosomal alpha-glucosidase;76 kDa lysosomal alpha-glucosidase;70 kDa lysosomal alpha-glucosidase	GAA	1154100
P23634	Plasma membrane calcium-transporting ATPase 4	ATP2B4	1152700
O75964	ATP synthase subunit g, mitochondrial	ATP5L	1148900
O00148;Q13838	ATP-dependent RNA helicase DDX39A;Spliceosome RNA helicase DDX39B	DDX39A;DDX39B	1143600
P23526	Adenosylhomocysteinase	AHCY	1133400
Q9BUF5	Tubulin beta-6 chain	TUBB6	1126400
Q92841	Probable ATP-dependent RNA helicase DDX17	DDX17	1123000
O00264	Membrane-associated progesterone receptor component 1	PGRMC1	1113500
P40261	Nicotinamide N-methyltransferase	NNMT	1105200
P05198	Eukaryotic translation initiation factor 2 subunit 1	EIF2S1	1101100
O60763	General vesicular transport factor p115	USO1	1099000
P07099	Epoxide hydrolase 1	EPHX1	1095700
Q92820	Gamma-glutamyl hydrolase	GGH	1094100
P62987;P62979;P0CG47;P0CG48	Ubiquitin-60S ribosomal protein L40;Ubiquitin;60S ribosomal protein L40;Ubiquitin-40S ribosomal protein S27a;Ubiquitin;40S ribosomal protein S27a;Polyubiquitin-B;Ubiquitin;Polyubiquitin-C;Ubiquitin	UBA52;RPS27A;UBB;UBC	1090000
O75955	Flotillin-1	FLOT1	1088300
P61160	Actin-related protein 2	ACTR2	1086900
O15372	Eukaryotic translation initiation factor 3 subunit H	EIF3H	1086700
Q15181	Inorganic pyrophosphatase	PPA1	1079100
P28331	NADH-ubiquinone oxidoreductase 75 kDa subunit, mitochondrial	NDUFS1	1076400
P62888	60S ribosomal protein L30	RPL30	1073400
Q9P0K7	Ankycorbin	RAI14	1072500
Q13151	Heterogeneous nuclear ribonucleoprotein A0	HNRNPA0	1068100
P46783;Q9NQ39	40S ribosomal protein S10;Putative 40S ribosomal protein S10-like	RPS10;RPS10P5	1043500
P30084	Enoyl-CoA hydratase, mitochondrial	ECHS1	1040900
Q06323	Proteasome activator complex subunit 1	PSME1	1040600
P53618	Coatomer subunit beta	COPB1	1039300
Q99613;B5ME19	Eukaryotic translation initiation factor 3 subunit C;Eukaryotic translation initiation factor 3 subunit C-like protein	EIF3C;EIF3CL	1023700
Q13011	Delta(3,5)-Delta(2,4)-dienoyl-CoA isomerase, mitochondrial	ECH1	1021400
Q9ULV4	Coronin-1C	CORO1C	1020300
P04899;P11488;P63096;P19087;P09471;P08754;A8MTJ3;P38405	Guanine nucleotide-binding protein G(i) subunit alpha-2;Guanine nucleotide-binding protein G(t) subunit alpha-1;Guanine nucleotide-binding protein G(i) subunit alpha-1;Guanine nucleotide-binding protein G(t) subunit alpha-2;Guanine nucleotide-binding protein G(o) subunit alpha;Guanine nucleotide-binding protein G(k) subunit alpha;Guanine nucleotide-binding protein G(t) subunit alpha-3;Guanine nucleotide-binding protein G(olf) subunit alpha	GNAI2;GNAT1;GNAI1;GNAT2;GNAO1;GNAI3;GNAT3;GNAL	1017200
P31040	Succinate dehydrogenase [ubiquinone] flavoprotein subunit, mitochondrial	SDHA	1013100
O75368	SH3 domain-binding glutamic acid-rich-like protein	SH3BGRL	1008100
O00571	ATP-dependent RNA helicase DDX3X	DDX3X	1005200
Q13509	Tubulin beta-3 chain	TUBB3	1004200
P53396	ATP-citrate synthase	ACLY	999740
P30740	Leukocyte elastase inhibitor	SERPINB1	999680
P43487	Ran-specific GTPase-activating protein	RANBP1	998010
O00303	Eukaryotic translation initiation factor 3 subunit F	EIF3F	992790
Q07955	Serine/arginine-rich splicing factor 1	SRSF1	986420
P46063	ATP-dependent DNA helicase Q1	RECQL	983180

P15559	NAD(P)H dehydrogenase [quinone] 1	NQO1	972270
O75367	Core histone macro-H2A.1	H2AFY	967870
P19367	Hexokinase-1	HK1	967870
O94979	Protein transport protein Sec31A	SEC31A	966080
P62750	60S ribosomal protein L23a	RPL23A	965610
P10619	Lysosomal protective protein;Lysosomal protective protein 32 kDa chain;Lysosomal protective protein 20 kDa chain	CTSA	962500
Q96BJ3	Axin interactor, dorsalization-associated protein	AIDA	956820
P36957	Dihydrolipoyllysine-residue succinyltransferase component of 2-oxoglutarate dehydrogenase complex, mitochondrial	DLST	955790
O00159	Unconventional myosin-Ic	MYO1C	951480
Q9Y265	RuvB-like 1	RUVBL1	948780
P36871	Phosphoglucomutase-1	PGM1	943830
Q96IU4	Alpha/beta hydrolase domain-containing protein 14B	ABHD14B	936180
Q00341	Vigilin	HDLBP	932920
P30050	60S ribosomal protein L12	RPL12	931420
Q14444	Caprin-1	CAPRIN1	929650
Q6NUK1	Calcium-binding mitochondrial carrier protein SCaMC-1	SLC25A24	924340
Q9NZN4	EH domain-containing protein 2	EHD2	915190
O15144	Actin-related protein 2/3 complex subunit 2	ARPC2	907250
P50281	Matrix metalloproteinase-14	MMP14	903660
P54577	Tyrosine--tRNA ligase, cytoplasmic;Tyrosine--tRNA ligase, cytoplasmic, N-terminally processed	YARS	903060
P42224	Signal transducer and activator of transcription 1-alpha/beta	STAT1	900100
Q9NRX4	14 kDa phosphohistidine phosphatase	PHPT1	893730
P27361	Mitogen-activated protein kinase 3	MAPK3	893240
P42356	Phosphatidylinositol 4-kinase alpha	PI4KA	891790
P48047	ATP synthase subunit O, mitochondrial	ATP5O	891110
O00483	Cytochrome c oxidase subunit NDUFA4	NDUFA4	884160
O75347	Tubulin-specific chaperone A	TBCA	879070
Q99436	Proteasome subunit beta type-7	PSMB7	875320
Q9UBI6	Guanine nucleotide-binding protein G(I)/G(S)/G(O) subunit gamma-12	GNG12	871230
P09496	Clathrin light chain A	CLTA	862250
Q99733	Nucleosome assembly protein 1-like 4	NAP1L4	858900
P39656	Dolichyl-diphosphooligosaccharide--protein glycosyltransferase 48 kDa subunit	DDOST	857770
Q15717;Q12926;P26378	ELAV-like protein 1;ELAV-like protein 2;ELAV-like protein 4	ELAVL1;ELAVL2;ELAVL4	854410
P14550	Alcohol dehydrogenase [NADP(+)]	AKR1A1	838030
Q99798	Aconitate hydratase, mitochondrial	ACO2	825710
P05413;P02689	Fatty acid-binding protein, heart;Myelin P2 protein	FABP3;PMP2	822950
Q01844	RNA-binding protein EWS	EWSR1	820640
P49588	Alanine--tRNA ligase, cytoplasmic	AARS	814260
P12004	Proliferating cell nuclear antigen	PCNA	812340
P20042	Eukaryotic translation initiation factor 2 subunit 2	EIF2S2	812290
Q13347	Eukaryotic translation initiation factor 3 subunit I	EIF3I	809450
P21281	V-type proton ATPase subunit B, brain isoform	ATP6V1B2	808160
Q15293	Reticulocalbin-1	RCN1	805730
Q7Z406	Myosin-14	MYH14	803260
P13473	Lysosome-associated membrane glycoprotein 2	LAMP2	799640
O60749;Q13596	Sorting nexin-2;Sorting nexin-1	SNX2;SNX1	795510
Q12906	Interleukin enhancer-binding factor 3	ILF3	789890
P51148;P20339	Ras-related protein Rab-5C;Ras-related protein Rab-5A	RAB5C;RAB5A	787600
O00567	Nucleolar protein 56	NOP56	785640
O95336	6-phosphogluconolactonase	PGLS	781510
P22314	Ubiquitin-like modifier-activating enzyme 1	UBA1	779500
P49257	Protein ERGIC-53	LMAN1	778500

O95394	Phosphoacetylglucosamine mutase	PGM3	771960
P13073	Cytochrome c oxidase subunit 4 isoform 1, mitochondrial	COX4I1	762340
O00764	Pyridoxal kinase	PDXK	760560
P35080	Profilin-2	PFN2	757220
Q16891	MICOS complex subunit MIC60	IMMT	749690
P63000;P60763;P15153	Ras-related C3 botulinum toxin substrate 1;Ras-related C3 botulinum toxin substrate 3;Ras-related C3 botulinum toxin substrate 2	RAC1;RAC3;RAC2	746620
P29966	Myristoylated alanine-rich C-kinase substrate	MARCKS	745930
O15511	Actin-related protein 2/3 complex subunit 5	ARPC5	740280
P26640	Valine--tRNA ligase	VARS	730680
Q15631	Translin	TSN	722470
Q15847	Adipogenesis regulatory factor	ADIRF	721330
P35659	Protein DEK	DEK	719870
P27695	DNA-(apurinic or apyrimidinic site) lyase;DNA-(apurinic or apyrimidinic site) lyase, mitochondrial	APEX1	719360
P09012	U1 small nuclear ribonucleoprotein A	SNRPA	716360
P30479;Q04826	HLA class I histocompatibility antigen, B-41 alpha chain;HLA class I histocompatibility antigen, B-40 alpha chain	HLA-B	713090
P48637	Glutathione synthetase	GSS	708190
P55060	Exportin-2	CSE1L	707450
P43243	Matrin-3	MATR3	701070
Q9Y678	Coatomer subunit gamma-1	COPG1	700950
P31943	Heterogeneous nuclear ribonucleoprotein H;Heterogeneous nuclear ribonucleoprotein H, N-terminally processed	HNRNPH1	697970
Q9BWM7	Sideroflexin-3	SFXN3	697860
Q96AC1	Fermitin family homolog 2	FERMT2	692960
P14868	Aspartate--tRNA ligase, cytoplasmic	DARS	691670
P61009	Signal peptidase complex subunit 3	SPCS3	690900
Q969M3	Protein YIPF5	YIPF5	688910
A0AVT1	Ubiquitin-like modifier-activating enzyme 6	UBA6	688790
P25787	Proteasome subunit alpha type-2	PSMA2	686450
Q9UJU6	Drebrin-like protein	DBNL	686220
Q9NVA2	Septin-11	11.Sep	672890
Q99873	Protein arginine N-methyltransferase 1	PRMT1	671740
Q9NUM4	Transmembrane protein 106B	TMEM106B	666100
P35611;P35612	Alpha-adducin;Beta-adducin	ADD1;ADD2	660910
Q16531	DNA damage-binding protein 1	DDB1	660230
P16278	Beta-galactosidase	GLB1	659270
P16930	Fumarylacetoacetase	FAH	657120
P62306	Small nuclear ribonucleoprotein F	SNRPF	656120
O43169	Cytochrome b5 type B	CYB5B	654690
Q9HDC9	Adipocyte plasma membrane-associated protein	APMAP	650160
Q32P28	Prolyl 3-hydroxylase 1	LEPRE1	649890
Q8WX93	Palladin	PALLD	647110
P21964	Catechol O-methyltransferase	COMT	646650
Q13148	TAR DNA-binding protein 43	TARDBP	646070
Q8NC51	Plasminogen activator inhibitor 1 RNA-binding protein	SERBP1	642620
P31930	Cytochrome b-c1 complex subunit 1, mitochondrial	UQCRC1	642050
P78559	Microtubule-associated protein 1A;MAP1A heavy chain;MAP1 light chain LC2	MAP1A	638600
P36873	Serine/threonine-protein phosphatase PP1-gamma catalytic subunit	PPP1CC	634070
P80723	Brain acid soluble protein 1	BASP1	626330
P55209	Nucleosome assembly protein 1-like 1	NAP1L1	622110
O75874	Isocitrate dehydrogenase [NADP] cytoplasmic	IDH1	621610
Q96G03	Phosphoglucomutase-2	PGM2	620880
Q15417	Calponin-3	CNN3	620680
Q99961;Q99962	Endophilin-A2;Endophilin-A1	SH3GL1;SH3GL2	619700
Q13263	Transcription intermediary factor 1-beta	TRIM28	616960

Q9H3P7	Golgi resident protein GCP60	ACBD3	616250
Q96QK1	Vacuolar protein sorting-associated protein 35	VPS35	615330
P62333	26S protease regulatory subunit 10B	PSMC6	611540
Q9Y2D5	A-kinase anchor protein 2	AKAP2	603040
P61019;Q8WUD1	Ras-related protein Rab-2A;Ras-related protein Rab-2B	RAB2A;RAB2B	602710
O43175	D-3-phosphoglycerate dehydrogenase	PHGDH	602000
O43865;Q96HN2	Putative adenosylhomocysteinase 2;Putative adenosylhomocysteinase 3	AHCYL1;AHCYL2	599920
Q9Y394	Dehydrogenase/reductase SDR family member 7	DHRS7	599720
Q96AY3	Peptidyl-prolyl cis-trans isomerase FKBP10	FKBP10	590690
Q9NR12	PDZ and LIM domain protein 7	PDLIM7	588230
P49721	Proteasome subunit beta type-2	PSMB2	587970
P49411	Elongation factor Tu, mitochondrial	TUFM	586340
Q14151;Q15424	Scaffold attachment factor B2;Scaffold attachment factor B1	SAFB2;SAFB	584840
O75643	U5 small nuclear ribonucleoprotein 200 kDa helicase	SNRNP200	583680
Q16630	Cleavage and polyadenylation specificity factor subunit 6	CPSF6	576260
P30043	Flavin reductase (NADPH)	BLVRB	575740
P40763	Signal transducer and activator of transcription 3	STAT3	575020
Q14914	Prostaglandin reductase 1	PTGR1	574520
Q13177;Q13153;O75914	Serine/threonine-protein kinase PAK 2;PAK-2p27;PAK-2p34;Serine/threonine-protein kinase PAK 1;Serine/threonine-protein kinase PAK 3	PAK2;PAK1;PAK3	572050
Q969H8	Myeloid-derived growth factor	MYDGF	571830
Q9Y6B6;Q9NR31	GTP-binding protein SAR1b;GTP-binding protein SAR1a	SAR1B;SAR1A	571740
P49915	GMP synthase [glutamine-hydrolyzing]	GMPS	568870
Q92616	Translational activator GCN1	GCN1L1	568500
P12955	Xaa-Pro dipeptidase	PEPD	566360
O43237	Cytoplasmic dynein 1 light intermediate chain 2	DYNC1LI2	561900
P22695	Cytochrome b-c1 complex subunit 2, mitochondrial	UQCRC2	558780
P22694;P17612	cAMP-dependent protein kinase catalytic subunit beta;cAMP-dependent protein kinase catalytic subunit alpha	PRKACB;PRKACA	557260
O14979	Heterogeneous nuclear ribonucleoprotein D-like	HNRNPDL	556850
P20073	Annexin A7	ANXA7	552140
P27487	Dipeptidyl peptidase 4;Dipeptidyl peptidase 4 membrane form;Dipeptidyl peptidase 4 soluble form	DPP4	547530
O95831	Apoptosis-inducing factor 1, mitochondrial	AIFM1	546690
Q16698	2,4-dienoyl-CoA reductase, mitochondrial	DECR1	546690
P33176;O60282;Q12840	Kinesin-1 heavy chain;Kinesin heavy chain isoform 5C;Kinesin heavy chain isoform 5A	KIF5B;KIF5C;KIF5A	543660
P61803	Dolichyl-diphosphooligosaccharide--protein glycosyltransferase subunit DAD1	DAD1	543360
Q9Y230	RuvB-like 2	RUVBL2	542020
P50479	PDZ and LIM domain protein 4	PDLIM4	540850
Q9HC38	Glyoxalase domain-containing protein 4	GLOD4	538090
O95573	Long-chain-fatty-acid--CoA ligase 3	ACSL3	536970
P55036	26S proteasome non-ATPase regulatory subunit 4	PSMD4	533880
Q92973	Transportin-1	TNPO1	530280
Q92791	Synaptonemal complex protein SC65	LEPREL4	529090
O94905	Erlin-2	ERLIN2	527210
P49419	Alpha-aminoadipic semialdehyde dehydrogenase	ALDH7A1	526620
P04040	Catalase	CAT	523210
P62714;P67775	Serine/threonine-protein phosphatase 2A catalytic subunit beta isoform;Serine/threonine-protein phosphatase 2A catalytic subunit alpha isoform	PPP2CB;PPP2CA	522360
P61006	Ras-related protein Rab-8A	RAB8A	515830
P51665	26S proteasome non-ATPase regulatory subunit 7	PSMD7	515260
P31942	Heterogeneous nuclear ribonucleoprotein H3	HNRNPH3	510880
P51688	N-sulphoglucosamine sulphohydrolase	SGSH	510150
P49458	Signal recognition particle 9 kDa protein	SRP9	507210

Q9Y277	Voltage-dependent anion-selective channel protein 3	VDAC3	503720
Q9Y2W1	Thyroid hormone receptor-associated protein 3	THRAP3	502450
Q13228	Selenium-binding protein 1	SELENBP1	498180
O00469	Procollagen-lysine,2-oxoglutarate 5-dioxygenase 2	PLOD2	497440
Q13643	Four and a half LIM domains protein 3	FHL3	497000
O43684	Mitotic checkpoint protein BUB3	BUB3	489980
Q9NRV9	Heme-binding protein 1	HEBP1	483320
Q14008	Cytoskeleton-associated protein 5	CKAP5	473930
P84074;P37235	Neuron-specific calcium-binding protein hippocalcin;Hippocalcin-like protein 1	HPCA;HPCAL1	473190
P04181	Ornithine aminotransferase, mitochondrial;Ornithine aminotransferase, hepatic form;Ornithine aminotransferase, renal form	OAT	473050
Q7L576;Q96F07	Cytoplasmic FMR1-interacting protein 1;Cytoplasmic FMR1-interacting protein 2	CYFIP1;CYFIP2	472430
P17980	26S protease regulatory subunit 6A	PSMC3	468540
P56192	Methionine--tRNA ligase, cytoplasmic	MARS	466240
Q14152	Eukaryotic translation initiation factor 3 subunit A	EIF3A	463890
Q9NVJ2;Q96BM9	ADP-ribosylation factor-like protein 8B;ADP-ribosylation factor-like protein 8A	ARL8B;ARL8A	463280
O95865	N(G),N(G)-dimethylarginine dimethylaminohydrolase 2	DDAH2	462050
Q8TCT9	Minor histocompatibility antigen H13	HM13	461220
Q9H6Z4	Ran-binding protein 3	RANBP3	459270
P27694	Replication protein A 70 kDa DNA-binding subunit;Replication protein A 70 kDa DNA-binding subunit, N-terminally processed	RPA1	457210
O95782;O94973	AP-2 complex subunit alpha-1;AP-2 complex subunit alpha-2	AP2A1;AP2A2	456700
P08134	Rho-related GTP-binding protein RhoC	RHOC	456380
P48449	Lanosterol synthase	LSS	454980
P29466	Caspase-1;Caspase-1 subunit p20;Caspase-1 subunit p10	CASP1	454200
Q12765	Secernin-1	SCRN1	454190
O95479	GDH/6PGL endoplasmic bifunctional protein;Glucose 1-dehydrogenase;6-phosphogluconolactonase	H6PD	449290
Q9C005	Protein dpy-30 homolog	DPY30	444460
Q9Y3I0	tRNA-splicing ligase RtcB homolog	RTCB	435340
Q16666	Gamma-interferon-inducible protein 16	IFI16	435130
P56537	Eukaryotic translation initiation factor 6	EIF6	435120
P08123	Collagen alpha-2(I) chain	COL1A2	434270
P31153	S-adenosylmethionine synthase isoform type-2	MAT2A	433060
Q06124	Tyrosine-protein phosphatase non-receptor type 11	PTPN11	431590
O75534	Cold shock domain-containing protein E1	CSDE1	431540
P42704	Leucine-rich PPR motif-containing protein, mitochondrial	LRPPRC	429700
P27824	Calnexin	CANX	427670
Q9Y371	Endophilin-B1	SH3GLB1	426970
Q15637	Splicing factor 1	SF1	423620
P28838	Cytosol aminopeptidase	LAP3	422500
P51991	Heterogeneous nuclear ribonucleoprotein A3	HNRNPA3	422480
P31689	DnaJ homolog subfamily A member 1	DNAJA1	420710
P28072	Proteasome subunit beta type-6	PSMB6	419930
Q9HD45	Transmembrane 9 superfamily member 3	TM9SF3	416080
O95816	BAG family molecular chaperone regulator 2	BAG2	412950
P78344	Eukaryotic translation initiation factor 4 gamma 2	EIF4G2	412830
Q15393	Splicing factor 3B subunit 3	SF3B3	409550
P38919	Eukaryotic initiation factor 4A-III;Eukaryotic initiation factor 4A-III, N-terminally processed	EIF4A3	407070
Q9NSD9	Phenylalanine--tRNA ligase beta subunit	FARSB	402800
P47914	60S ribosomal protein L29	RPL29	402620
Q9H845	Acyl-CoA dehydrogenase family member 9, mitochondrial	ACAD9	400350

P22234	Multifunctional protein ADE2;Phosphoribosylaminoimidazole-succinocarboxamide synthase;Phosphoribosylaminoimidazole carboxylase	PAICS	400290
O00754	Lysosomal alpha-mannosidase;Lysosomal alpha-mannosidase A peptide;Lysosomal alpha-mannosidase B peptide;Lysosomal alpha-mannosidase C peptide;Lysosomal alpha-mannosidase D peptide;Lysosomal alpha-mannosidase E peptide	MAN2B1	399350
Q93052	Lipoma-preferred partner	LPP	397740
Q14240	Eukaryotic initiation factor 4A-II;Eukaryotic initiation factor 4A-II, N-terminally processed	EIF4A2	396700
O75533	Splicing factor 3B subunit 1	SF3B1	394000
P49748	Very long-chain specific acyl-CoA dehydrogenase, mitochondrial	ACADVL	393250
P07954	Fumarate hydratase, mitochondrial	FH	390100
O75340	Programmed cell death protein 6	PDCD6	388600
P49189	4-trimethylaminobutyraldehyde dehydrogenase	ALDH9A1	385500
Q9UHX1	Poly(U)-binding-splicing factor PUF60	PUF60	382400
Q96CX2	BTB/POZ domain-containing protein KCTD12	KCTD12	380380
Q8NHP8	Putative phospholipase B-like 2;Putative phospholipase B-like 2 32 kDa form;Putative phospholipase B-like 2 45 kDa form	PLBD2	378140
P51153	Ras-related protein Rab-13	RAB13	377670
P08708	40S ribosomal protein S17	RPS17	374510
O75436	Vacuolar protein sorting-associated protein 26A	VPS26A	374350
P61421	V-type proton ATPase subunit d 1	ATP6V0D1	368630
Q08209;P16298	Serine/threonine-protein phosphatase 2B catalytic subunit alpha isoform;Serine/threonine-protein phosphatase 2B catalytic subunit beta isoform	PPP3CA;PPP3CB	368480
Q96FQ6	Protein S100-A16	S100A16	366890
P22087	rRNA 2-O-methyltransferase fibrillarin	FBL	363980
Q08945	FACT complex subunit SSRP1	SSRP1	363720
P34932	Heat shock 70 kDa protein 4	HSPA4	362920
P63208	S-phase kinase-associated protein 1	SKP1	362400
P62195	26S protease regulatory subunit 8	PSMC5	362270
Q8TD19	Serine/threonine-protein kinase Nek9	NEK9	361600
Q13885;Q9BVA1	Tubulin beta-2A chain;Tubulin beta-2B chain	TUBB2A;TUBB2B	357680
Q96IX5	Up-regulated during skeletal muscle growth protein 5	USMG5	356170
Q02790	Peptidyl-prolyl cis-trans isomerase FKBP4;Peptidyl-prolyl cis-trans isomerase FKBP4, N-terminally processed	FKBP4	354660
O15027	Protein transport protein Sec16A	SEC16A	354030
O75475	PC4 and SFRS1-interacting protein	PSIP1	353000
Q9UIJ7	GTP:AMP phosphotransferase AK3, mitochondrial	AK3	350590
P08621	U1 small nuclear ribonucleoprotein 70 kDa	SNRNP70	350020
O95425	Supervillin	SVIL	346940
Q96N66	Lysophospholipid acyltransferase 7	MBOAT7	346570
Q5JTV8	Torsin-1A-interacting protein 1	TOR1AIP1	345430
Q8WWM7	Ataxin-2-like protein	ATXN2L	344810
P30153	Serine/threonine-protein phosphatase 2A 65 kDa regulatory subunit A alpha isoform	PPP2R1A	344450
Q9UHG3	Prenylcysteine oxidase 1	PCYOX1	343600
Q02809	Procollagen-lysine,2-oxoglutarate 5-dioxygenase 1	PLOD1	343170
Q96HC4	PDZ and LIM domain protein 5	PDLIM5	342170
O43242	26S proteasome non-ATPase regulatory subunit 3	PSMD3	338260
Q99829	Copine-1	CPNE1	337030
P02786	Transferrin receptor protein 1;Transferrin receptor protein 1, serum form	TFRC	336940
P09417	Dihydropteridine reductase	QDPR	334240
Q9BXB7	Spermatogenesis-associated protein 16	SPATA16	334020
Q13765;E9PAV3	Nascent polypeptide-associated complex subunit alpha;Nascent polypeptide-associated complex subunit alpha, muscle-specific form	NACA	333870

Q6IAA8	Ragulator complex protein LAMTOR1	LAMTOR1	333440
Q9HCU0	Endosialin	CD248	330530
Q9UHB9	Signal recognition particle subunit SRP68	SRP68	329950
P00492	Hypoxanthine-guanine phosphoribosyltransferase	HPRT1	329230
P04844	Dolichyl-diphosphooligosaccharide--protein glycosyltransferase subunit 2	RPN2	328910
O94826	Mitochondrial import receptor subunit TOM70	TOMM70A	328370
Q9H4M9	EH domain-containing protein 1	EHD1	326270
P23588	Eukaryotic translation initiation factor 4B	EIF4B	325120
Q9P2J5	Leucine--tRNA ligase, cytoplasmic	LARS	323060
P00568;Q9Y6K8	Adenylate kinase isoenzyme 1;Adenylate kinase isoenzyme 5	AK1;AK5	321590
CON__Q3SX09			319620
Q15560;P23193	Transcription elongation factor A protein 2;Transcription elongation factor A protein 1	TCEA2;TCEA1	317490
Q9UHL4	Dipeptidyl peptidase 2	DPP7	316890
Q15785	Mitochondrial import receptor subunit TOM34	TOMM34	315280
Q6DN90	IQ motif and SEC7 domain-containing protein 1	IQSEC1	315280
Q96D15	Reticulocalbin-3	RCN3	313430
Q15056	Eukaryotic translation initiation factor 4H	EIF4H	312490
Q15126	Phosphomevalonate kinase	PMVK	312380
P21589	5-nucleotidase	NT5E	311700
P62495	Eukaryotic peptide chain release factor subunit 1	ETF1	311280
Q92520	Protein FAM3C	FAM3C	303260
Q8NBJ5	Procollagen galactosyltransferase 1	COLGALT1	302900
Q99729	Heterogeneous nuclear ribonucleoprotein A/B	HNRNPAB	299620
O60443	Non-syndromic hearing impairment protein 5	DFNA5	298940
P13804	Electron transfer flavoprotein subunit alpha, mitochondrial	ETFA	297760
Q53TN4	Cytochrome b reductase 1	CYBRD1	296310
O43776	Asparagine--tRNA ligase, cytoplasmic	NARS	290810
CON__P35908;P35908	Keratin, type II cytoskeletal 2 epidermal	KRT2	290010
Q86VP6	Cullin-associated NEDD8-dissociated protein 1	CAND1	287610
Q14203	Dynactin subunit 1	DCTN1	287100
Q13616	Cullin-1	CUL1	286970
O00231	26S proteasome non-ATPase regulatory subunit 11	PSMD11	286640
Q13425	Beta-2-syntrophin	SNTB2	286530
P05455	Lupus La protein	SSB	285160
O94874	E3 UFM1-protein ligase 1	UFL1	284930
Q07021	Complement component 1 Q subcomponent-binding protein, mitochondrial	C1QBP	284310
Q8TCJ2	Dolichyl-diphosphooligosaccharide--protein glycosyltransferase subunit STT3B	STT3B	283430
O00203	AP-3 complex subunit beta-1	AP3B1	282590
Q08378	Golgin subfamily A member 3	GOLGA3	281510
P24666	Low molecular weight phosphotyrosine protein phosphatase	ACP1	281400
Q92597	Protein NDRG1	NDRG1	281340
P47897	Glutamine--tRNA ligase	QARS	280990
P61020	Ras-related protein Rab-5B	RAB5B	280720
Q8WVY7	Ubiquitin-like domain-containing CTD phosphatase 1	UBLCP1	278910
Q8NFI4;P50502;Q8IZP2	Putative protein FAM10A5;Hsc70-interacting protein;Putative protein FAM10A4	ST13P5;ST13;ST13P4	278150
Q9Y316	Protein MEMO1	MEMO1	277960
P55884	Eukaryotic translation initiation factor 3 subunit B	EIF3B	276120
P82979	SAP domain-containing ribonucleoprotein	SARNP	275220
Q13310	Polyadenylate-binding protein 4	PABPC4	274570
P42785	Lysosomal Pro-X carboxypeptidase	PRCP	274010
P30085	UMP-CMP kinase	CMPK1	272620
Q16795	NADH dehydrogenase [ubiquinone] 1 alpha subcomplex subunit 9, mitochondrial	NDUFA9	272120

P24928	DNA-directed RNA polymerase II subunit RPB1	POLR2A	271130
P49821	NADH dehydrogenase [ubiquinone] flavoprotein 1, mitochondrial	NDUFV1	270130
P23246	Splicing factor, proline- and glutamine-rich	SFPQ	265820
P49755	Transmembrane emp24 domain-containing protein 10	TMED10	263980
Q15369	Transcription elongation factor B polypeptide 1	TCEB1	263540
P0DN76;Q01081	Splicing factor U2AF 35 kDa subunit	U2AF1	263220
P23142	Fibulin-1	FBLN1	263170
Q06210	Glutamine--fructose-6-phosphate aminotransferase [isomerizing] 1	GFPT1	258580
P08253	72 kDa type IV collagenase;PEX	MMP2	257850
Q9Y2X3	Nucleolar protein 58	NOP58	257420
P31937	3-hydroxyisobutyrate dehydrogenase, mitochondrial	HIBADH	256730
P11586	C-1-tetrahydrofolate synthase, cytoplasmic;Methylenetetrahydrofolate dehydrogenase;Methenyltetrahydrofolate cyclohydrolase;Formyltetrahydrofolate synthetase;C-1-tetrahydrofolate synthase, cytoplasmic, N-terminally processed	MTHFD1	254760
O14773	Tripeptidyl-peptidase 1	TPP1	254050
Q7L523;Q5VZM2	Ras-related GTP-binding protein A;Ras-related GTP-binding protein B	RRAGA;RRAGB	253580
Q96JY6	PDZ and LIM domain protein 2	PDLIM2	251470
Q9UQ80	Proliferation-associated protein 2G4	PA2G4	250680
O14617	AP-3 complex subunit delta-1	AP3D1	249670
Q9NZ32	Actin-related protein 10	ACTR10	248490
O14880	Microsomal glutathione S-transferase 3	MGST3	247760
Q13547;Q92769	Histone deacetylase 1;Histone deacetylase 2	HDAC1;HDAC2	247640
Q27J81	Inverted formin-2	INF2	246030
Q9UKV3	Apoptotic chromatin condensation inducer in the nucleus	ACIN1	245390
Q15124	Phosphoglucomutase-like protein 5	PGM5	242850
P20810	Calpastatin	CAST	241760
O60271;Q9UPT6	C-Jun-amino-terminal kinase-interacting protein 4;C-Jun-amino-terminal kinase-interacting protein 3	SPAG9;MAPK8IP3	241640
Q99426	Tubulin-folding cofactor B	TBCB	239020
O60716	Catenin delta-1	CTNND1	238950
Q15654	Thyroid receptor-interacting protein 6	TRIP6	238460
Q9NZ08	Endoplasmic reticulum aminopeptidase 1	ERAP1	237520
Q14677	Clathrin interactor 1	CLINT1	234090
Q92598;O95757	Heat shock protein 105 kDa;Heat shock 70 kDa protein 4L	HSPH1;HSPA4L	230960
P50552	Vasodilator-stimulated phosphoprotein	VASP	227140
P04216	Thy-1 membrane glycoprotein	THY1	226720
Q02952	A-kinase anchor protein 12	AKAP12	223410
Q12931	Heat shock protein 75 kDa, mitochondrial	TRAP1	222920
O60884	DnaJ homolog subfamily A member 2	DNAJA2	222460
Q53H12	Acylglycerol kinase, mitochondrial	AGK	221780
Q9NTJ5	Phosphatidylinositide phosphatase SAC1	SACM1L	221640
P67870	Casein kinase II subunit beta	CSNK2B	220500
P46926;Q8TDQ7	Glucosamine-6-phosphate isomerase 1;Glucosamine-6-phosphate isomerase 2	GNPDA1;GNPDA2	220050
Q9BQB6	Vitamin K epoxide reductase complex subunit 1	VKORC1	219210
Q8WVJ2	NudC domain-containing protein 2	NUDCD2	217520
Q6P2Q9	Pre-mRNA-processing-splicing factor 8	PRPF8	216600
P26368	Splicing factor U2AF 65 kDa subunit	U2AF2	216470
P51159	Ras-related protein Rab-27A	RAB27A	216320
P15586	N-acetylglucosamine-6-sulfatase	GNS	214810
Q9HB71	Calcyclin-binding protein	CACYBP	214050
P17844	Probable ATP-dependent RNA helicase DDX5	DDX5	209290
Q63ZY3	KN motif and ankyrin repeat domain-containing protein 2	KANK2	207960

Q9H4A4	Aminopeptidase B	RNPEP	206860
P05023;P13637;P50993	Sodium/potassium-transporting ATPase subunit alpha-1;Sodium/potassium-transporting ATPase subunit alpha-3;Sodium/potassium-transporting ATPase subunit alpha-2	ATP1A1;ATP1A3;ATP1A2	206610
O76074	cGMP-specific 3,5-cyclic phosphodiesterase	PDE5A	203330
CON__P01030;CON__ENSEMBL:ENSBTAP00000007350			202230
P54920	Alpha-soluble NSF attachment protein	NAPA	201540
O60568	Procollagen-lysine,2-oxoglutarate 5-dioxygenase 3	PLOD3	200530
P29590	Protein PML	PML	199540
Q8TB61	Adenosine 3-phospho 5-phosphosulfate transporter 1	SLC35B2	198090
P07996	Thrombospondin-1	THBS1	196940
P17813	Endoglin	ENG	195490
Q9H772	Gremlin-2	GREM2	195330
Q8WZ42	Titin	TTN	194890
Q15370	Transcription elongation factor B polypeptide 2	TCEB2	194560
REV__P11137			194050
Q9H910	Hematological and neurological expressed 1-like protein	HN1L	190600
Q14192	Four and a half LIM domains protein 2	FHL2	190220
P43686	26S protease regulatory subunit 6B	PSMC4	189300
O43681	ATPase ASNA1	ASNA1	187760
O00560	Syntenin-1	SDCBP	185780
P61764	Syntaxin-binding protein 1	STXBP1	184680
CON__P05787;P05787;CON__H-INV:HIT00002992931	Keratin, type II cytoskeletal 8	KRT8	183700
Q9Y4K1	Absent in melanoma 1 protein	AIM1	182630
Q9BTW9	Tubulin-specific chaperone D	TBCD	181570
O43670	BUB3-interacting and GLEBS motif-containing protein ZNF207	ZNF207	181500
O00115	Deoxyribonuclease-2-alpha	DNASE2	181050
P03956	Interstitial collagenase;22 kDa interstitial collagenase;27 kDa interstitial collagenase	MMP1	180420
Q9UJ70	N-acetyl-D-glucosamine kinase	NAGK	179920
P18846;P16220	Cyclic AMP-dependent transcription factor ATF-1;Cyclic AMP-responsive element-binding protein 1	ATF1;CREB1	178040
P12270	Nucleoprotein TPR	TPR	176500
O95340	Bifunctional 3-phosphoadenosine 5-phosphosulfate synthase 2;Sulfate adenylyltransferase;Adenylyl-sulfate kinase	PAPSS2	175810
P35754	Glutaredoxin-1	GLRX	174470
Q9NR28	Diablo homolog, mitochondrial	DIABLO	173460
P78347	General transcription factor II-I	GTF2I	171900
Q12882	Dihydropyrimidine dehydrogenase [NADP(+)]	DPYD	171850
Q16832	Discoidin domain-containing receptor 2	DDR2	171850
Q16527	Cysteine and glycine-rich protein 2	CSRP2	171090
O95980	Reversion-inducing cysteine-rich protein with Kazal motifs	RECK	170120
Q9Y263	Phospholipase A-2-activating protein	PLAA	170120
Q00169;P48739	Phosphatidylinositol transfer protein alpha isoform;Phosphatidylinositol transfer protein beta isoform	PITPNA;PITPNB	168390
Q969V3	Nicalin	NCLN	168060
Q6DD88	Atlastin-3	ATL3	167740
P11717	Cation-independent mannose-6-phosphate receptor	IGF2R	166610
Q9NSE4	Isoleucine--tRNA ligase, mitochondrial	IARS2	165230
P16615;O14983;Q93084	Sarcoplasmic/endoplasmic reticulum calcium ATPase 2;Sarcoplasmic/endoplasmic reticulum calcium ATPase 1;Sarcoplasmic/endoplasmic reticulum calcium ATPase 3	ATP2A2;ATP2A1;ATP2A3	164580

P55769	NHP2-like protein 1;NHP2-like protein 1, N-terminally processed	NHP2L1	164230
Q3KQU3	MAP7 domain-containing protein 1	MAP7D1	163600
O15321	Transmembrane 9 superfamily member 1	TM9SF1	163540
P29218	Inositol monophosphatase 1	IMPA1	163320
Q9H074	Polyadenylate-binding protein-interacting protein 1	PAIP1	163160
Q8IXB1	DnaJ homolog subfamily C member 10	DNAJC10	163020
Q13561	Dynactin subunit 2	DCTN2	161950
Q86TX2;P49753	Acyl-coenzyme A thioesterase 1;Acyl-coenzyme A thioesterase 2, mitochondrial	ACOT1;ACOT2	161540
P07711	Cathepsin L1;Cathepsin L1 heavy chain;Cathepsin L1 light chain	CTSL	160630
Q13428	Treacle protein	TCOF1	160510
Q9NY33	Dipeptidyl peptidase 3	DPP3	158930
Q07866;Q9H0B6	Kinesin light chain 1;Kinesin light chain 2	KLC1;KLC2	158910
P05783	Keratin, type I cytoskeletal 18	KRT18	158410
Q9UQE7	Structural maintenance of chromosomes protein 3	SMC3	157960
Q9NP61	ADP-ribosylation factor GTPase-activating protein 3	ARFGAP3	157870
P30048	Thioredoxin-dependent peroxide reductase, mitochondrial	PRDX3	157440
P20933	N(4)-(beta-N-acetylglucosaminyl)-L-asparaginase;Glycosylasparaginase alpha chain;Glycosylasparaginase beta chain	AGA	157260
P41091;Q2VIR3	Eukaryotic translation initiation factor 2 subunit 3;Putative eukaryotic translation initiation factor 2 subunit 3-like protein	EIF2S3;EIF2S3L	156870
P46977	Dolichyl-diphosphooligosaccharide--protein glycosyltransferase subunit STT3A	STT3A	154620
Q14566	DNA replication licensing factor MCM6	MCM6	154010
Q9GZZ9	Ubiquitin-like modifier-activating enzyme 5	UBA5	151440
P28065	Proteasome subunit beta type-9	PSMB9	151280
Q15746	Myosin light chain kinase, smooth muscle;Myosin light chain kinase, smooth muscle, deglutamylated form	MYLK	151110
Q96RF0	Sorting nexin-18	SNX18	150750
P40616	ADP-ribosylation factor-like protein 1	ARL1	150440
Q9BTY7	Protein HGH1 homolog	HGH1	150220
O60888	Protein CutA	CUTA	150190
Q96KG9	N-terminal kinase-like protein	SCYL1	150010
Q6IBS0	Twinfilin-2	TWF2	149710
P52630	Signal transducer and activator of transcription 2	STAT2	149310
O15067	Phosphoribosylformylglycinamidine synthase	PFAS	147520
Q16762	Thiosulfate sulfurtransferase	TST	146890
Q96GG9	DCN1-like protein 1	DCUN1D1	146130
CON__P34955			145600
Q08380	Galectin-3-binding protein	LGALS3BP	145290
Q9P2T1	GMP reductase 2	GMPR2	144690
O43324	Eukaryotic translation elongation factor 1 epsilon-1	EEF1E1	144010
Q9NUP9;Q9HAP6;O14910	Protein lin-7 homolog C;Protein lin-7 homolog B;Protein lin-7 homolog A	LIN7C;LIN7B;LIN7A	143080
Q96HE7	ERO1-like protein alpha	ERO1L	143020
Q9NR50	Translation initiation factor eIF-2B subunit gamma	EIF2B3	138200
P11047	Laminin subunit gamma-1	LAMC1	135240
Q86UE4	Protein LYRIC	MTDH	134260
P02452	Collagen alpha-1(I) chain	COL1A1	134240
Q15392	Delta(24)-sterol reductase	DHCR24	134050
O14579	Coatomer subunit epsilon	COPE	133550
Q9NR45	Sialic acid synthase	NANS	133180
O15173	Membrane-associated progesterone receptor component 2	PGRMC2	132560
Q5SW79	Centrosomal protein of 170 kDa	CEP170	131220
Q9H1E5	Thioredoxin-related transmembrane protein 4	TMX4	130920
Q9H223	EH domain-containing protein 4	EHD4	129090

Q9H444	Charged multivesicular body protein 4b	CHMP4B	129070
P23381	Tryptophan--tRNA ligase, cytoplasmic;T1-TrpRS;T2-TrpRS	WARS	128900
P50914	60S ribosomal protein L14	RPL14	128700
P09874	Poly [ADP-ribose] polymerase 1	PARP1	126330
O43795	Unconventional myosin-Ib	MYO1B	123850
P27708	CAD protein;Glutamine-dependent carbamoyl-phosphate synthase;Aspartate carbamoyltransferase;Dihydroorotase	CAD	122540
Q9BX40	Protein LSM14 homolog B	LSM14B	122530
Q9UKV8	Protein argonaute-2	AGO2	122040
P52907	F-actin-capping protein subunit alpha-1	CAPZA1	121410
Q9Y3C6	Peptidyl-prolyl cis-trans isomerase-like 1	PPIL1	121370
P25205	DNA replication licensing factor MCM3	MCM3	120040
Q13242	Serine/arginine-rich splicing factor 9	SRSF9	118990
Q08AM6	Protein VAC14 homolog	VAC14	118530
Q9Y2Z0	Suppressor of G2 allele of SKP1 homolog	SUGT1	118400
P22061	Protein-L-isoaspartate(D-aspartate) O-methyltransferase	PCMT1	117580
Q96P70	Importin-9	IPO9	115450
P49591	Serine--tRNA ligase, cytoplasmic	SARS	115160
Q15046	Lysine--tRNA ligase	KARS	113950
Q92896	Golgi apparatus protein 1	GLG1	113680
Q14766	Latent-transforming growth factor beta-binding protein 1	LTBP1	113150
P45954	Short/branched chain specific acyl-CoA dehydrogenase, mitochondrial	ACADSB	111540
Q9Y2Q5	Ragulator complex protein LAMTOR2	LAMTOR2	111190
Q13131	5-AMP-activated protein kinase catalytic subunit alpha-1	PRKAA1	107560
Q16643	Drebrin	DBN1	106710
P37840	Alpha-synuclein	SNCA	105240
Q96P48	Arf-GAP with Rho-GAP domain, ANK repeat and PH domain-containing protein 1	ARAP1	104720
P52943	Cysteine-rich protein 2	CRIP2	104080
P43307	Translocon-associated protein subunit alpha	SSR1	103760
P50416	Carnitine O-palmitoyltransferase 1, liver isoform	CPT1A	100090
Q96N67;Q96HP0	Dedicator of cytokinesis protein 7;Dedicator of cytokinesis protein 6	DOCK7;DOCK6	99696
Q9UHD9;Q9UMX0;Q9NRR5	Ubiquilin-2;Ubiquilin-1;Ubiquilin-4	UBQLN2;UBQLN1;UBQLN4	99122
P49757;Q9Y6R0	Protein numb homolog;Numb-like protein	NUMB;NUMBL	97772
Q8IV08	Phospholipase D3	PLD3	97096
Q9BZQ8	Protein Niban	FAM129A	94143
P57740	Nuclear pore complex protein Nup107	NUP107	93017
Q9BQA1	Methylosome protein 50	WDR77	91591
Q9Y282	Endoplasmic reticulum-Golgi intermediate compartment protein 3	ERGIC3	90780
P52888	Thimet oligopeptidase	THOP1	90676
P36542	ATP synthase subunit gamma, mitochondrial	ATP5C1	90590
Q13620	Cullin-4B	CUL4B	89497
Q5NDL2	EGF domain-specific O-linked N-acetylglucosamine transferase	EOGT	86037
O00429	Dynamin-1-like protein	DNM1L	84263
P55010	Eukaryotic translation initiation factor 5	EIF5	83396
Q6ZMZ3	Nesprin-3	SYNE3	82149
Q86X76	Nitrilase homolog 1	NIT1	81779
Q9UPN3	Microtubule-actin cross-linking factor 1, isoforms 1/2/3/5	MACF1	81572
Q15436	Protein transport protein Sec23A	SEC23A	81357
P46087	Probable 28S rRNA (cytosine(4447)-C(5))-methyltransferase	NOP2	81251
O43581	Synaptotagmin-7	SYT7	81046
O15305	Phosphomannomutase 2	PMM2	80459
Q9BTU6	Phosphatidylinositol 4-kinase type 2-alpha	PI4K2A	80451
P35221	Catenin alpha-1	CTNNA1	80177

O60669	Monocarboxylate transporter 2	SLC16A7	79232
P54802	Alpha-N-acetylglucosaminidase;Alpha-N-acetylglucosaminidase 82 kDa form;Alpha-N-acetylglucosaminidase 77 kDa form	NAGLU	77623
Q9Y4L1	Hypoxia up-regulated protein 1	HYOU1	75419
Q9Y5M8	Signal recognition particle receptor subunit beta	SRPRB	74786
Q9UIA9	Exportin-7	XPO7	73473
O14786	Neuropilin-1	NRP1	73449
Q9H8Y8	Golgi reassembly-stacking protein 2	GORASP2	72791
O75746	Calcium-binding mitochondrial carrier protein Aralar1	SLC25A12	72483
O00186	Syntaxin-binding protein 3	STXBP3	72345
Q9BSJ8	Extended synaptotagmin-1	ESYT1	72182
O95433	Activator of 90 kDa heat shock protein ATPase homolog 1	AHSA1	71182
Q9UI12	V-type proton ATPase subunit H	ATP6V1H	70524
Q9BUP3	Oxidoreductase HTATIP2	HTATIP2	68686
Q14980	Nuclear mitotic apparatus protein 1	NUMA1	68637
Q9H8H3	Methyltransferase-like protein 7A	METTL7A	68023
Q15427	Splicing factor 3B subunit 4	SF3B4	67960
O75828	Carbonyl reductase [NADPH] 3	CBR3	66761
P23497	Nuclear autoantigen Sp-100	SP100	64852
Q9UPU5	Ubiquitin carboxyl-terminal hydrolase 24	USP24	62915
O14972	Down syndrome critical region protein 3	DSCR3	62781
Q12888	Tumor suppressor p53-binding protein 1	TP53BP1	62208
Q9H269	Vacuolar protein sorting-associated protein 16 homolog	VPS16	61635
Q9BT78	COP9 signalosome complex subunit 4	COPS4	60050
P42167	Lamina-associated polypeptide 2, isoforms beta/gamma;Thymopoietin;Thymopentin	TMPO	57913
Q8NCN5	Pyruvate dehydrogenase phosphatase regulatory subunit, mitochondrial	PDPR	57913
P36551	Oxygen-dependent coproporphyrinogen-III oxidase, mitochondrial	CPOX	56702
P11216;P11217;P06737	Glycogen phosphorylase, brain form;Glycogen phosphorylase, muscle form;Glycogen phosphorylase, liver form	PYGB;PYGM;PYGL	56465
Q7Z2W4	Zinc finger CCCH-type antiviral protein 1	ZC3HAV1	55702
Q9Y3Z3	Deoxynucleoside triphosphate triphosphohydrolase SAMHD1	SAMHD1	55458
O95400	CD2 antigen cytoplasmic tail-binding protein 2	CD2BP2	54922
CON__Q922U2;CON__Q5XQN5;CON__Q8BGZ7;CON__P50446;CON__P13647;P13647	Keratin, type II cytoskeletal 5	KRT5	54561
P35749	Myosin-11	MYH11	51751
P62191	26S protease regulatory subunit 4	PSMC1	51722
CON__Q0IIK2;CON__Q29443			50882
Q8IUD2	ELKS/Rab6-interacting/CAST family member 1	ERC1	50355
P10909	Clusterin;Clusterin beta chain;Clusterin alpha chain	CLU	50062
P20337	Ras-related protein Rab-3B	RAB3B	49938
Q9BZE4	Nucleolar GTP-binding protein 1	GTPBP4	49041
P61018	Ras-related protein Rab-4B	RAB4B	47012
Q4G0N4	NAD kinase 2, mitochondrial	NADK2	45094
Q15006	ER membrane protein complex subunit 2	EMC2	44087
Q9Y5U9	Immediate early response 3-interacting protein 1	IER3IP1	42940
Q9Y6E0	Serine/threonine-protein kinase 24;Serine/threonine-protein kinase 24 36 kDa subunit;Serine/threonine-protein kinase 24 12 kDa subunit	STK24	42587
Q9NXR7	BRCA1-A complex subunit BRE	BRE	41797

REV__A0A0B4J1V0			41075
Q7Z417	Nuclear fragile X mental retardation-interacting protein 2	NUFIP2	40779
P13798	Acylamino-acid-releasing enzyme	APEH	36804
P11387	DNA topoisomerase 1	TOP1	29437
Q12965	Unconventional myosin-Ie	MYO1E	28604
CON__ENSEMBL:ENSBTAP00000018574			25572

Table S 2. List of proteins identified in LC-MS/MS analysis of hVFF embedded within collagen matrix, analyzed by MaxQuant by searching the public SwissProt human database plus rat collagens, based on a 1 % FDR. Proteins are listed in order of descending intensities.

Majority protein IDs	Protein names	Gene names	Intensity
P02769;CON__P02769			254200000
P02452	Collagen alpha-1(I) chain	COL1A1	170320000
Q9NYQ7	Cadherin EGF LAG seven-pass G-type receptor 3	CELSR3	90015000
CON__P12763			67011000
P08670	Vimentin	VIM	46949000
CON__P34955			39755000
Q86WI1	Fibrocystin-L	PKHD1L1	30880000
P02751	Fibronectin;Anastellin;Ugl-Y1;Ugl-Y2;Ugl-Y3	FN1	23811000
CON__Q0IIK2;CON__Q29443			16539000
P63261;P60709	Actin, cytoplasmic 2;Actin, cytoplasmic 2, N-terminally processed;Actin, cytoplasmic 1;Actin, cytoplasmic 1, N-terminally processed	ACTG1;ACTB	15015000
P07355;A6NMY6	Annexin A2;Putative annexin A2-like protein	ANXA2;ANXA2P2	13162000
P12111	Collagen alpha-3(VI) chain	COL6A3	12952000
P02787	Serotransferrin	TF	9166100
CON__P00735			7800900
CON__ENSEMBL:ENSBTAP00000024146			7495500
CON__P15497			6314200
REV__A6NEH8			6261200
P78539	Sushi repeat-containing protein SRPX	SRPX	5421500
CON__Q2UVX4			5337800
P14618	Pyruvate kinase PKM	PKM	4628900
P06703	Protein S100-A6	S100A6	4436400
CON__P81644			4128200
P68371;P04350	Tubulin beta-4B chain;Tubulin beta-4A chain	TUBB4B;TUBB4A	4034800
P05556	Integrin beta-1	ITGB1	3784300
REV__Q96RT1			3564600
CON__REFSEQ:XP_001252647;CON__A2I7N3			3547400
P08758	Annexin A5	ANXA5	3504000
P12109	Collagen alpha-1(VI) chain	COL6A1	3425400
P08238	Heat shock protein HSP 90-beta	HSP90AB1	3181000
CON__ENSEMBL:ENSBTAP00000018229			2864200
P04406	Glyceraldehyde-3-phosphate dehydrogenase	GAPDH	2728100
CON__Q3KUS7			2575900
CON__Q3SZ57			2412100
P02545	Prelamin-A/C;Lamin-A/C	LMNA	2326500

CON__Q3SX09			2325100
CON__Q9TTE1;CON__A2I7N1			2302800
P07996	Thrombospondin-1	THBS1	1895500
P23284	Peptidyl-prolyl cis-trans isomerase B	PPIB	1733300
P62987;P62979;P0CG47;P0CG48	Ubiquitin-60S ribosomal protein L40;Ubiquitin;60S ribosomal protein L40;Ubiquitin-40S ribosomal protein S27a;Ubiquitin;40S ribosomal protein S27a;Polyubiquitin-B;Ubiquitin;Polyubiquitin-C;Ubiquitin	UBA52;RPS27A;UBB;UBC	1730000
P09382	Galectin-1	LGALS1	1728100
CON__Q3SZR3			1637600
P35579	Myosin-9	MYH9	1522400
P02656	Apolipoprotein C-III	APOC3	1510500
CON__Q3SZV7			1494800
P67936	Tropomyosin alpha-4 chain	TPM4	1431700
Q5VTE0;P68104;Q05639	Putative elongation factor 1-alpha-like 3;Elongation factor 1-alpha 1;Elongation factor 1-alpha 2	EEF1A1P5;EEF1A1;EEF1A2	1419000
CON__P02070			1397700
O60938	Keratocan	KERA	1336800
CON__Q3Y5Z3			1328400
P07237	Protein disulfide-isomerase	P4HB	1316100
P07585	Decorin	DCN	1285900
CON__Q58D62			1283200
P23528;Q9Y281	Cofilin-1;Cofilin-2	CFL1;CFL2	1177000
CON__Q9TRI1			1174700
CON__P28800			1077400
Q14766	Latent-transforming growth factor beta-binding protein 1	LTBP1	1060500
P80297;P02795;P13640;P80294;P04731	Metallothionein-1X;Metallothionein-2;Metallothionein-1G;Metallothionein-1H;Metallothionein-1A	MT1X;MT2A;MT1G;MT1H;MT1A	1007000
CON__Q3T052			998400
CON__Q3ZBS7			940760
P08123	Collagen alpha-2(I) chain	COL1A2	814010
P11021	78 kDa glucose-regulated protein	HSPA5	805760
P15144	Aminopeptidase N	ANPEP	805170
P63267;P68032;P62736;P68133	Actin, gamma-enteric smooth muscle;Actin, alpha cardiac muscle 1;Actin, aortic smooth muscle;Actin, alpha skeletal muscle	ACTG2;ACTC1;ACTA2;ACTA1	780740
CON__Q1RMK2			670130
P06733	Alpha-enolase	ENO1	656610
P21589	5-nucleotidase	NT5E	649250
P17301	Integrin alpha-2	ITGA2	639370
P13667	Protein disulfide-isomerase A4	PDIA4	617610
P60660	Myosin light polypeptide 6	MYL6	616720
P11142	Heat shock cognate 71 kDa protein	HSPA8	603640
P04083	Annexin A1	ANXA1	571420
CON__P06868			560260
P04264;CON__P04264	Keratin, type II cytoskeletal 1	KRT1	550260
P98160	Basement membrane-specific heparan sulfate proteoglycan core protein;Endorepellin;LG3 peptide	HSPG2	512480
CON__P05787;P05787;CON__H-INV:HIT000292931	Keratin, type II cytoskeletal 8	KRT8	497260
P04075;P00883	Fructose-bisphosphate aldolase A	ALDOA	490660
P10809	60 kDa heat shock protein, mitochondrial	HSPD1	485410
Q71U36;P68363;P0DPH8;P0DPH7;Q6PEY2	Tubulin alpha-1A chain;Tubulin alpha-1B chain;Tubulin alpha-3E chain	TUBA1A;TUBA1B;TUBA3E	480610
P11047	Laminin subunit gamma-1	LAMC1	474620

P61981	14-3-3 protein gamma;14-3-3 protein gamma, N-terminally processed	YWHAG	461400
P31949	Protein S100-A11;Protein S100-A11, N-terminally processed	S100A11	461100
P60842	Eukaryotic initiation factor 4A-I	EIF4A1	450950
CON__ENSEMBL:ENSBTAP00000016046			442580
Q15149	Plectin	PLEC	440050
P61586	Transforming protein RhoA	RHOA	436940
P62879;P62873;P16520	Guanine nucleotide-binding protein G(I)/G(S)/G(T) subunit beta-2;Guanine nucleotide-binding protein G(I)/G(S)/G(T) subunit beta-1;Guanine nucleotide-binding protein G(I)/G(S)/G(T) subunit beta-3	GNB2;GNB1;GNB3	435220
P08133	Annexin A6	ANXA6	431900
P06576	ATP synthase subunit beta, mitochondrial	ATP5B	420190
Q8NHW5;P05388	60S acidic ribosomal protein P0-like;60S acidic ribosomal protein P0	RPLP0P6;RPLP0	416320
P00740	Coagulation factor IX;Coagulation factor IXa light chain;Coagulation factor IXa heavy chain	F9	411010
P07437	Tubulin beta chain	TUBB	407050
Q9Y3Z3	Deoxynucleoside triphosphate triphosphohydrolase SAMHD1	SAMHD1	405490
P21796	Voltage-dependent anion-selective channel protein 1	VDAC1	376960
P62280	40S ribosomal protein S11	RPS11	375550
Q9Y240	C-type lectin domain family 11 member A	CLEC11A	354390
CON__P01030;CON__ENSEMBL:ENSBTAP00000007350			347110
Q00610	Clathrin heavy chain 1	CLTC	346390
P63104	14-3-3 protein zeta/delta	YWHAZ	345890
P07900	Heat shock protein HSP 90-alpha	HSP90AA1	345720
P13639	Elongation factor 2	EEF2	338170
P14314	Glucosidase 2 subunit beta	PRKCSH	335480
P26038	Moesin	MSN	314830
P21980	Protein-glutamine gamma-glutamyltransferase 2	TGM2	312850
P40926	Malate dehydrogenase, mitochondrial	MDH2	294080
Q7Z406	Myosin-14	MYH14	293210
P05067	Amyloid beta A4 protein;N-APP;Soluble APP-alpha;Soluble APP-beta;C99;Beta-amyloid protein 42;Beta-amyloid protein 40;C83;P3(42);P3(40);C80;Gamma-secretase C-terminal fragment 59;Gamma-secretase C-terminal fragment 57;Gamma-secretase C-terminal fragment 50;C31	APP	286550
P07858	Cathepsin B;Cathepsin B light chain;Cathepsin B heavy chain	CTSB	286150
CON__P41361			282930
P62937	Peptidyl-prolyl cis-trans isomerase A;Peptidyl-prolyl cis-trans isomerase A, N-terminally processed	PPIA	282490
Q99715	Collagen alpha-1(XII) chain	COL12A1	274870
CON__P00978			271760
P83731	60S ribosomal protein L24	RPL24	262000
P62942	Peptidyl-prolyl cis-trans isomerase FKBP1A	FKBP1A	244640
P21810	Biglycan	BGN	239530
P25189	Myelin protein P0	MPZ	238710
P24534	Elongation factor 1-beta	EEF1B2	238510
P21333	Filamin-A	FLNA	237490
P08253	72 kDa type IV collagenase;PEX	MMP2	232620
P29401	Transketolase	TKT	221330
CON__Q0V8M9			214600
P62888	60S ribosomal protein L30	RPL30	213270

Q13509	Tubulin beta-3 chain	TUBB3	211800
P60468	Protein transport protein Sec61 subunit beta	SEC61B	210610
Q9NQC3	Reticulon-4	RTN4	198970
P05783	Keratin, type I cytoskeletal 18	KRT18	198100
Q8TCT9	Minor histocompatibility antigen H13	HM13	194370
CON__ENSEMBL:ENSBTAP00000018574			185660
P62424	60S ribosomal protein L7a	RPL7A	183370
P25705	ATP synthase subunit alpha, mitochondrial	ATP5A1	165500
Q8IUX7	Adipocyte enhancer-binding protein 1	AEBP1	163550
P50990	T-complex protein 1 subunit theta	CCT8	158920
P08865	40S ribosomal protein SA	RPSA	156530
P30519	Heme oxygenase 2	HMOX2	153050
P29692	Elongation factor 1-delta	EEF1D	151000
P62820;Q9H0U4	Ras-related protein Rab-1A;Ras-related protein Rab-1B	RAB1A;RAB1B	149080
O43707	Alpha-actinin-4	ACTN4	147830
Q12907	Vesicular integral-membrane protein VIP36	LMAN2	147670
P40939	Trifunctional enzyme subunit alpha, mitochondrial;Long-chain enoyl-CoA hydratase;Long chain 3-hydroxyacyl-CoA dehydrogenase	HADHA	146760
P60174	Triosephosphate isomerase	TPI1	145040
Q07021	Complement component 1 Q subcomponent-binding protein, mitochondrial	C1QBP	144550
Q8NFI4;P50502;Q8IZP2	Putative protein FAM10A5;Hsc70-interacting protein;Putative protein FAM10A4	ST13P5;ST13;ST13P4	142780
CON__Q3SZH5			142180
Q16363	Laminin subunit alpha-4	LAMA4	141710
Q15942	Zyxin	ZYX	140780
P06748	Nucleophosmin	NPM1	134460
CON__ENSEMBL:ENSBTAP00000034412			133940
Q9Y3B3	Transmembrane emp24 domain-containing protein 7	TMED7	131760
Q8WZ42	Titin	TTN	126160
Q14520	Hyaluronan-binding protein 2;Hyaluronan-binding protein 2 50 kDa heavy chain;Hyaluronan-binding protein 2 50 kDa heavy chain alternate form;Hyaluronan-binding protein 2 27 kDa light chain;Hyaluronan-binding protein 2 27 kDa light chain alternate form	HABP2	123480
Q14974	Importin subunit beta-1	KPNB1	121200
P23396	40S ribosomal protein S3	RPS3	118180
CON__P13645;P13645;CON__P02535-1	Keratin, type I cytoskeletal 10	KRT10	111930
P09525	Annexin A4	ANXA4	109880
P09651;Q32P51	Heterogeneous nuclear ribonucleoprotein A1;Heterogeneous nuclear ribonucleoprotein A1, N-terminally processed;Heterogeneous nuclear ribonucleoprotein A1-like 2	HNRNPA1;HNRNPA1L2	108600

P30464;P30484;Q95365;P30466;Q29940;P30685;P30491;P30490;P18464;P30481;P18463;P30498;P30495;P30493;P30492;P18465;P10319;Q29960	HLA class I histocompatibility antigen, B-15 alpha chain;HLA class I histocompatibility antigen, B-46 alpha chain;HLA class I histocompatibility antigen, B-38 alpha chain;HLA class I histocompatibility antigen, B-18 alpha chain;HLA class I histocompatibility antigen, B-59 alpha chain;HLA class I histocompatibility antigen, B-35 alpha chain;HLA class I histocompatibility antigen, B-53 alpha chain;HLA class I histocompatibility antigen, B-52 alpha chain;HLA class I histocompatibility antigen, B-51 alpha chain;HLA class I histocompatibility antigen, B-44 alpha chain;HLA class I histocompatibility antigen, B-37 alpha chain;HLA class I histocompatibility antigen, B-78 alpha chain;HLA class I histocompatibility antigen, B-56 alpha chain;HLA class I histocompatibility antigen, B-55 alpha chain;HLA class I histocompatibility antigen, B-54 alpha chain;HLA class I histocompatibility antigen, B-57 alpha chain;HLA class I histocompatibility antigen, B-58 alpha chain;HLA class I histocompatibility antigen, Cw-16 alpha chain	HLA-B;HLA-C	106560
Q99878;Q96KK5;Q9BTM1;Q93077;Q7L7L0;P20671;P0C0S8;P04908;Q16777;Q6FI13;Q8IUE6;P16104;Q96QV6	Histone H2A type 1-J;Histone H2A type 1-H;Histone H2A.J;Histone H2A type 1-C;Histone H2A type 3;Histone H2A type 1-D;Histone H2A type 1;Histone H2A type 1-B/E;Histone H2A type 2-C;Histone H2A type 2-A;Histone H2A type 2-B;Histone H2AX;Histone H2A type 1-A	HIST1H2AJ;HIST1H2AH;H2AFJ;HIST1H2AC;HIST3H2A;HIST1H2AD;HIST1H2AG;HIST1H2AB;HIST2H2AC;HIST2H2AA3;HIST2H2AB;H2AFX;HIST1H2AA	106270
P22314	Ubiquitin-like modifier-activating enzyme 1	UBA1	105300
P22626	Heterogeneous nuclear ribonucleoproteins A2/B1	HNRNPA2B1	104720
P18085	ADP-ribosylation factor 4	ARF4	103170
REV__Q8IZY5			101580
Q99536	Synaptic vesicle membrane protein VAT-1 homolog	VAT1	101270
P27105	Erythrocyte band 7 integral membrane protein	STOM	95354
P30101	Protein disulfide-isomerase A3	PDIA3	92675
P23634	Plasma membrane calcium-transporting ATPase 4	ATP2B4	91484
Q14108	Lysosome membrane protein 2	SCARB2	86760
P98095	Fibulin-2	FBLN2	86413
P53396	ATP-citrate synthase	ACLY	84048
P35606	Coatomer subunit beta	COPB2	82748
P18669	Phosphoglycerate mutase 1	PGAM1	73093
P28300	Protein-lysine 6-oxidase	LOX	70432
Q14315	Filamin-C	FLNC	69511
P12882;Q9Y623;Q9UKX2;P13535	Myosin-1;Myosin-4;Myosin-2;Myosin-8	MYH1;MYH4;MYH2;MYH8	66050
P04632	Calpain small subunit 1	CAPNS1	65260
Q9UBI6	Guanine nucleotide-binding protein G(I)/G(S)/G(O) subunit gamma-12	GNG12	65241
O75955	Flotillin-1	FLOT1	64411
P61247	40S ribosomal protein S3a	RPS3A	57480
P34932	Heat shock 70 kDa protein 4	HSPA4	55862
Q01813;P17858	ATP-dependent 6-phosphofructokinase, platelet type;ATP-dependent 6-phosphofructokinase, liver type	PFKP;PFKL	51649
O95573	Long-chain-fatty-acid--CoA ligase 3	ACSL3	49797
Q9H078	Caseinolytic peptidase B protein homolog	CLPB	47749
Q96D15	Reticulocalbin-3	RCN3	46860
O43242	26S proteasome non-ATPase regulatory subunit 3	PSMD3	39637
Q96PK6	RNA-binding protein 14	RBM14	35474
O00560	Syntenin-1	SDCBP	22660
Q02846	Retinal guanylyl cyclase 1	GUCY2D	14861

Table S 3. List of proteins identified in LC-MS/MS analysis of collagen matrix without hVFF, analyzed by MaxQuant by searching the public SwissProt human database plus rat collagens, based on a 1 % FDR. Proteins are listed in order of descending intensities.

Majority protein IDs	Protein names	Gene names	Intensity
CON__P12763			61373000
CON__P34955			27205000
CON__P15497			25923000
REV__A2RRP1			20178000
CON__Q0IIK2;CON__Q29443			19670000
Q8NBJ4	Golgi membrane protein 1	GOLM1	17497000
CON__Q2UVX4			7558000
P02787	Serotransferrin	TF	6977600
P00761;CON__P00761			6273900
CON__P02768-1;P02768	Serum albumin	ALB	6194800
REV__Q9ULC6			5699600
CON__P00735			4808600
P63261;P60709	Actin, cytoplasmic 2;Actin, cytoplasmic 2, N-terminally processed;Actin, cytoplasmic 1;Actin, cytoplasmic 1, N-terminally processed	ACTG1;ACTB	3721900
REV__Q96RT1			3247100
CON__ENSEMBL:ENSBTAP00000024146			2695100
CON__ENSEMBL:ENSBTAP00000018229			2578600
CON__Q95121			2252500
P02461	Collagen alpha-1(III) chain	COL3A1	2051500
CON__Q3ZBS7			1956200
Q53TN4	Cytochrome b reductase 1	CYBRD1	1378100
P08123	Collagen alpha-2(I) chain	COL1A2	1277100
CON__Q58D62			1134600
CON__P02070			1078200
P02656	Apolipoprotein C-III	APOC3	1065000
P04264;CON__P04264	Keratin, type II cytoskeletal 1	KRT1	927230
CON__Q9TRI1			789540
CON__REFSEQ:XP_001252647;CON__A2I7N3			727710
CON__ENSEMBL:ENSBTAP00000018574			712110
CON__Q3SX09			542050
CON__Q3T052			513210
P14618	Pyruvate kinase PKM	PKM	461250
CON__Q3SZH5			448880
P10809	60 kDa heat shock protein, mitochondrial	HSPD1	406010
CON__Q3SZ57			395400
CON__P00978			371490
CON__Q2KJ62;CON__P01044-1;CON__P01045-1			369620
CON__Q0V8M9			357450
CON__P13645;P13645;CON__P02535-1	Keratin, type I cytoskeletal 10	KRT10	319900

P00740	Coagulation factor IX;Coagulation factor IXa light chain;Coagulation factor IXa heavy chain	F9	299430
CON__Q03247			292660
P13639	Elongation factor 2	EEF2	277770
P12883;P13533	Myosin-7;Myosin-6	MYH7;MYH6	277050
CON__P41361			263990
CON__Q3MHN5			261220
P68371;P04350	Tubulin beta-4B chain;Tubulin beta-4A chain	TUBB4B;TUBB4A	224970
CON__P05787;P05787;CON__H-INV:HIT000292931	Keratin, type II cytoskeletal 8	KRT8	192500
CON__Q3SZR3			180650
P12110	Collagen alpha-2(VI) chain	COL6A2	175360
P00338	L-lactate dehydrogenase A chain	LDHA	167070
P35030	Trypsin-3	PRSS3	163790
CON__P17697			158300
CON__P06868			154880
CON__Q3KUS7			135480
CON__ENSEMBL:ENSBTAP00000034412			133420
Q16778;P33778;P23527;P06899;Q8N257	Histone H2B type 2-E;Histone H2B type 1-B;Histone H2B type 1-O;Histone H2B type 1-J;Histone H2B type 3-B	HIST2H2BE;HIST1H2BB;HIST1H2BO;HIST1H2BJ;HIST3H2BB	131320
P29401	Transketolase	TKT	126830
P04083	Annexin A1	ANXA1	126670
P12111	Collagen alpha-3(VI) chain	COL6A3	114470
CON__P04258			112560
P08670	Vimentin	VIM	108990
CON__Q29RQ1			103480
P23528;Q9Y281	Cofilin-1;Cofilin-2	CFL1;CFL2	93950
P80297;P02795;P13640;P80294;P04731	Metallothionein-1X;Metallothionein-2;Metallothionein-1G;Metallothionein-1H;Metallothionein-1A	MT1X;MT2A;MT1G;MT1H;MT1A	92232
CON__Q32PJ2			90160
P04114	Apolipoprotein B-100;Apolipoprotein B-48	APOB	80255
P04259;CON__P48668;CON__P04259;CON__P02538;P48668;P02538	Keratin, type II cytoskeletal 6B;Keratin, type II cytoskeletal 6C;Keratin, type II cytoskeletal 6A	KRT6B;KRT6C;KRT6A	74559
P09651;Q32P51	Heterogeneous nuclear ribonucleoprotein A1;Heterogeneous nuclear ribonucleoprotein A1, N-terminally processed;Heterogeneous nuclear ribonucleoprotein A1-like 2	HNRNPA1;HNRNPA1L2	72269
Q15365;Q15366	Poly(rC)-binding protein 1;Poly(rC)-binding protein 2	PCBP1;PCBP2	71158
P0DOX7;P01834	Ig kappa chain C region	IGKC	63173
P12882;Q9Y623;Q9UKX2;P13535	Myosin-1;Myosin-4;Myosin-2;Myosin-8	MYH1;MYH4;MYH2;MYH8	58343
CON__Q3MHN2;P02748	Complement component C9;Complement component C9a;Complement component C9b	C9	49136
P06748	Nucleophosmin	NPM1	49012
CON__Q2KJF1			48880
P0DP25;P0DP24;P0DP23			48699
P23142	Fibulin-1	FBLN1	44935
P16403;P10412;P16402;P22492;Q02539	Histone H1.2;Histone H1.4;Histone H1.3;Histone H1t;Histone H1.1	HIST1H1C;HIST1H1E;HIST1H1D;HIST1H1T;HIST1H1A	30868
P06576	ATP synthase subunit beta, mitochondrial	ATP5B	27723
O00311	Cell division cycle 7-related protein kinase	CDC7	16125

Q99547	M-phase phosphoprotein 6	MPHOSPH6	13039
H3BRN8	Uncharacterized protein C15orf65	C15orf65	8661,3